PROCESSING AND PROPERTIES OF SILICON NITRIDE CERAMICS

by

Jacqueline Margot Nel

A thesis submitted to the Faculty of Engineering, University of Cape Town in fulfilment of the degree of Master of Science in Applied Science.

Department of Materials Engineering
University of Cape Town

September 1993

Summary

Silicon nitride, Si_3N_4, ceramics were produced using either silicon or silicon nitride powder. The silicon was reaction bonded in nitrogen atmosphere to form reaction bonded Si_3N_4, which was then sintered between 1700°C and 1800°C to form a dense Si_3N_4 ceramic. The silicon nitride powder compacts were also sintered between 1700°C and 1800°C. In order to achieve densification Y_2O_3-Al_2O_3 additive combination was used in both processing routes.

The physical and mechanical properties of the Si_3N_4 materials was found to be dependent on the processing conditions. The post sintered reaction bonded Si_3N_4 materials had the highest densities and hardness values, while the sintered Si_3N_4 materials had the highest strength and toughness values. The microstructure was also influenced to a great extent by the processing conditions, and this in turn influenced the mechanical properties of the ceramics.

Contents

1. Introduction

The importance of silicon nitride, Si_3N_4, as an engineering ceramic has increased dramatically in the last two decades, and silicon nitride is being used extensively in commercial applications were high strength, hardness and toughness are required. This study reviews the status of two of the less costly processing routes which do not utilize pressure to produce the final silicon nitride product, namely the reaction bonded silicon nitride from silicon and the subsequent sintering of this product, and the sintering of silicon nitride powder using pressureless sintering.

The aim of the study was to produce silicon nitride materials with high density, and compare the properties such as hardness, strength and toughness obtained using the reaction bonded silicon nitride and sintered silicon nitride routes mentioned above.

The effect of processing conditions, such as variations in sintering temperture and their effect on the properties and microstructures, were investigated. The presence of Si_2ON_2 in reaction bonded Si_3N_4 and its influence on the resulting post sintered reaction bonded Si_3N_4 was also studied. The post sintered reaction bonded silicon nitride (PSRBSN) and sintered Si_3N_4 are of particular interest since both these routes produce dense Si_3N_4. The PSRBSN is produced from the less costly silicon powder which is then argon sintered and nitrided using lengthy sintering schedules to produce a relatively low density reaction bonded Si_3N_4. This reaction bonded Si_3N_4 is then sintered to produce a dense Si_3N_4. The sintered Si_3N_4, on the other hand, utilises more costly Si_3N_4 powder which is sintered using shorter sintering schedules. A higher concentration of additive is, however, necessary to sinter the Si_3N_4 powder in comparison to the reaction bonded route. A well documented additive combination which produces high density Si_3N_4 materials was used, namely yttria (Y_2O_3) and alumina (Al_2O_3). The microstructures of the materials were also examined with the purpose of interpreting the physical and mechanical properties.

2. Review of Literature

2.1. INTRODUCTION TO SILICON NITRIDE

Silicon nitride, Si_3N_4, has become an increasingly important engineering ceramic, with applications in areas requiring high strength (room and elevated temperatures), hardness, toughness and wear resistance, such as bearings, seal faces, piston liners and welding nozzles, to name but a few. A large body of literature has appeared in the last twenty years. Reviews detailing the progress in the processing, properties and microstructure have been compiled by Moulson (1979), Messier and Croft (1982), Riley (1984), Riley (1987) and Griel (1989). In this review general comments have been referenced to the reviewers, while specific results have been referenced to the original researchers.

One of the first references to silicon nitride is reported to be a German patent by Mehnrer in 1895. Nitrogen was passed over a mixture of carbon and silica in a heated furnace to form the Si_3N_4. Another early reference is that of Sinding Larsen in 1909 who patented the process of reducing silica in a carbon arc furnace and reacting the silicon vapour with nitrogen.

Considerable improvements have recently been made in the performance of Si_3N_4. These can be largely attributed to an understanding of the reaction mechanism and the availability of pure silicon and Si_3N_4 powders. Si_3N_4 has relatively low density ($3.18 g/cm^3$), moderate microhardness (19 - 25GPa), high strength (400 - 900MPa at room temperature), strength retention to elevated temperatures (200 - 500MPa at 1400°C), low thermal expansion and a high dissociation temperature (1882°C). These properties coupled with the high chemical stability, wear resistance, thermal shock resistance and corrosion resistance makes Si_3N_4 a good candidate for engineering applications (Moulson (1979), Lange(1980), Messier and Croft(1982), and Sorrel (1982)).

The retention of strength at high temperatures, the high dissociation temperature, thermal shock and creep resistance are attributed to the high covalency in the Si_3N_4 structure. The covalent, directional character of the bonds, however also results in low self-diffusivity and this makes self-sintering difficult. The current study is concerned with producing Si_3N_4 bodies using two processing routes and utilizing both yttria (Y_2O_3) and alumina (Al_2O_3)

sintering aids. The evaluation of the resulting properties of these materials and comparison of the two processing routes also form part of this study.

2.1.1 Crystallography

Crystalline silicon nitride exists in two hexagonal forms, α and ß. The ß-structure belongs to space group $P6_3/m$ and the α-Si_3N_4 to space group $P3_1/C$.

There has been considerable controversy regarding the nature of the α-structure (Kohatsu et al (1974), Moulson (1979) and Messier and Croft(1982)). From earlier structure determinations it was proposed that the α-Si_3N_4 was an oxynitride with oxygen atoms replacing nitrogen atoms in some of the sites and some nitrogen sites being left vacant for charge neutrality. It was therefore proposed that the α and ß structures were high and low oxygen potential modifications rather than low and high temperature polymorphs. More recently it was established that the bond lengths obtained did not suggest sufficient oxygen content or its segregation in any nitrogen site (Kohatsu et al (1974)). It has therefore been concluded that the development of either α or ß-Si_3N_4 is determined by particular growth mechanisms rather than thermodynamic considerations (Moulson (1979)).

The Si_3N_4 structures are made up of layers of basal planes shown in Figure 2.1(a). This plane consists of a hexagonal array of basic units in the form of puckered 8-membered rings, Figure 2.1(b). This arrangement results in a void of 1.5Å diameter in the basal plane. The ß-structure is made up of identical layers and the basal planes are stacked in sequence AAAAA . .. (Messier and Croft(1982) and Shaw (1981)). This structure is not strained and channels occur where the voids are superimposed. The α-structure is more strained since the second basal plane is rotated with respect to the first in a stacking sequence ABABAB . . .. Because of the rotation the voids are no longer superimposed and thus form pockets and not channels.

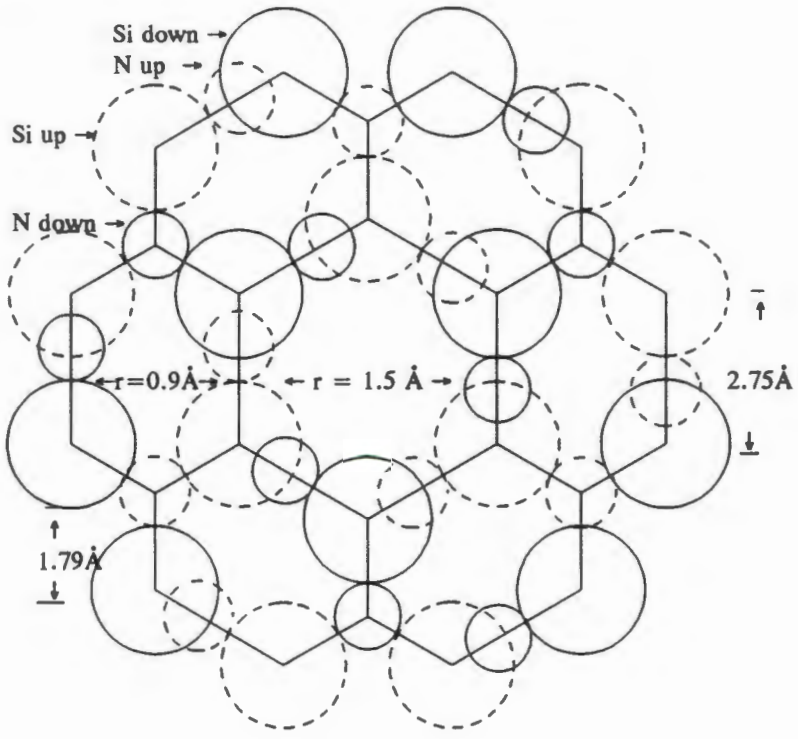

(a)

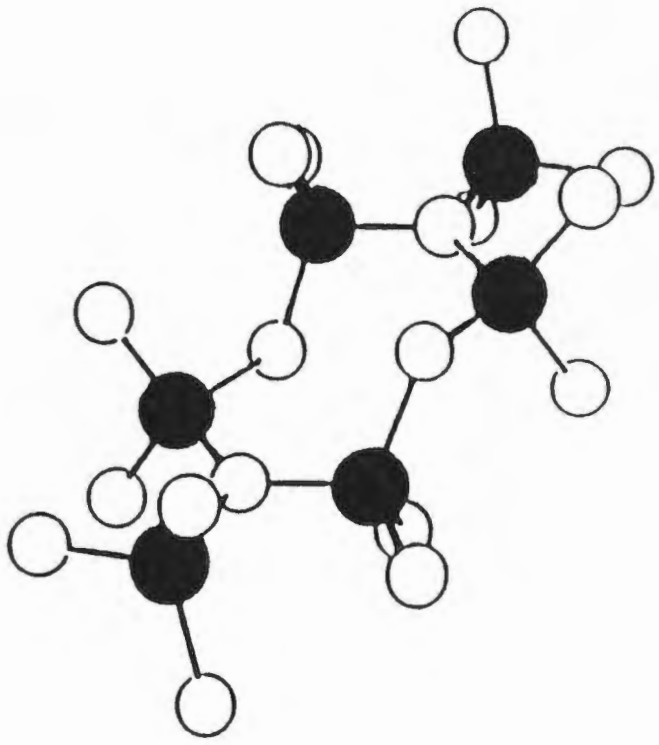

(b)

Figure 2.1: Schematic of a) the Basal Plane and b) 8 membered ring which make up the Si_3N_4 structure.

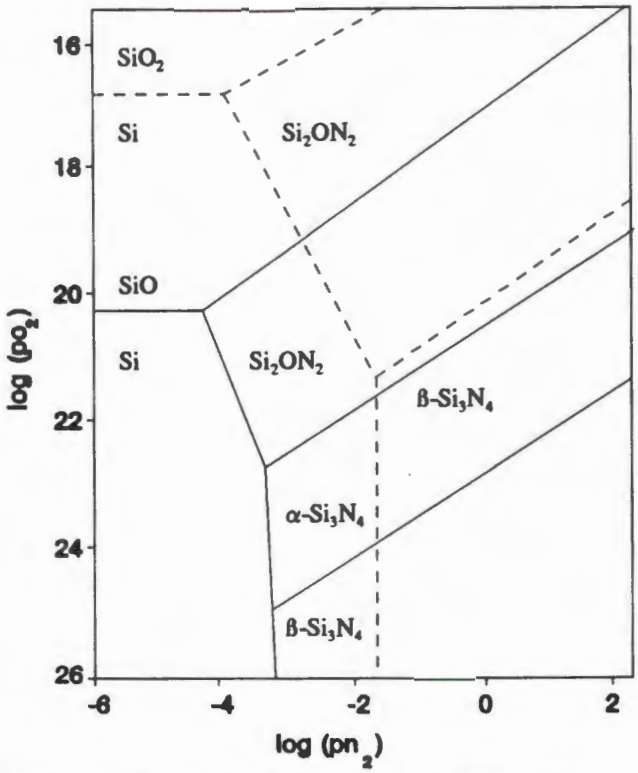

Figure 2.2: Thermochemical stability of the Si-O-N system at 1600K (solid lines) and 1800K (dotted lines) (after Jack (1979)).

2.1.2 Phase Equilibria

The first phase diagram data for the Si-O-N system assumed that the α-Si_3N_4 phase was an oxynitride (Grieveson et al (1968)). This was found not to be the case and a new equilibrium diagram was devised (Jack (1979)). The dotted lines in Figure 2.2 represent the thermochemical stability at 1800K and the solid lines are at 1600K.

Silicon nitride forms from its elements according to the following reactions (Moulson (1979)):

$3\,Si\,(s) + 2\,N_2\,(g) \rightarrow Si_3N_4\,(s) \quad \Delta G^\circ \sim -723 + 0.315T kJmol^{-1}$

$3\,Si\,(l) + 2\,N_2\,(g) \rightarrow Si_3N_4\,(s) \quad \Delta G^\circ \sim -874 + 0.405T kJmol^{-1}$

$3\,Si\,(g) + 2\,N_2\,(g) \rightarrow Si_3N_4\,(s) \quad \Delta G^\circ \sim -2080 + 0.757T kJmol^{-1}$

X-ray data have shown that both α- and ß-Si_3N_4 are present when calculating these thermodynamic data and therefore the crystalline forms have not been specified above.

2.1.3 Review of Study

To produce Si_3N_4 components, various methods are used, such as reaction bonding, pressureless sintering, hot pressing, gas pressure sintering and hot isostatic pressing. The former two methods have been used during this study and will be discussed in more detail in sections 2.2 and 2.3 respectively. Due to the slow rate of self-diffusivity of Si_3N_4, additives (usually oxides) are needed during the sintering of Si_3N_4 in order to reach near theoretical density. These additions complicate the chemistry of the systems and consequently only a limited number of phase diagrams are available. These will be explored in more detail in section 2.4. The mechanical properties are reviewed in section 2.5 and the microstructures in section 2.6.

2.2 REACTION BONDED AND POST-SINTERED SILICON NITRIDE

Reaction bonding, sometimes referred to as reaction sintering, is a formation reaction coupled with the development of strength in a bulk compact of powder (Riley (1977)).

Reaction bonding of silicon nitride by the nitridation of silicon results in a ceramic material composed predominantly of Si_3N_4, with residual Si and impurities. This reaction is accompanied by approximately 22% volume increase and a theoretical mass gain of 66.67% (Messier and Croft (1982)), but no dimensional changes occur in the compact. The volume increase is accommodated in the interconnecting porosity and results in a decrease in porosity without dimensional change. The final density is then only dependent on the green density of the compact. Theoretically a green density of 1.913 g/cm^3 should result in fully dense Si_3N_4 (3.18g.cm^{-3}), but in practice the maximum density obtainable is approximately 2.7 g/cm^3 (Riley (1977)). This is due to a large extent to pore closure in the compact and the loss of material due to evaporation. Typical densities are in the order of 2.4 g/cm^3, and a mass gain of 60 - 61% is more realistic (Messier and Croft (1982)).

This section will give a brief overview of the production of reaction bonded silicon nitride, RBSN, a technique used during this study.

2.2.1 Nitriding Schedules

Prior to the nitridation of the pressed silicon compact, it is common practice to include an argon sintering step at temperatures between 1150°C and 1200°C. This step imparts strength to the silicon compact enabling easier machining prior to nitriding. This step also results in the coarsening of the green structure, increases the permeability of the compact and results in the reduction of some SiO_2 (Arundale and Moulson (1977), Riley (1983)).

The next step is the nitridation of the Si. The melting point of Si is 1410°C, and it has been found that full nitridation is difficult below this temperature. Two stage nitriding has become common practice with typical schedule of 24 - 50 hours at 1350°C followed by 10 - 24 hours at 1450°C (Riley (1977)).

Due to the exothermic nature of the reaction, temperature gradients of up to 40°C are produced in the compact. The exothermic reaction also results in inadequate temperature control when using conventional methods. Ideally the reactants should be able to control the temperature, therefore, a rate controlled nitriding cycle has been developed (Mangles (1981a)). Some self-regulating procedures are described in detail by Mangles (1981a) and Mustel and Broussaud (1984). It was, however, not possible to use this method during this study, but the two stage sintering cycle was implemented.

2.2.2 Nitriding Mechanisms

Silicon is spontaneously oxidised at room temperature and this oxide layer has an inhibiting effect on the nitridation. Nitridation can occur underneath the thin oxide layer, but the reaction is slow and the resulting nitride film acts as a further barrier (Riley (1977)). It is only when this oxide layer is removed or disrupted that nitridation can occur to any appreciable extent. The techniques listed below are used singly or in combination, and all appear to have a catalytic effect on the nitridation process (Riley (1983)).

1. Vacuum Pre-treatment at 1000 - 1200°C

   SiO_2 (c) → SiO (g) + ½ O_2 (g) Oxygen partial pressure must be < 1mPa
2. Hydrogen Pre-treatment

   SiO_2 (c) + H_2 (g) → SiO (g) + H_2O (g)
3. Metallic Fluoride addition

   2 MF_2 (c) + SiO_2 (c) → SiF_4 + 2 MO (c)
4. Transition metal addition

   Si (c) + SiO_2 (c) → 2SiO (g)

After the removal of the oxide layer, nitridation of the Si takes place at various rates.

Atkinson et al (1976) studied the kinetics and morphology of the growth of Si_3N_4 on pure Si. Their proposed mechanism is illustrated in Figure 2.3. N_2 gas molecules are chemisorbed onto the clean Si surface and nitrided nuclei form rapidly, Figure 2.3(a). The chemisorbed coverage is usually low, and as the nuclei grow they deplete the neighbouring Si surface of

chemisorbed nitrogen. Each nucleus is therefore surrounded by a nitrogen depleted zone. At low temperatures the initial nuclei mainly grow laterally (Figure 2.3(b)), but at higher temperatures the grain growth takes place vertically. The nitrogen is supplied by chemisorbtion and surface diffusion and the Si by surface diffusion and/or evaporation-condensation. As the nuclei grow the surrounding Si surface is depressed by the removal of Si and nuclei growth occurs around the edge of the depression (Figure 2.3 (c and d)). The nuclei approach each other and as the Si is supplied from a decreasing area, the depressions deepen and undercut the nitride (Figure 2.3 (d)). The growth of the nitride is now predominantly perpendicular to the Si surface. The channels through which the Si is supplied to the reaction surface are sealed off when the nitride growths coalesce (Figure 2.3 (e)). This makes the transport of Si to the reaction surface increasingly difficult and the rate of nitridation decreases proportionately to the closure of the channels until the reaction stops completely. Before closure of the channels, new nitride nuclei can form on the surface of the silicon within the pores (Figure 2.3(f)). Braun et al (1988) studied the nitridation of Si by thermogravimetry. The kinetic parameters and reaction mechanisms were found to be dependent on the various grades of Si used. The initial reaction was found to be mainly a phase boundary reaction, with variations in the reaction orders, while the main nitridation ranged from phase boundary reaction to first order reaction to a two dimensional diffusion.

The products of nitridation consist of both α and ß-Si_3N_4. It is generally accepted that the α-Si_3N_4 is formed by a vapour phase reaction involving silicon or silicon monoxide vapour. This phase will be the dominant phase as long as the temperature is held below 1410°C (Riley (1977)). The ß-Si_3N_4 forms via the direct nitridation of liquid silicon and at higher nitriding temperatures more ß-Si_3N_4 is formed. This means that the proportions of the two phases can be controlled along with the microstructure of the material by controlling the temperature.

2.2.3 Effects of Impurities or Additions to the Nitriding System

Iron impurities in the Si powder can influence the nitridation reaction in various ways. It can disrupt the SiO_2 film present on the Si by devitrification and thus expose the Si to nitrogen (Moser et al (1986)) or it can react with the silicon to form Fe-Si liquids which promotes the

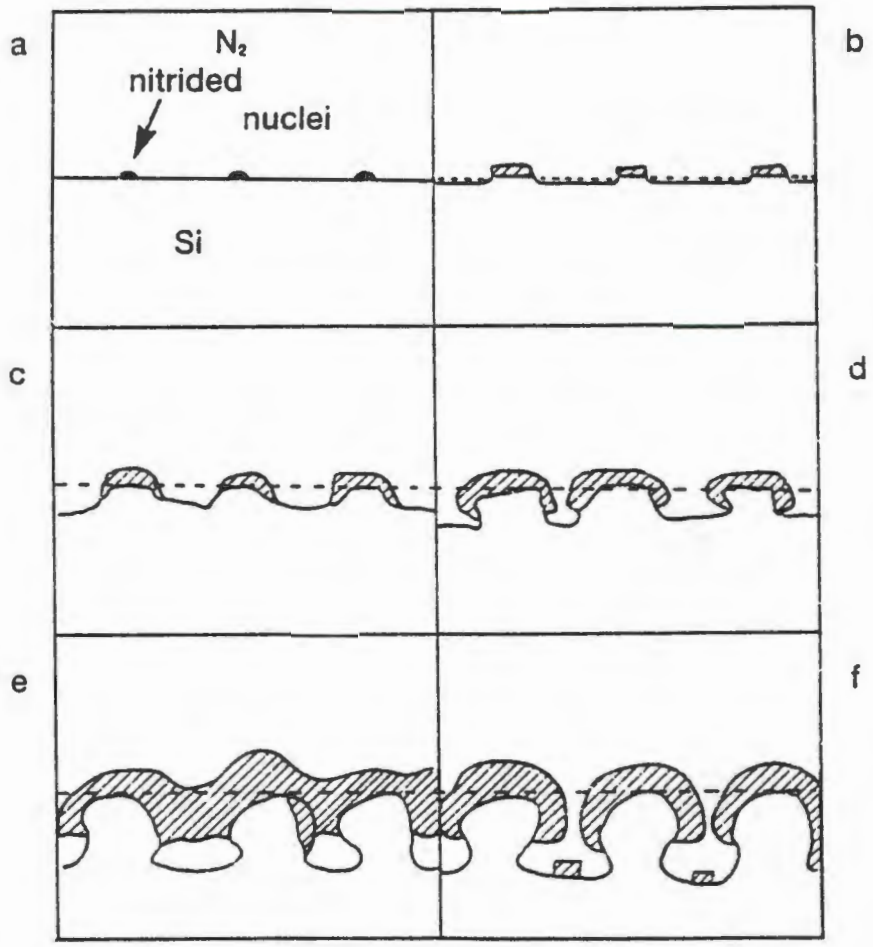

Figure 2.3: Mechanism of the Nitridation of Silicon (Atkinson et al (1976)).

growth of ß-Si_3N_4 (Moulson (1979)).

The natural thin oxide layer can be removed as previously discussed, but deliberately oxidised powders ($\sim 1\mu$m thick layer of oxide) can not be nitrided (Moulson (1979)). The reactivity of these oxidised powders can be completely restored by adding 10 wt% Fe.

Large quantities of oxygen or water present in the nitriding gas appear, however, to have very little effect on the nitridation reaction (Moulson (1979), Riley (1983)). The addition of H_2O has also been found in some cases to enhance the α-Si_3N_4 formation (Moulson (1979)).

The presence of hydrogen in the nitriding atmosphere accelerates silicon nitride formation and a small percentage of hydrogen is mixed with the nitrogen during the production of high density RBSN (Lu and Riley (1984)). The hydrogen facilitates the removal of the protective silica film, and can also increase the rate of nitriding by acting as an oxygen sink or by increasing the SiO partial pressure in the Si by reduction of SiO_2.

2.2.4 Post-Sintering RBSN (PSRBSN)

RBSN materials can be easily formed into the shape needed and, due to the fact that no shrinkage occurs, there is a high degree of dimensional control. The density of these materials, however, is low (80 - 85% theoretical) and this results in limited strength and other mechanical properties (Mangels and Tennenhouse (1980) and Mangels (1981b)). Other methods of processing Si_3N_4, such as hot-pressing and sintering Si_3N_4, meet the mechanical properties required, but there is a shrinkage of up to 20% (Ziegler (1983)) and the amount of sintering aids necessary for densification is high.

Post sintering of RBSN has been investigated by numerous groups and some advantages of this method of processing are listed below (Giachello and Popper (1979a) and Mangels (1981b)):

1. The readily available Si can be formed into complex shapes by techniques which are well established (slip-casting and injection moulding) or by machining the shape after sintering under argon. This allows the shaping of the components without the use of expensive diamond tooling.
2. The green density of the RBSN is relatively high, which results in linear shrinkages of only 5 - 10%.
3. The sintering process can be carried out at atmospheric pressure.
4. Smaller quantities of sintering aids are necessary than for normal pressureless sintering.

Pure silicon nitride does not self-sinter due to the covalent nature of the bonds, and so sintering aids, generally oxides, have to be added. These additives react with the surface silica to form an oxynitride liquid phase at high temperature which promotes shrinkage and

the transformation of α-Si_3N_4 to ß-Si_3N_4 (Hampshire and Jack (1983)). This liquid phase sintering mechanism will be dealt with in more detail in section 2.3.2.

The additives used in PSRBSN are the same as those used in sintered Si_3N_4 (See section 2.3). There are two techniques used to introduce the sintering additive to the RBSN component. The first technique is the impregnation/diffusion of the additive into the RBSN compact and the second is intimate mixing with the Si before nitriding (Giachello and Popper (1979(a)) and Mangels (1981(b))).

The sintering temperatures for PSRBSN vary with the additive used, but they range from 1700°C (pressureless sintering) to 2000°C (using N_2 over-pressure). In order to minimize the decomposition of Si_3N_4 which occurs at these temperatures, the compacts may be embedded in a powder bed consisting usually of Si_3N_4, BN and additives (Mangels and Tennenhouse (1981) and Barnett and Nel (1989)). Other advantages of the powder are to support and separate the compacts in the crucible, prevent reaction with the carbonaceous atmosphere resulting from graphite elements, and lastly, to prevent the migration of additives from the compact.

2.2.5 Transformation of α- to ß-Si_3N_4

The transformation of α-Si_3N_4 to ß-Si_3N_4 during sintering is usually complete at the temperatures used to sinter, since the transformation starts at ~1650°C (Park and Kim (1988)). α-Si_3N_4 has been densified without transformation but the strengths are reported to be much lower than those of materials which have undergone transformation (Messier and Croft (1982)). The transformation process does not necessarily occur simultaneously with the shrinkage which commences with the formation of the liquid phase. These two processes are dependent on the additives used and differ from one additive to the other, eg. MgO results in nearly complete densification and only partial transformation, whereas Y_2O_3 gives a complete transformation with limited densification (Hampshire and Jack (1983)).

Hampshire and Jack (1983) showed that the activation energies for transformation were the same for the two additives and they were also similar to the dissociation energy of the Si-N

bond. This, along with other studies, (Messier and Croft (1982)) indicates that the transformation of α to ß-Si_3N_4 can be classified as a reconstructive transformation of secondary co-ordination. The reverse transformation from ß to α-Si_3N_4 has not been observed.

Park and Kim (1988) studied the effect of free Si on the α-ß transformation. They found that the fraction ß-Si_3N_4 gradually increased when free Si was present in pure Si_3N_4 powder. In the absence of Si at 1700°C, however, no α-ß transformation was observed. It was concluded that the Si which is molten at the temperatures in question (1600 - 1800°C) acts as a suitable liquid phase for the transformation in the same way as other sintering aids. In another study Park et al(1987) found that the size of the free Si particles also influenced the extent of transformation. In an earlier study Mukerji (1984), found that α-ß transformation did occur in pure Si_3N_4 after 1 hour at 1820°C, which is 120°C higher than that used by Park and Kim (1988).

Although iron is known to promote the formation of ß-Si_3N_4 via the ferrosilicon liquid phase during reaction bonding of Si_3N_4, when iron is added to α-Si_3N_4 powder and sintered, it has no effect on the transformation of α to ß-Si_3N_4 (Chakraborty and Mukerji (1986)).

2.3 SINTERED SILICON NITRIDE

2.3.1 Pressureless Sintering

Pure silicon nitride powder cannot be sintered at reasonable temperatures (<2000°C) and pressures (<10MPa), (Riley (1984), Mukerji (1984) and Lange (1983)), due to the low diffusion coefficients of Si and N. There is also a high loss of material at temperatures above 1600°C when no nitrogen overpressure (1 - 10MPa) or powder beds are used. When no additive is used, the α-ß transformation takes place at higher temperatures (1800°C) and the ß-Si_3N_4 grains are acicular with high aspect ratios. These grains form a rigid structure which prevents densification and shrinkage (Mukerji (1984)). The incorporation of sintering aids introduces a competitive material transport route which accelerates densification (Riley (1983)). The sintering aids (or additives) are usually oxides or nitrides which react with the SiO_2 on the Si_3N_4 powder particles to form a liquid phase above their eutectic temperature. The reaction which takes place at temperatures up to 1800°C is:

$$Si_3N_4 + SiO_2 + \text{Additive/s} + \text{(other impurities)} \rightarrow Si_3N_4 + \text{Liquid} \rightarrow Si_3N_4 + \text{2nd Phase}$$

In this temperature range the decomposition of silicon nitride becomes important. This problem can be solved either by raising the pressure (Wötting and Ziegler (1988(a))) or by embedding the compact in a powder bed during sintering (Popper (1978)).

By careful selection of the powder bed it is possible to control not only the decomposition of the Si_3N_4, but also the loss of volatile additives. In a study by Giachello et al (1979(b)) it was found that when using a suitably doped bed the results obtained were comparable to materials which were gas pressure sintered. The addition of additives of similar composition to the sintering aid to the powder bed inhibited the migration of the additives from the compact. It was also found that the presence of additives in the powder bed could be used to sinter pure Si_3N_4. The minimum amount of sintering aid necessary diffused into the compact from the bed thus facilitating sintering and densification.

2.3.2 Liquid Phase Sintering

Liquid phase sintering, LPS, is the only mechanism by which Si_3N_4 can be sintered at easily attainable temperatures and pressures (below 2000°C and 100MPa). As mentioned previously, the sintering aid/s react with the silica which is present on the surface of the Si_3N_4 particles. At a sufficiently high temperature this reaction produces a liquid phase by which densification can take place.

LPS can best be defined as sintering involving the coexistence of a liquid phase and particulate solid phase during some parts of the heat treatment. The most common method of LPS involves two powders of differing chemistries which are mixed together. A liquid phase forms either by the melting of the one component or the formation of a eutectic (German (1985)).

The forces acting on the system due to the surface energies must be considered in LPS. On melting the liquid tends to coat the solid particles, and pores will be formed in the liquid phase. The liquid-vapour pore surface area decreases and consequently the overall lowering of the surface energy is the driving force for densification (Kingery (1959)). Each pore has a negative pressure which is equivalent to placing the system under an equal hydrostatic pressure. An equivalent pressure is exerted by the small radii of curvature in capillary depressions on the surface. These pressures provide an appreciable driving force throughout the sintering process, making it possible to sinter compacts without external pressure (Kingery (1959)). For high performance applications, however, external pressure techniques are often used in conjunction with additives to obtain the high density products necessary.

The densification process in classic LPS takes place in three overlapping stages, particle rearrangement, solution-precipitation, and solid state controlled sintering. Each of these stages are shown in Figure 3.1 and will be dealt with in more detail below.

2.3.2.1 Particle Rearrangement

On initial liquid formation there is rapid densification due to the capillary pressure which tends to rearrange the solid particles in such a way that better packing and

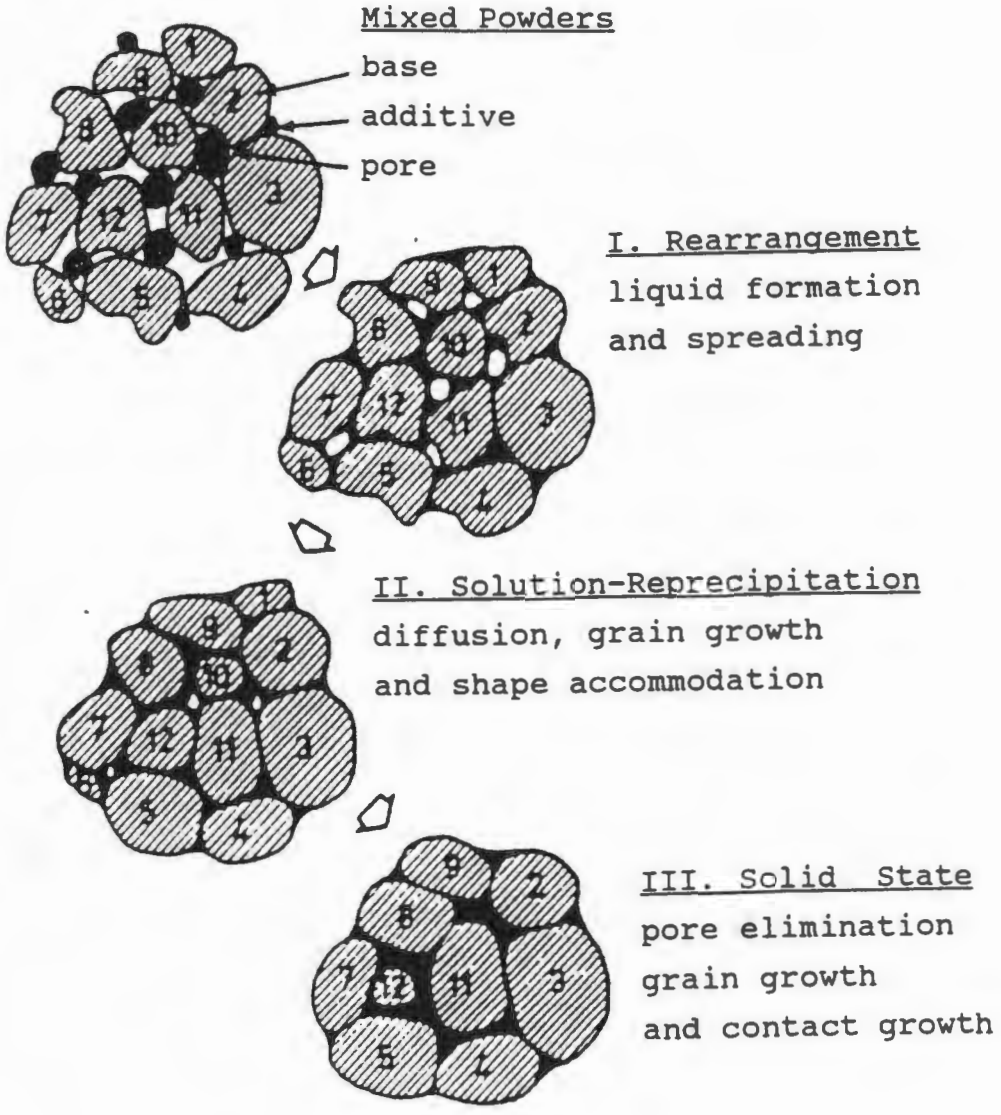

Figure 2.4: Schematic diagram of the stages during liquid phase sintering (German (1985)).

a decrease in porosity is achieved (Kingery (1959), German (1985)). The densification rate is dependent on the viscosity of the liquid formed while the extent of densification via rearrangement is dependent on the volume fraction of liquid present, particle size distribution and morphology, and the solubility of the solid (ie Si_3N_4) in the liquid (German (1985)). During the initial stages the amount and composition of the liquid phase is changing continuously by dissolution of additives and Si_3N_4, which changes the wetting, spreading and flow behaviour of the liquid. This process of particle movement and densification is extremely slow in Si_3N_4 compared to liquid metals due to the comparatively high viscosity of the silicate

liquids which are formed. Fully dense compacts can be obtained by rearrangement if there is sufficient liquid present (estimated at 35 vol%). Irregularly shaped particles and high green densities can inhibit the rearrangement process (Prokesová and Pánek (1989)). The compaction of powders can result in particle contact which may form solid state bonds during heating, thus preventing rearrangement (German (1985)). The rearrangement rate in Si_3N_4 is dependent on the size and shape of the powders used, and the ß-Si_3N_4 content. A high ß-Si_3N_4 content is reported to halt the rearrangement process before completion (Prokesová and Pánek (1989)).

2.3.2.2 Solution-Reprecipitation

Various other events run concurrent to the rearrangement stage. These are usually overshadowed because of the fast kinetics of the rearrangement. As the rearrangement is inhibited, solubility and diffusion effects begin to dominate. A general attribute of this stage is the microstructural coarsening. Particle contact points and small grains are areas of high solubility due mainly to the pressure induced by the capillary forces present. Diffusion along the concentration gradients in these areas of high solubility results in material transport to regions of lower solubility (Kingery (1959)). Powders with high α-Si_3N_4 contents have a higher solubility since this phase becomes thermodynamically unstable with respect to ß-Si_3N_4 at high temperature and this causes the α-Si_3N_4 to dissolve more readily (Wötting and Ziegler (1986(a))).

The shape of the grains can be altered during the solution-reprecipitation process to allow tighter packing of the grains, resulting in the elimination of some of the porosity. The shapes of the grains are determined by the relative solid-liquid and solid-solid interfacial energies, quantity of liquid, liquid immiscibility, viscosity and anisotropy in the surface energy of the solid (German (1985)).

In the Si_3N_4 system the dissolution of the α-Si_3N_4 and the reprecipitation of the material as ß-Si_3N_4 is the driving force in this second stage of LPS. When little or no ß-Si_3N_4 is present in the starting powder, supersaturation of the liquid phase by

α-Si_3N_4 must be attained before nucleation and subsequent growth of elongated ß-Si_3N_4 will take place. When ß-Si_3N_4 particles are present, no supersaturation is necessary to precipitate the ß-Si_3N_4. The growth of ß-Si_3N_4 grains takes place continuously under near equilibrium conditions. This results in the growth of ß-Si_3N_4 grains to spherical particles compared to the rod-like grains when no ß-Si_3N_4 is present (Wötting and Ziegler (1986(a))). Weiss and Kayser (1983) discuss two possible mechanisms for the growth of ß-grains at the expense of the α-grains. The first is directional grain growth which takes place when the ß-particles are much smaller than the α-particles, and the second is a modified Ostwald ripening when the ß-particles become larger than the α-particles.

The shrinkage in Si_3N_4 was found to be directly related to the amount of α-Si_3N_4 which has transformed to ß-Si_3N_4. According to classic LPS the shrinkage has the following proportionality:

$$\frac{V}{V_o} \alpha\ t^{n-1}$$

where t = time, n = 3 if solution into or precipitation from the liquid phase is rate controlling and n = 5 if diffusion through the liquid is rate controlling. This relationship assumes non-spherical particles (German (1985)).

2.3.2.3 Solid State Controlled Sintering

The dominant processes in this final stage are active throughout the LPS cycle, but due to the relative slowness the contribution of solid state sintering is not significant at low temperatures. During this stage the densification is reduced due to the existence of a solid skeleton, but the microstructural coarsening continues. The typical compact exhibits considerable grain growth by the onset of this stage and with continued sintering these grains continue to grow and pore sizes change by a process of solution-reprecipitation. Long heating schedules and subsequent annealing enhance the grain growth and also results in the reduction of the aspect ratio (German (1985)).

Solution-reprecipitation continues during this stage, resulting in grain growth, grain shape accommodation and final pore removal. The final porosity is usually less than 5%. The rigidity of the microstructural skeleton often inhibits the elimination of porosity. Factors which can further inhibit this final densification are trapped gas in the pores, decomposition of the sintered components, gross packing defects and reaction products involving the atmosphere. The microstructural changes which occur during this final stage of sintering are dictated by the volume fraction of liquid and the size and shape of the grains, and this influences properties such as wear resistance and strength (German (1985)).

During the sintering of Si_3N_4, gas is released during the decomposition of the reaction products. This results in a complex dependence on the sintering time - temperature combination due to simultaneous densification and decomposition. A compromise has to be reached between densification and decomposition which usually results in short sintering times being preferred.

2.3.3 Influence of other parameters on sintering

An increase in temperature during sintering promotes densification by decreasing the viscosity of the liquid phase thus facilitating the rearrangement. The lower viscosity also enhances the coarsening of the grains and reduces the aspect ratio thus reducing the mechanical properties. The temperature can only be increased to $\sim 1800°C$ when a high nitrogen overpressure is not used. Above this temperature the Si_3N_4 starts to dissociate rapidly (Wötting and Ziegler (1986(a) and (c))).

The application of pressure during sintering, be it uniaxial mechanical pressure during hot pressing or isostatic gas pressure during hot isostatic pressing, assists the rearrangement process and the solution of α-Si_3N_4. This leads to improved densification rates, increased nucleation rates and a finer-grained microstructure (German (1985), Greskovich (1976)).

The densification, microstructure and properties of the materials also depend on the type and amount of additives used during processing. A large amount of additive usually results in

high densities, but the liquid phase often forms a glassy intergranular phase which lowers the high temperature properties. When reducing the additive concentration, the following characteristics of the Si_3N_4 powder become important for the best sintering results (Wötting and Ziegler (1986(a) and (c))):

- High fineness for large surface area which results in high sintering activity.
- Equiaxed particles for optimum green density packing.
- High α-Si_3N_4 content to favour the formation of the elongated interlocking ß-Si_3N_4.
- Low O_2 content, but sufficiently high for liquid phase formation.
- Low carbon content to avoid reduction of the oxygen layer on the powder at high temperatures.
- Low impurity levels of elements such as Ca, Fe, Al, Mg and inclusions of WC for good high temperature properties and homogeneous microstructure.

2.4 ADDITIVES

Additives are used to promote sintering of Si_3N_4 via a liquid phase (See section 2.3.2). Some of the more commonly used additives are Y_2O_3, MgO, Ce_2O_3, ZrO_2, Al_2O_3 and AlN. Additives can be used singly, but are usually used in conjunction with one or more additives to get the desired properties in the final material.

The additives react with the SiO_2 surface layer and the Si_3N_4 in the Si_3N_4 particle to form an oxynitride liquid which allows liquid phase sintering to occur at high temperatures (Hampshire (1984)). The temperature of the initial liquid formation varies with each additive, and is lower than the lowest solidus temperature in the corresponding metal oxide-silica system. This lowering of the eutectic temperature is due to the presence of nitrogen in the system. For example MgO forms a liquid phase at 1390°C and Y_2O_3 at 1450°C in the Si_3N_4 system compared to 1543°C and 1660°C respectively in the SiO_2 system. Additional additives will lower this eutectic still further (Lange (1983(b))) and can also increase the amount of liquid phase present (Hampshire (1984)).

Few phase diagrams are available for the nitride systems, and therefore other means must be used to determine the effectiveness of novel additives. When comparing the standard free energies of formation of successful additives such as Y_2O_3, it has been found that the standard free energy of oxidation of the metal to metal oxide, ΔG_3 ($Y \rightarrow Y_2O_3$) and the metal nitride to oxide, ΔG_4 ($YN \rightarrow Y_2O_3$) were both less than the standard free energies of oxidation of Si_3N_4 to SiO_2 (ΔG_1) and SiO (ΔG_2). Figure 2.5 shows some of these values for a number of metal oxides, some of which have been used successfully as additives in the silicon nitride system (Negita (1985)).

The additives also influence the viscosity of the liquid phase. For example a Y_2O_3 containing liquid phase has a higher viscosity than a MgO containing liquid phase (Hampshire and Pomeroy (1985), Hwang and Tein (1983)). This influences the solution-precipitation stage of sintering and therefore the α-ß phase transformation and densification are also affected. The more viscous the liquid phase the faster the transformation appears to take place (Hwang and Tein (1983)), but this can also result in lower densification (Hampshire and Jack (1983)).

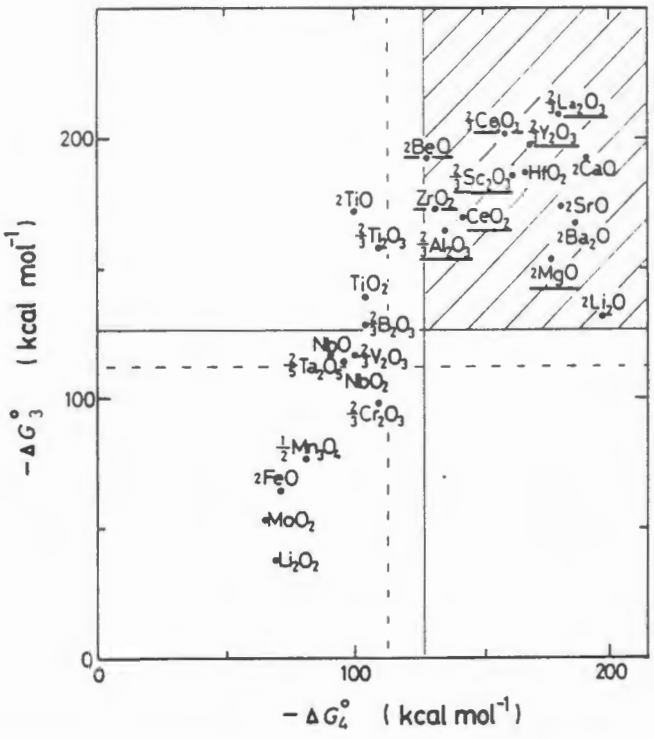

Figure 2.5: Plot of standard free energies for metal oxides at 2000K. Dotted line-ΔG_2 for $Si_3N_4 \rightarrow SiO$, solid line-ΔG_1 for $Si_3N_4 \rightarrow SiO_2$ (Negita (1985)).

The various additives can be divided into three basic classes (Lorenz et al (1982)):

1. those which exhibit extended solid solution formation with Si_3N_4, eg Al_2O_3, AlN, SiO_2 and BeO, Be_3N_2, $BeSiN_2$.
2. those that do not exhibit extended solid solution formation with Si_3N_4, eg MgO, ZrO_2, Y_2O_3
3. a combination of the first and second class, eg Al_2O_3-AlN-SiO_2-Y_2O_3.

The additives from the first class can result in a single phase alloy, while the insoluble additives in the second and third classes necessarily form multiphase systems with amorphous and/or crystalline phases.

2.4.1 Solid-solution Forming Additives

The most commonly used solid solution additives used in Si_3N_4 are Al_2O_3, AlN and SiO_2. These additives are used in varying amounts with Si_3N_4 and form a group of materials referred to as SiAlONs. ß-SiAlON is formed from ß-Si_3N_4 by substituting Al in the place of Si, and O in the place of N in the structure. There is a wide range of compositions that are formed in this manner, and some of these are shown in Figure 2.6. α-SiAlON is formed

from α-Si_3N_4 where Si is replaced by Al in the structure. In order to balance the valence difference of these two elements, N is either replaced by O or metal cations are introduced into the interstitial sites in the matrix resulting in the following composition: $M_x(Si,Al)_{12}(N,O)_{16}$, where $x \leq 2$ (Lorenz et al (1982), Boskovic et al (1978), Jack (1991)).

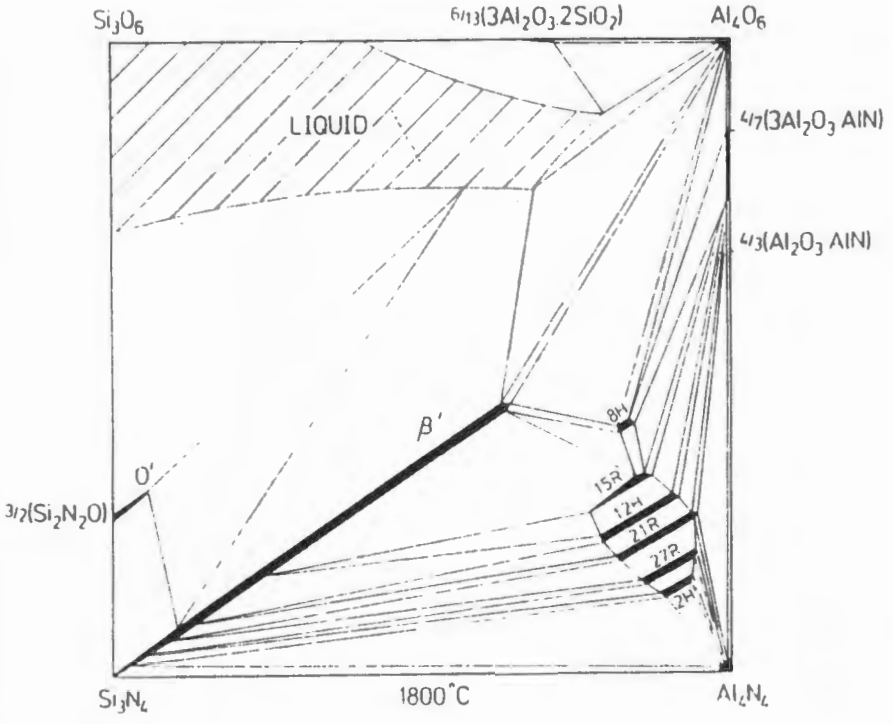

Figure 2.6: The Si-Al-O-N quaternary phase diagram at 1800°C (after Jack (1991).

Be-based additives have also been found to form a solid solution in Si_3N_4. One of the more important Be-based additives is $BeSiN_2$. It was first used by Palm and Greskovich (1980) and is prepared by mixing equimolar amounts of Be_3N_2 and Si_3N_4 and heat treating this mixture to a temperature of 1600 °C (Pasco and Greskovich (1982)). This additive is used in materials which are to be hot pressed or gas pressure sintered, since it has a low oxygen content and therefore there is less liquid phase present during sintering. Despite these pressure methods, Greskovich et al (1983) found that there was insufficient oxygen content in the system to facilitate the sintering process. It was found that an oxygen content of between 1.4% and 7% was needed to react the additive with the surface SiO_2 on the Si_3N_4.

The oxygen is introduced by a controlled oxidation of the additive or the mixed powders. The sintering then takes place via the liquid phase as previously discussed, where the $BeSiN_2$ reacts with the SiO_2 and this forms a solid solution which is taken up in the ß-Si_3N_4 matrix in the form of $Be_{0.1}Si_{2.9}N_{3.8}O_{0.2}$. The materials produced using the $BeSiN_2$ additives have good oxidation and creep resistance, and the strengths are retained up to temperatures of 1400°C in air (Pasco and Greskovich (1983)).

2.4.2 Non Solid-solution Forming Additives

The following two additive systems, Mg-O-Si-N and Y-Si-O-N , when used on their own do not form solid solutions with Si_3N_4, but they are often used in conjunction with other additives such as Al_2O_3, which then result in a combination of solid solution and other multi-phase compositions. These two systems will be discussed in more detail below.

2.4.2.1 Mg-O-Si-N System

After the discovery in 1961 by Deeley et al that MgO acted as a sintering aid during the hot pressing of Si_3N_4, it became the most widely used additive in commercial and experimental products. The first phase diagram of this system, however, was only determined in 1978, Figure 2.7, (Lange (1978)). Because of the low eutectic temperature, 1390°C, and low viscosity of the resulting liquid phase, MgO promotes good densification in the Si_3N_4 products, but does not promote the transformation of the α-phase to ß-Si_3N_4. The resulting liquid phase is not conducive to crystallization on cooling and the high temperature properties, particularly flexural strength, degrade rapidly above 1000°C due to the low liquid formation temperature (Rae et al (1977), Hampshire and Pomeroy (1985)).

MgO has been used as additive in all methods of processing of Si_3N_4. Successful addition of low quantities of MgO have been used predominantly in hot pressing and post sintering of RBSN and better high temperature strength and oxidation resistance are reported (Clarke and Lange (1980)). Gazza (1982) used 5wt% MgO to hot press Si_3N_4, and obtained a material with a flexural 3-point bend strength of 800MPa. Giachello and Popper (1979) used the same amount of additive in RBSN

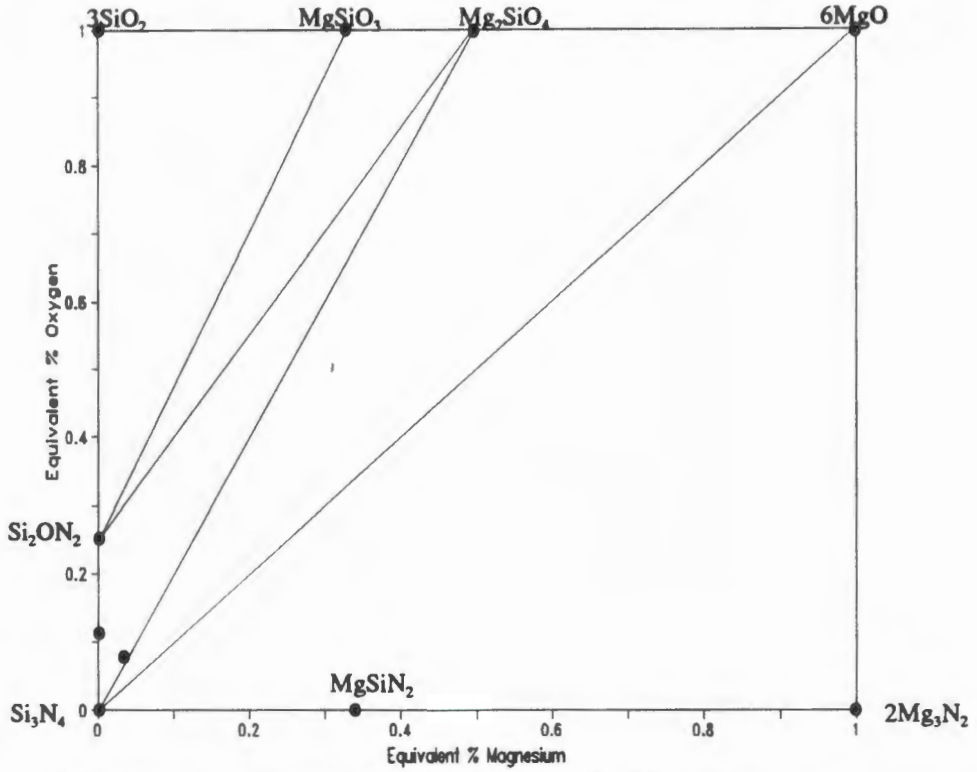

Figure 2.7: Equivalence phase diagram of Si-Mg-O-N system (after Lange (1978)).

materials and found the resulting products to be in the same density range as those pressureless sintered, but the strengths were higher. When less MgO was used in RBSN, 2.4wt%, a strength of ~500MPa and densities of 3.2g/cm^3 were obtained (Mangels and Tennenhouse (1980)).

MgO has also been used in conjunction with Al_2O_3 to sinter Si_3N_4 (Barta and Manella (1981)). It was established that the Al_2O_3 was essential for pressureless sintering of Si_3N_4 to full density, since it forms an even lower temperature liquid phase eutectic than MgO on its own, and a lower sintering temperature of 1650°C was sufficient. They also observed that the addition of Al_2O_3 inhibited the decomposition of the Si_3N_4 during sintering.

2.4.2.2 Y-Si-O-N System

During the late 1970's there was a general move from MgO additives towards the more refractory oxides, such as Y_2O_3. These additives resulted in higher eutectic temperatures which also resulted in less high temperature degradation of strength.

On sintering Si_3N_4 with only Y_2O_3 as additive, the densities were lower than those materials sintered using MgO additives (Giachello and Popper (1979)), and the properties of the material were very dependent on the heating rate used and not only on the final sintering temperature (Campbell and Dutta (1982)). Higher sintering temperatures are also necessary when using only Y_2O_3 as additive (above 1750°C). The grain boundaries of these materials, particularly those with ~6wt% Y_2O_3 have been crystallized, and this has improved the high temperature properties and oxidation resistance of the resulting material over those with MgO in the additive system. Crystallization of $Y_2Si_2O_7$ in the intergranular phase was found to increase the number of dislocations in the product, resulting from the induced stresses after crystallization, and this adversely affected the mechanical properties. These dislocations were, however, easily reduced by prolonged annealing at 1500°C thus improving the properties (Lee et al (1988)).

Y_2O_3 was initially used in conjunction with MgO, and it was found that very little MgO was necessary to obtain good densification of the material during pressureless sintering, ~1% MgO + ~8% Y_2O_3 (Martinengo et al (1978), Giachello and Popper (1979) and Hampshire and Pomeroy (1985)). This low concentration of MgO was sufficient to maintain the high densification rate, while the Y_2O_3 resulted in the transformation of the α-Si_3N_4 to ß-Si_3N_4. When higher MgO concentrations were used, the α-ß transformation was inhibited. Devitrification of the glassy grain boundary phase is possible and after devitrification the oxidation resistance improves significantly (Martinengo et al (1978)). The flexural strength does not degrade as dramatically above 900°C as the MgO doped materials, while the room temperature strengths are not significantly different. It was established that the Y_2O_3-MgO additive combination resulted in higher densities and faster sintering times than either MgO or Y_2O_3 additives on their own (Giachello and Popper (1979),Giachello et al (1980)).

The densities of RBSN materials increased and significant grain growth was observed after sintering with Y_2O_3 at higher temperatures, up to 1925°C. On

varying the Y_2O_3 concentration from 4 - 8wt% grain coarsening occurred with little densification when lower Y_2O_3 concentrations were used. At higher temperatures and higher Y_2O_3 concentrations, exaggerated grain growth occurred which resulted in lower room temperature strengths (Mangels and Tennenhouse (1981)). Room temperature properties and microstructures of both MgO and Y_2O_3 doped post sintered RBSN were comparable to those of hot pressed Si_3N_4, with the added advantage of being able to produce complex, near-net shapes (Mangels (1981)).

The Y_2O_3 doped materials, which have not undergone devitrification of the grain boundary phase, undergo oxidation at higher temperatures, but the strength is retained up to 900°C. Above this temperature the decrease in the strength is due to the viscous flow of the glassy grain boundary phase (Govila et al (1985)).

Employing pressure during sintering, such as HIP or hot pressing, requires less Y_2O_3 addition since the processing pressure increases and lower temperatures can also be used (Yeheskel et al (1984) and Pejryd (1989)). The high temperature strength in these materials can be maintained up to a temperature of 1200°C when less additives are used (Micski and Bergman (1990)).

The presence of SiO_2 (from the surface of Si_3N_4 particles or added in excess) in the Y_2O_3 doped Si_3N_4 system results in the formation of quaternary phases in the grain boundaries. These phases can be crystalline or amorphous glasses. Figure 2.8 shows the phase diagram at 1630°C for the Y-Si-O-N system. A number of crystalline phases which have been identified in the Si_3N_4 products are shown in the diagram, such as $Y_2Si_2O_7$.

The effect of using Al_2O_3 in the Y-Si-O-N system is to improve the densification of the compact and this is facilitated by the reduction of the liquid phase formation temperature, which also reduces the viscosity of the liquid phase (Smith and Quackenbush (1980), Galasso and Veltri (1981)). It has been established, however, that Al_2O_3 hinders the crystallization of the liquid phase which results in the

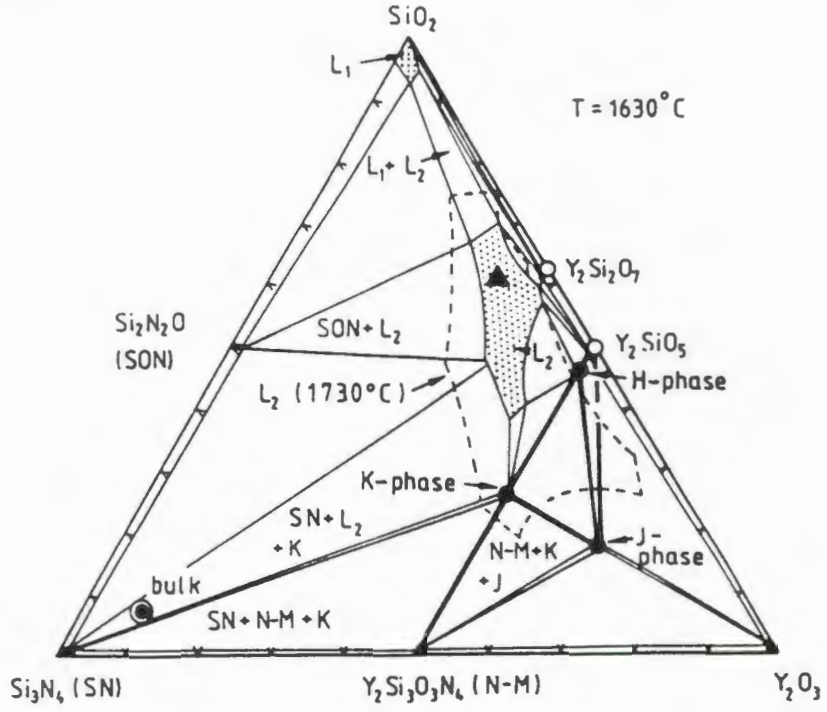

Figure 2.8: Phase Diagram of the Y-Si-O-N system at 1630°C. The dotted line represents the liquid phase at 1700°C (Braue et al (1986)).

degradation of high temperature properties. Braue et al (1986) overcame this problem by adding small quantities of ZrO_2 (~ 1wt%) to the system which then acted as a nucleating agent in the devitrification of the glassy phase during annealing. This improved the strength above 900°C significantly.

Non-oxide additions have also been successfully used with Y_2O_3 in Si_3N_4 sintering. The addition of AlN to the Y_2O_3-Al_2O_3 combination has been found to have a stabilizing effect on the strength at elevated temperatures. The materials retain their strengths up to 1200°C (Komeya et al (1990)). Further addition of a few percent HfO_2 to the above system resulted in a material that increased in strength as the temperature increased, giving its highest strength at 1300°C (Komeya et al (1990), Kameda et al (1990)). The HfO_2 was identified as discrete particles in the material, and did not form part of a glassy phase. A further advantage of the hafnia addition is that it promotes the crystallization of the grain boundary phases and inhibits grain growth.

2.4.2.3 Other Additives

A number of other additives and additive combinations have also been studied. A few will be discussed briefly.

Rare earth oxides other than Y_2O_3, have also been used to sinter Si_3N_4. Because of the high melting temperatures of these oxides, the sintering temperatures necessary to reach high densities are relatively high, above 1700°C, when these oxides are used on their own. Rare earth oxides are often used in conjunction with other oxides such as SiO_2, Al_2O_3 or Y_2O_3 (Mieskowski and Sanders (1985) and Hirosaki et al (1988)). The high temperature strengths of these rare earth oxide doped materials have been found to be superior to those sintered with Al_2O_3 or MgO with Y_2O_3 (Hirosaki et al (1990)). The oxidation resistance of these materials is less than the Y_2O_3 doped Si_3N_4, but they are, however, within an order of magnitude of those materials sintered with Y_2O_3 (Mieskowski and Sanders (1985)).

Y_2O_3-ZrO_2 (TZP) additions in Si_3N_4 can improve the room temperature strength and fracture toughness via a microcracking mechanism due to transformation of the ZrO_2 (Kobayashi and Wada (1981)). Up to 70% of the room temperature strength can be retained to temperatures of up to 1200°C. The oxidation resistance of these materials has been found to be much higher than, for example, the MgO-Si_3N_4 materials (Dutta and Buzek (1984)). A minimum of 6.6wt% of Y_2O_3 in the ZrO_2 was necessary to produce the best oxidation resistance. A lower concentration resulted in the Y_2O_3 migrated out of the ZrO_2 lattice, thus destabilizing the ZrO_2. Above this minimum amount of Y_2O_3, the ZrO_2 was retained in the tetragonal phase (Lange et al (1987)).

For better wear properties, Tanaka and Hidetoshi (1984) added fairly large amounts of TiN (5-45wt%). These composite materials combined the wear resistance and high toughness of the TiN with the hardness, strength and thermal shock resistance of the Si_3N_4.

2.4.3 Addition of Additives

Additives are generally dispersed in the Si_3N_4 powder by combining the individual powders and mixing them by mechanical methods such as ball or attrition milling. These methods, however, do not always result in a homogeneous distribution of the additives, which in turn generates flaws in the microstructure on sintering. These inhomogeneities can also result in the impeding of the formation of ternary phases which are required during sintering or on cooling to recrystallize from the liquid phase.

Chemical routes for the formation and manipulation of submicron oxide powders have been widely used (Roy (1987)), but the non-oxide powder preparation has generally followed the mixed powder route. The decreasing grain size and increasing purity constraints necessary for the production of advanced Si_3N_4 products requires processing techniques which eliminate the uncontrolled external and internal physical and chemical contamination. Colloidal processing techniques provide an improved method for the homogeneous distribution of sintering additives, especially in very small quantities, compared to mechanical mixing techniques. This results in a significant reduction of the amount of additive required for sintering and hence the high temperature properties improve due to less intergranular glassy phase present after sintering (Kulig et al (1989)).

2.5 MECHANICAL PROPERTIES

2.5.1 Hardness

The hardness of Si_3N_4 has been found to be dependent on the process used to produce the material, the composition of the material and the phases present (McColm (1990)).

Greskovich and Gazza (1985) studied the effect of the phase transformation from $\alpha \rightarrow ß$ on hardness of hot pressed Si_3N_4. It was found that as the α-content decreased from 85% to 20%, the hardness decreased from 20.9GPa to 16.4GPa. The value further decreased to below 16GPa after full transformation. The maximum hardness reported for pure fully dense ß-Si_3N_4 is 20GPa (using a 500g load) (Greskovich and Yeh (1983)). α-Si_3N_4 formed by CVD is reported to be 34.4GPa (using 100g load) (McColm(1990)). These two values show that the α-Si_3N_4 is harder than ß-Si_3N_4, even though two different loads were used. McColm (1990) reported that the load dependence for microhardness was negligible at loads higher than 200g. A reduction of $\sim$25% was shown from 100g to 200g, bringing the above value to $\sim$27GPa, which is still higher than that of ß-Si_3N_4.

Paterson (1988) reported deviations in macrohardness values for loads between 1 and 5kg. These deviations differed for different materials manufactured by RBSN methods, and it was suggested that interactions occur with the microstructure on indentation. Above 10kg the hardness was found to be invariant implying that at these loads the interaction with microstructure is essentially independent of local microstructural variations present in Si_3N_4.

A study of the influences of a number of properties in hot pressed and sintered Si_3N_4, and reaction sintered and liquid phase sintered SiAlON found that the hot pressed Si_3N_4 gave the highest microhardness (Mukhopadhyay et al (1990 and 1991)). It was also found that with an increase in density, (grain size)$^{-0.5}$ and Young's Modulus, the hardness increased. There was also a definite decrease in hardness with an increase in open porosity. The strength generally increases with an increase in hardness.

The hardness of RBSN materials increase with density, but the deviations in the values between different materials at similar densities has been attributed to the variations in the

microstructure. As the ß-Si_3N_4 content increased, the hardness was found to decrease in the absence of Si_2ON_2. However, in the presence of Si_2ON_2, the hardness of the material containing 50% ß-Si_3N_4 and > 15% Si_2ON_2 was found to increase to 12.8GPa from a nominal 6 - 7GPa (Paterson (1988)).

2.5.2 Toughness

A number of toughening mechanisms are used in ceramics. Ceramics, however, do not generally exhibit plastic deformation by dislocation movement to any significant extent. The resistance to fracture is provided by the lattice of the material itself. The toughness of ceramics can therefore be improved by modifying the microstructure to such an extent as to reduce the stresses near the crack tips (Wiederhorn (1984)).

This can be accomplished in three basic ways (Wiederhorn (1984), Schubert and Petzow (1988)):

- transformation toughening which occurs in tetragonally stabilized ZrO_2
- whisker and fibre reinforcement
- particle reinforcement

The inclusion reinforcements have one drawback, in that the large inclusions which favourably influence the crack path through the material, and thus improve toughness values, are also the fracture controlling defects. There are also difficulties in the dispersion, densification and stability of the inclusions, particularly whiskers and fibres in the matrix.

Si_3N_4 has the unique advantage in that the ß-Si_3N_4 microstructure consists of elongated grains, which could be described as the in-situ growth of "whiskers" or "fibres". When the grains have cross-sections of $> 1\mu m$ they seemed to positively influence the toughness, while diameters of $< 1\mu m$ negatively influenced the toughness. Two toughening methods have been identified in Si_3N_4, namely, crack deflection and crack branching. The occurrence of these toughening characteristics increases with an increase in the population of grains with diameters larger than $1\mu m$. A maximum toughness of 9.7MPa.$m^{½}$ was obtained by controlled in-situ grain growth (Matsuhiro and Takahashi (1989)).

Since the ß-phase of Si_3N_4 has an elongated structure and α-Si_3N_4 an equiaxed grain structure it would therefore be expected that a relationship would exist between the toughness and the ß-Si_3N_4 phase fraction. This relationship was found to be linear, increasing from $\sim 5MPa.m^{½}$ in an α-Si_3N_4 material to $>6MPa.m^{½}$ in a ß-Si_3N_4 material (Hamasaki et al (1990)). The ß-content played a greater role in influencing the toughness than the various additive concentrations which were used in HIP-Si_3N_4, and the ß-phase content in turn was directly related to the sintering temperature.

The additives used to sinter Si_3N_4 can have a marked effect on the toughness. An additive of particular interest in this respect is ZrO_2. The toughness of Si_3N_4 has been found to improve due to microcracking and transformation (Claussen and John (1978)) and increases (up to $7.6MPa.m^{½}$), with an increase (up to 30 vol%) in ZrO_2 additions (Lange (1987)).

2.5.3 Strength

At temperatures below the softening point of the intergranular, glassy phase, Si_3N_4 materials which are mechanically stressed fail as a result of process-induced microstructural flaws or defects that result from shaping or load application. The fracture strength can be derived from the fracture toughness, K_{Ic}, and the size of the defect, a, resulting in the following relationship (Neil et al (1988))

$$\sigma = \gamma \frac{K_{Ic}}{\sqrt{\pi a}}$$

where γ is a geometric factor characterising the shape and location of the defects. From this equation it follows that the strength, σ, increases either when the fracture toughness increases or when the critical size of the defects are reduced (Heinrich (1980)). The toughness improvement methods have been discussed in the previous section.

As far as the defects are concerned, their absolute size is not the only factor to be considered. The number of defects or more specifically, the defect density plays a critical role in the fracture strength of a material. Therefore the distribution function of defect size and frequency together determine the fracture statistics (Petzow et al (1991)).

The improvement of the fracture strength by reducing the defect size is accomplished by the improvement of the consecutive ceramic processing steps. Many of the coarse microstructural defects found in ceramics result from incorrect processing techniques during the processing of the powder. Mechanical and chemical impurities can be introduced by careless working practices, concentration gradients can be caused by inhomogeneous distribution of additives and local density variations as a result of agglomerates are some examples of these defects. These defects cannot be eliminated by sintering or hot pressing. Other process-related defects originate at later stages of processing and include firstly pressing defects, caused by uneven distribution of pressure in the die, over pressure during pressing or machining defects of the die. The second group of defects are caused by sintering conditions, which influence the grain boundaries, triple points and crystalline phases. These defects are the most frequent, and although the majority of the defects are subcritical, there are exceptions, such as excessive grain growth, which can result in grains of up to 100μm or more. Figure 2.9 shows the frequency distribution of the three major defect categories as a function of their size (Petzow et al (1991)). The improvement methods used during processing can also be supplemented by non-destructive testing methods which result in early elimination of critical defect containing components. This approach is used extensively in commercial production of advanced ceramics (Neil (1988)).

The strength of the materials also depends on the size of the specimen (Davidge 1986). The effect of specimen size on the strength of sintered silicon nitride has been studied for both 3-point and 4-point bend strength methods (Katayama and Hattori (1982)). It was found that as the volume of the specimen increased, the strength deteriorated. Soma et al (1985) confirmed this relationship between specimen volume and strength and also found that it was also valid for tensile specimens.

At temperatures higher than the softening point of the glassy grain boundary phases, permanent inelastic deformation (creep) occurs when specimens are mechanically stressed. The deformation may come about by the sliding of the grain boundaries. The strength is therefore dependent on the temperature and the load time (Weiss (1981)). Additional failure modes of oxidation and stress corrosion are also encountered in Si_3N_4 (Petzow et al (1991)).

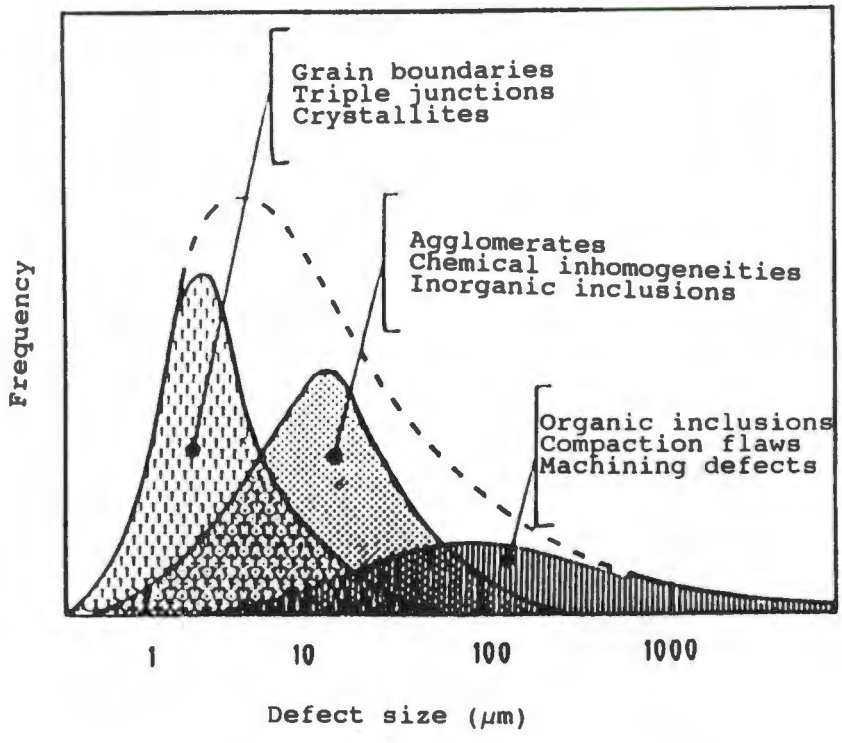

Figure 2.9: Quantitative representation of the defect distributions as a function of the defect size (Petzow et al (1991)).

To improve the creep resistance, and therefore the high temperature strength, the glassy grain boundary phases have to be eliminated. The additives, however, which cause the glassy phases are essential for the sintering process. Besides reducing these phases to a minimum, the glassy phase can further be decreased by crystallization after densification has taken place. This devitrification leads to a stiffening of the structure at high temperatures. The grain boundary sliding and viscous flow can therefore be reduced, resulting in a higher retention of strength above 1000°C and in some systems can even result in an increase in strength as shown in Figure 2.10 (Petzow et al (1991)).

2.5.3.1 RBSN and Sintered RBSN

Since the strength of materials is dependant on the size of the defects or pores present, the strength of RBSN is highly dependant on the density of the nitrided compact. The room temperature strengths of RBSN were found to decrease from 200MPa to 100MPa when the density decreased from 2.6g/cm^3 to 2.2g/cm^3 (Evans and Davidge (1970) and Heinrich (1980)). By optimizing the processing conditions strengths of up to 320MPa were obtained with a material having a density of

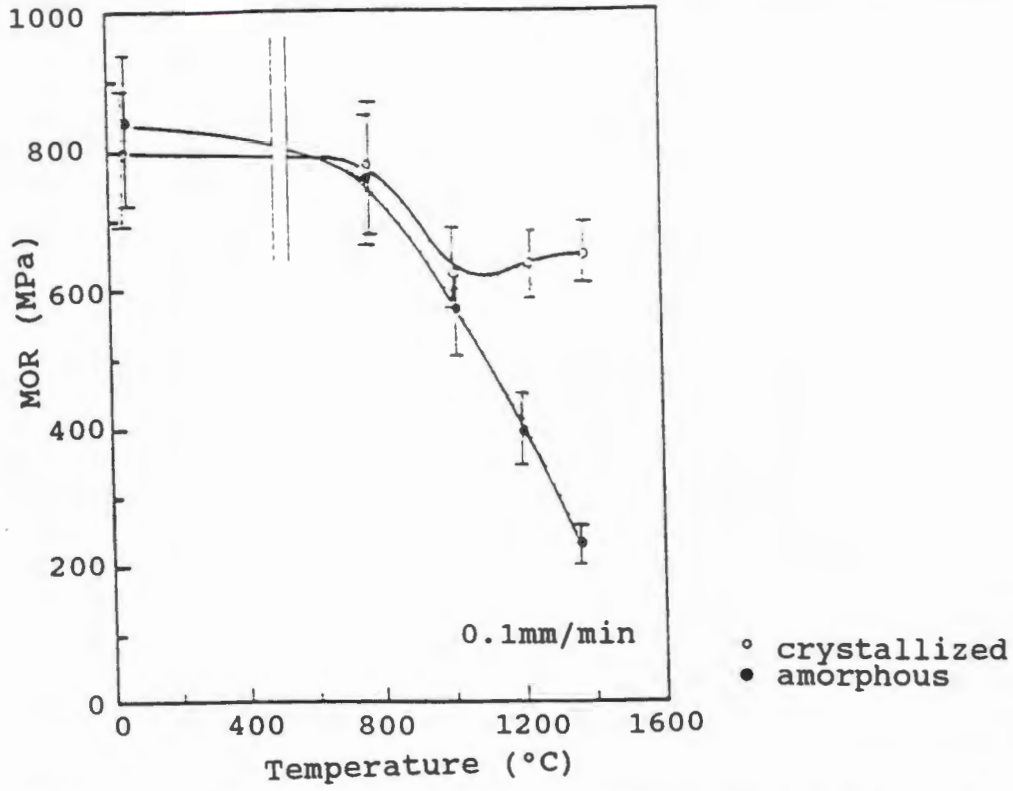

Figure 2.10: High temperature flexural strength of silicon nitride ceramics using Y_2O_3 additive with crystallized and amorphous grain boundary phases (Petzow et al (1991)).

2.5g/cm^3 (Heinrich et al (1982)). At higher temperatures, up to 1200°C, RBSN retains room temperature strength and in some cases even increases in strength (Noakes and Pratt (1970), Mukhopadhyah and Chakraborty (1988)). This phenomenon has been attributed to the limited ability of the material to deform plastically, since additives which encourage the grain boundary sliding are absent. Early studies of RBSN produced materials with a room temperature strength ranging from 150MPa to 230MPa, while the high temperature (1200°C) strengths ranged from 196 to 210MPa (Noakes and Pratt (1970), Evans and Davidge (1970)).

The influence of the phases present after nitriding on strength is difficult to establish, since the processing conditions often alter both the composition, particularly the α/β ratio and the pore size distribution simultaneously, both of which can influence the strength. A number of studies have reported that a high proportion of β-Si_3N_4 is associated with lower strength (Jennings et al (1976), Elias et al (1976)), while others have reported no influence on strength with a variation in the α/β ratio (Mangles and Cassidy (1973)). Heinrich (1980) examined the effect

of α/β ratio change on strength and managed to keep the macropore size constant, while the micropore size increased with an increase in α-content. It was found that the strength decreased with a decrease in α-content.

The starting materials have a significant influence on the properties of the RBSN. When a finer silicon powder is used, the resulting fine grain structure and the smaller pores, result in higher strengths (Messier and Wong (1973), Heinrich (1983)). An increase in strength of up to 50% at a constant density has been reported if the particle size of the original silicon is decreased from a distribution of 37-63 μm to <10 μm (Riley (1989)). Using high purity, laser synthesised, fine silicon powder, values of 75% higher than the average strength have been obtained (Ritter et al (1988)).

The room temperature strength of RBSN can be further improved if additives are present and post-sintering heat treatments are carried out (Giachello and Popper (1979)). The strength of these materials depends on the additive used and the processing conditions. The strength of PSRBSN can double, even treble, the strengths of RBSN and this can be seen in the summary of strengths set out in Table 2.1.

2.5.3.2 Sintered Si_3N_4

The limiting factors regarding strength are the same in sintered Si_3N_4 as for RBSN and post-sintered RBSN, ie, pore/defect size and density. A number of factors influence these features and therefore the strength, such as sintering temperature, rate of heating, additive concentrations and compositions and pressure used during sintering, to name but a few.

It has been found that for slow heating rates, densities are higher compared to those for higher rates and, with this increase in density, the strength also increases. A drawback to slow heating rates is that more grain growth often takes place, due to the extended time spent in the liquid phase range, which results in excessive solid

Table 2.1: Strengths of Si_3N_4 materials produced by various methods.

Material	Room temp strength	Configuration	Reference	Comments
RBSN	100 - 280	3-point	Evans and Davidge (1970)	~70 - 200MPa in 4-point*
RBSN	320	4-point	Heinrich et al (1982)	
RBSN (SiH_4 laser synthesised Si)	531	ball-on-ring	Ritter et al (1988)	~480MPa in 4-point
PSRBSN 0.9% MgO	480	3-point	Giachello and Popper (1979)	~340MPa in 4-point
PSRBSN 8%Y_2O_3	560 - 823	4-point	Govila et al (1985)	
SSN 8%Y_2O_3+1%MgO	585	3-point	Giachello et al (1980)	~410MPa in 4-point
SSN 6%Y_2O_3+2%Al_2O_3	705	4-point	Quackenbush et al (1981)	
SSN 6% Y_2O_3	580	4-point	Quackenbush et al (1981)	
SSN 5%Y_2O_3+3%Al_2O_3	750	3-point	Goto et al (1990)	Hot pressed ~525MPa in 4-point
SSN Y_2O_3+Al_2O_3	1360	3-point	Komeda et al (1990)	Hot Pressed ~952MPa in 4-point

* - 4-point bend test is taken as 30% less than the 3-point bend.

state sintering of which grain growth is a characteristic (Campbell and Dutta (1982)). This can lead to a decrease in the strength values. If grain growth can be controlled (less additive) subsequent heat treatments to crystallize as much of the grain boundary phase as possible can improve the densities and strengths (particularly at high temperature) (Braue et al (1986)).

The composition of the additive used during sintering has a marked effect on the final density of the material, and therefore on the strength of the materials, both at room temperature and high temperature. This can be seen both from Tables 2.1 and 2.2 and Figure 2.11. Table 2.2 shows recent results obtained using alternative additives in sintered Si_3N_4 (Chang-Chun et al (1988) and Kobayashi and Wada (1988)).

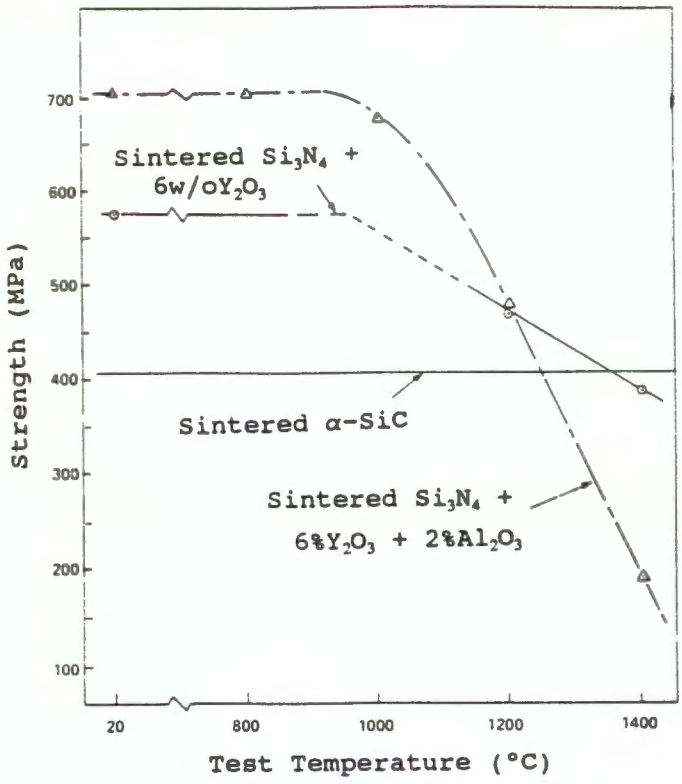

Figure 2.11: 4-point bend strengths of 2 Si_3N_4 materials (Quackenbush et al (1981)).

Table 2.2: Strengths of various sintered Si_3N_4 materials produced with different additives.

Additive	Strength	Configuration	Reference	Comments
AlN	609	3-pt	Chang-Chun et al (1988)	~426MPa in 4-point*
ZrN	917	3-pt		~640MPa in 4-point
AlN+ZrN	686	3-pt		~480MPa in 4-point
MgO.Al_2O_3	544	3-pt		~380MPa in 4-point
MgO	667	3-pt		~467MPa in 4-point
Y_2O_3-ZrO_2(Y_2O_3)	800	3-pt	Kobayashi and Wada (1988)	~560MPa in 4-point
Y_2O_3-ZrO_2(MgO)	1100	3-pt		~770MPa in 4-point

* - 4-point bend test is taken as 30% less than the 3-point bend.

The influence of sintering temperature on strength is shown in Figure 2.12, where the strength of four Si_3N_4 materials, sintered at various temperatures is shown. There is no definite trend in the results and the effect of sintering temperature is highly dependent on the additive used.

If pressure is exerted during sintering, be it by hot pressing, hot isostatic pressing or gas pressure sintering, it does generally improve mechanical properties such as strength significantly compared to pressureless sintering, as can be seen in Table 2.1, but these processes require capital intensive equipment which results in high cost of the final materials produced.

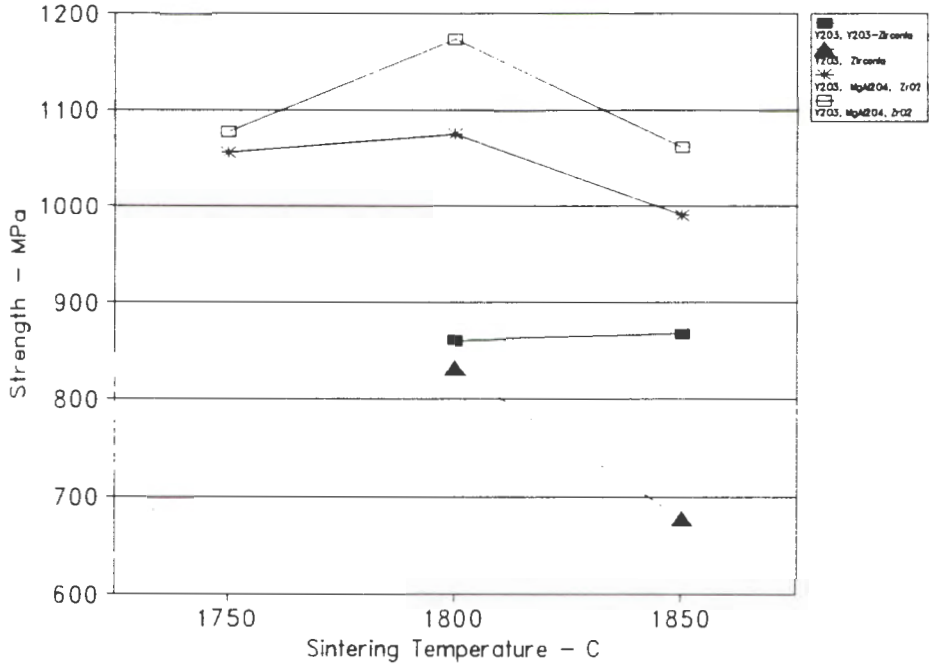

Figure 2.12: Variation of strength with sintering temperature (Kobayashi and Wada (1988)).

2.6 MICROSTRUCTURE

The various processing methods and conditions of both Si_3N_4 powder and the sintered product influence the final microstructure of the Si_3N_4 material. Factors which have been the subjects of numerous studies are:

- starting powders, both silicon and silicon nitride (Kleebe and Ziegler (1986), Jennings et al (1988)).
- sintering temperature and heating rates (Mangels (1981), Mangels and Tennenhouse (1981), Jennings et al (1988(b)).
- gas purity or gas mixtures used and pressure of gas during processing (Mangels (1981)).
- additives used to facilitate sintering (Mangels and Tennenhouse (1981), Hampshire and Pomeroy (1985)).

The two polymorphs of Si_3N_4 have distinct microstructural characteristics. The α-Si_3N_4 can produce two distinct microconstituents, the α-phase needles and the α-phase matte, while the ß-Si_3N_4 usually also form needles. Each of these morphologies result from different formation sequences which are influenced by the reaction conditions, but most processing conditions lead to more than one of the above morphologies being present (Jennings and Richman (1976)).

2.6.1 Reaction Bonded Si_3N_4

The dominant form of silicon nitride present in RBSN is α-Si_3N_4, since reaction temperatures are usually below the transformation temperature. The α-needles are very common, and occur in most RBSN materials, but they are particularly numerous in materials produced from less pure silicon powder when the reaction temperature is between 1350 and 1400°C. These needles have a high aspect ratio (length to width) of around 25 (Jennings et al (1976(b))). These needles have often been found to have globular features at one of the ends. These globular features have been found to be rich in iron (Russel et al (1985)).

The α-matte is the other α-phase morphology in RBSN and is a fine grained structure that is favoured by fine, pure silicon starting powder, slow heating rates, and reaction

temperatures below 1400°C with no gas flow (Jennings et al (1976(b))). The α-morphology is usually the predominant phase present and the grains are essentially submicron, 0.5 - 1 μm.

The ß-phase formation in RBSN is favoured by the use of less pure, coarser silicon powder, which is heated rapidly in a flowing nitrogen atmosphere to high temperatures above 1450°C, and it therefore forms predominantly out of liquid silicon (Jennings et al (1976(b))and Riley (1977)). It has also been reported that ß-Si_3N_4 forms preferentially when silicon reacts with active or atomic nitrogen, while α-Si_3N_4 forms when N_2 is present in the molecular form (Jennings et al (1988(b)).

A relationship between the α/ß ratio and the pore size was reported by Danforth et al (1979). As the α-content increased, the largest pore size in the product decreased, and for a constant α/ß ratio, the largest pore size was dependant on the original particle size of the silicon powder, the coarse powder producing the larger pores. Another factor influencing the pore structure of the RBSN is the purity of the starting powder. When high levels of metallic impurities are present, larger pores are present after nitriding compared to high purity powder materials (Kleebe and Ziegler (1988)).

The effect of the gas composition on the final microstructure of the RBSN is also significant. When no change occurs in the composition of the gas during the reaction process, a wide distribution of pores is observed with pores of up to 30 μm in diameter. When these gas compositions are varied, ie increasing H_2 or He content as the reaction takes place to a final composition of ~25% H_2 or ~50% He, the structures are more uniform and the pore size is reduced to less than 20 μm. This in turn improves the mechanical properties of the material. When argon is introduced to the N_2 gas, the pores are larger and there is evidence of unreacted silicon (Mangels (1981(a))).

RBSN generally consist of a high α-content (75-85%) with the balance being ß-Si_3N_4 and intergranular phase, if additives have been used. RBSN has been reported to be predominantly submicron α-Si_3N_4, with some larger ß-Si_3N_4 grains, 1-5 μm (Mangels and

Tennenhouse (1980)). Using a rate-controlled, self regulating sintering technique the microstructural uniformity and pore size and distribution can be further improved (Mangles (1981(a))).

When additives are introduced to the RBSN and further heat treatments are carried out, the predominantly α-Si_3N_4 material undergoes transformation and densification takes place. This results in major changes in the microstructure. These resulting microstructures depend on the temperature used during sintering and the amount and composition of the additives used, however, in all cases the post-sintered RBSN materials have shown that apart from transformation from α to ß-Si_3N_4, the grains grew to greater than the original submicron size after sintering.

Using MgO as a sintering aid at low concentrations of approximately 3wt% has resulted in microstructures similar to those obtained for hot pressed Si_3N_4 with the same additives, namely elongated ß-Si_3N_4 grains of up to 5 μm in length (Mangels and Tennenhouse (1980), Mangels (1981(b))).

Y_2O_3 additions require higher temperatures than MgO for sintering to take place. The ß-Si_3N_4 grains can vary in size and shape but they are generally needle-like between 0.5 and 5 μm in length with larger grains being found around pores (Mangels (1981(b)), Bradley and Karasek (1987)). At higher temperatures, above 1850°C, exaggerated grain growth can take place and needle-like grains of 15-20 μm, having definite hexagonal shape have been observed. At lower Y_2O_3 concentrations less densification occurs due to less liquid phase being available to facilitate the densification, and the sintering results in lower density, but larger grained material (Mangels and Tennenhouse (1981(b))). The addition of Al_2O_3 to the Y_2O_3 improves the density and results in an intergranular phase which develops at lower temperature.

2.6.2 Sintered Si_3N_4

The microstructures which develop in pressureless sintered Si_3N_4, when Si_3N_4 powders are used in conjunction with additives as the starting material, are ultimately determined by the

phases present in the starting powder, particularly the polymorph of Si_3N_4 which forms the major phase.

It has been found that when an α-Si_3N_4 starting powder is used, the resulting microstructure after sintering has fibrous needle-like ß-grains, while a higher ß-content in the starting powder results in equiaxed grains being formed (Lange (1980)). The fibrous structure produced from high α-content starting powders have been found to be advantageous for higher toughness properties.

As with the sintering of RBSN materials, the various sintering additives have an influence on the resulting microstructure, often with very similar results, for example MgO enhances densification, while Y_2O_3 enhances transformation from α to ß (Hampshire (1984)).

The effect of the MgO content in the presence of Y_2O_3 has been studied extensively. It can be concluded that the small amounts of MgO, not only assists densification, but also enhances the elongated growth of the resulting ß-Si_3N_4 grains, resulting in higher aspect ratios. It is proposed that the aspect ratio of the grains does not only depend on the amount of liquid phase present, but also on the viscosity of the liquid phase (Hampshire (1984)). This was confirmed when studies of Y_2O_3-MgO doped Si_3N_4 showed that as the viscosity of the liquid phase increased and volume decreased, the growth of the ß-Si_3N_4 grains occurred mainly along the crystallographic c-axis to reduce the surface energy to volume ratio (Hampshire and Pomeroy (1985)). In low viscosity liquids, the grains are able to grow in all directions. Similar observations have been made in systems using Y_2O_3-Al_2O_3 sintering aids (Wötting and Ziegler (1984)).

When using Y_2O_3-Al_2O_3 additives, a wide range of microstructures have been observed, ranging from fairly equiaxed fine (<2 μm) grains to larger (>2 μm) occasionally elongated grains, depending on the amount of additives and their respective ratios, and the processing conditions (Tajima et al (1988)). After sintering the additives are found in thin layers between the grains (grain boundaries) and in pockets where more than two grains come together (Bonnel (1989)).

In order to improve the mechanical properties of the Si_3N_4 materials (pressureless sintered or post sintered RBSN) the low melting point glassy grain boundary phases have to be minimized. This is often achieved by subsequent heat treatments after the sintering process during which the grain boundary phases are recrystallized (Tsuge et al (1975), Komeya et al (1990)).

Yttria has little or no solubility in Si_3N_4 and therefore most of the Y_2O_3 used as additive is found in the grain boundary phases, be they crystalline or glassy (Bradley and Karasek(1987)). The grain boundaries in both sintered Si_3N_4 and post sintered RBSN have been generally found to be associated with Y-Si-O-N and Y-Si-O phases which can vary in composition according to the factors mentioned at the beginning of this section (Bradley and Karasek(1987), Lee and Hilmas (1989)). If other additives are used in conjunction with the Y_2O_3, such as Al_2O_3, the Al can also be present in these silicates. Al is not, however, usually found in the crystalline grain boundary areas, but in the remaining amorphous phases and in solid solution with Si_3N_4 (Cinibulk et al (1990)).

3. Experimental Procedures

3.1 MATERIAL PROCESSING

3.1.1 Reaction Bonded Silicon Nitride

An outline of the steps used in the production of reaction bonded silicon nitride (RBSN) materials during this study is shown in Figure 3.1.

3.1.1.1 Powder Processing

The CU600 grade silicon used for the production of reaction bonded Si_3N_4 was obtained locally from Elkem. The silicon was milled down to a mean particle size (d_{50}) of ~ 10 μm by crushing and ball milling. It was then milled further in an attrition mill for 2½ hours together with additives (Y_2O_3 and Al_2O_3), ZrO_2 milling media and iso-propanol. Iso-propanol was used to prevent the oxidation of the silicon. After attrition milling a particle size distribution analysis was carried out and it was found to have reduced the d_{50} to 3 μm. 4wt% polyethylene glycol binder was added to the slurry at the end of the milling cycle, and mixed in thoroughly. After milling the powder was oven dried at 75°C overnight and then sieved through a 125 μm sieve. The composition of the powder used is shown in Table 3.1. Assuming full conversion of the silicon to Si_3N_4, the Y_2O_3 and Al_2O_3 contents in the final product would be 8wt% and 2wt% respectively, resulting in a total of 10wt% additive.

Table 3.1: Composition of Powders used for RBSN materials

Composition - wt%			ZrO_2 Milling Media	Iso-propanol	Polyethylene glycol
Si	Y_2O_3	Al_2O_3			
86	11	3	660g/100g powder	83ml/100g powder	4wt%

3.1.1.2 Formation Methods

Samples were produced from the powders by uniaxial pressing in dies to form small 10mm diameter discs or 50mmx8mm bars of ~6mm thick for further evaluation. The pressure used during uniaxial pressing of RBSN was 5MPa on both these forms. The samples were then vacuum sealed in plastic bags and cold isostatically pressed (CIPped). The pressure was varied during the CIPping process in order to determine

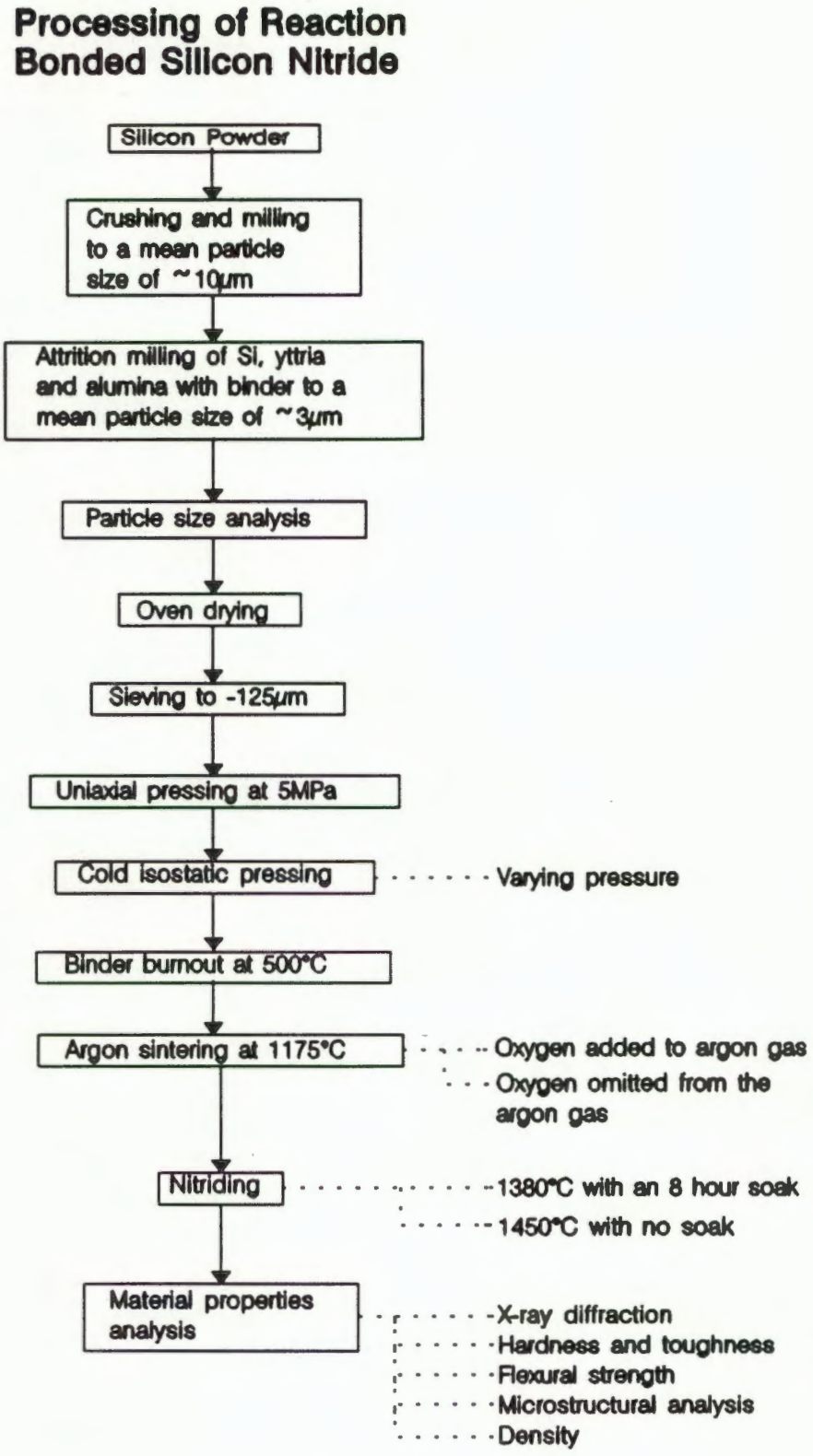

Figure 3.1: A flow diagram showing the process steps used in the formation of reaction bonded silicon nitride.

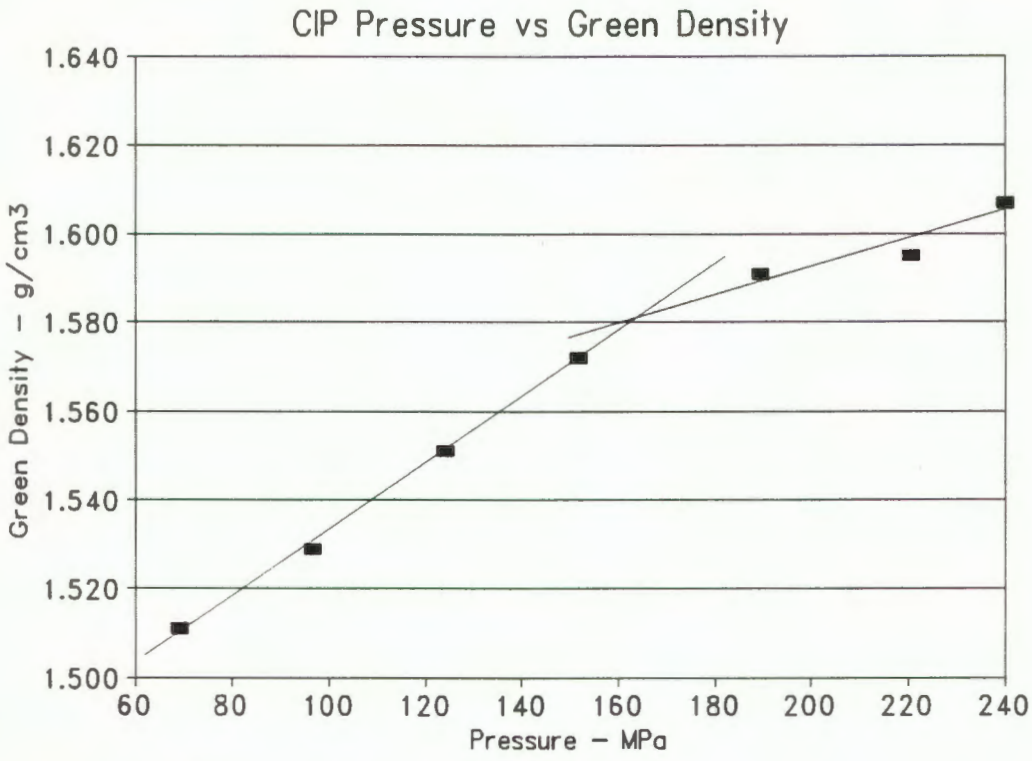

Figure 3.2: CIPping trials for Silicon powder compacts.

the optimum pressure required. The results from this trial is shown in Figure 3.2. A point of inflection is obtained when plotting the green density vs the CIP pressure. At lower pressures the powder is compressed resulting in the filling up of large pores. As the pressure increases the number contact points between powder particles increases. This results in the inhibiting of further compaction without the fracturing of the particles. At higher pressures the particles do start to fracture and a further increase in green density is achieved with an increase in pressure, but this increase is not as significant as that achieved at lower pressures. The point of inflection is an indication of a change between these two mechanisms. The optimum pressure for compaction is taken at or just below this point, that is before any major fracturing of the powder particles occurs, thus maintaining the partially spherical shape of the particles. In this study this pressure was just above 160MPa. All further CIPping was done at 160MPa for the Si powders, since a further increase in pressure did not increase the green density significantly.

3.1.1.3 Heat Treatments

The polyethylene glycol was removed from the Si compacts prior to the reaction bonding of Si and N_2. The binder removal was carried out at 500°C in air for 1 hour. A vacuum or inert gas would have resulted in residual carbon being present in the compact, and this would then react with the silicon to form SiC. No oxidation of the Si was observed and the mass loss ranged between 3.1 and 3.6%.

The following argon sintering heating schedule was used:

Room Temperature - 1175°C	235°Ch^{-1}
1175°C soak	5 hours
1175 - Room Temperature	250°Ch^{-1}

During one of the argon sintering cycles oxygen was introduced and the results were compared with materials where this was not done.

The argon sintered silicon compacts from both the pure argon sintering and the argon-oxygen sintering cycles were nitrided. The nitriding schedules had very slow heating rates in the reaction regions due to the exothermic nature of the reaction. The following schedules (with the heating rate being slowed down twice before reaching the final maximum temperature) were effective in reaction bonding Si and N_2:

1	Room Temp - 950°C	240°Ch^{-1}
	950 - 1350°C	20°Ch^{-1}
	1350 - 1450°C	5°Ch^{-1}
	1450°C - Room Temp	240°Ch^{-1}
2	Room Temp - 950°C	240°Ch^{-1}
	950 - 1350°C	20°Ch^{-1}
	1350 - 1380°C	5°Ch^{-1}
	1380°C soak	8 h
	1380°C - Room Temp	Furnace cool

The 2 step heating schedule is described by Riley (1977). The nitriding was carried out in a furnace that was constructed at the Division of Materials Science and Technology, CSIR, Pretoria.

3.1.2 Post Sintered Reaction Bonded Si_3N_4

An overview of the post sintered reaction bonded Si_3N_4 process is shown in Figure 3.3. The powder processing, formation methods, argon sintering and nitriding cycles were the same as for the reaction bonded silicon nitride. Therefore the effect of the presence of oxygen during argon sintering, and the effect of nitriding temperature on the final post-sintered product were studied.

3.1.2.1 Heat Treatments

The nitrided products were post sintered in a Centorr furnace using three cycles shown below with either pure argon or pure nitrogen atmospheres.

1. Argon atmosphere

Room temperature - 1800°C	350°Ch^{-1}
1800°C soak	1 h
1800°C - Room Temperature	350°Ch^{-1}

2. Nitrogen Atmosphere

Room temperature - 1750°C	350°Ch^{-1}
1750°C soak	1 h
1750°C - Room Temperature	350°Ch^{-1}

3. Nitrogen Atmosphere

Room temperature - 1800°C	350°Ch^{-1}
1800°C soak	1 h
1800°C - Room Temperature	350°Ch^{-1}

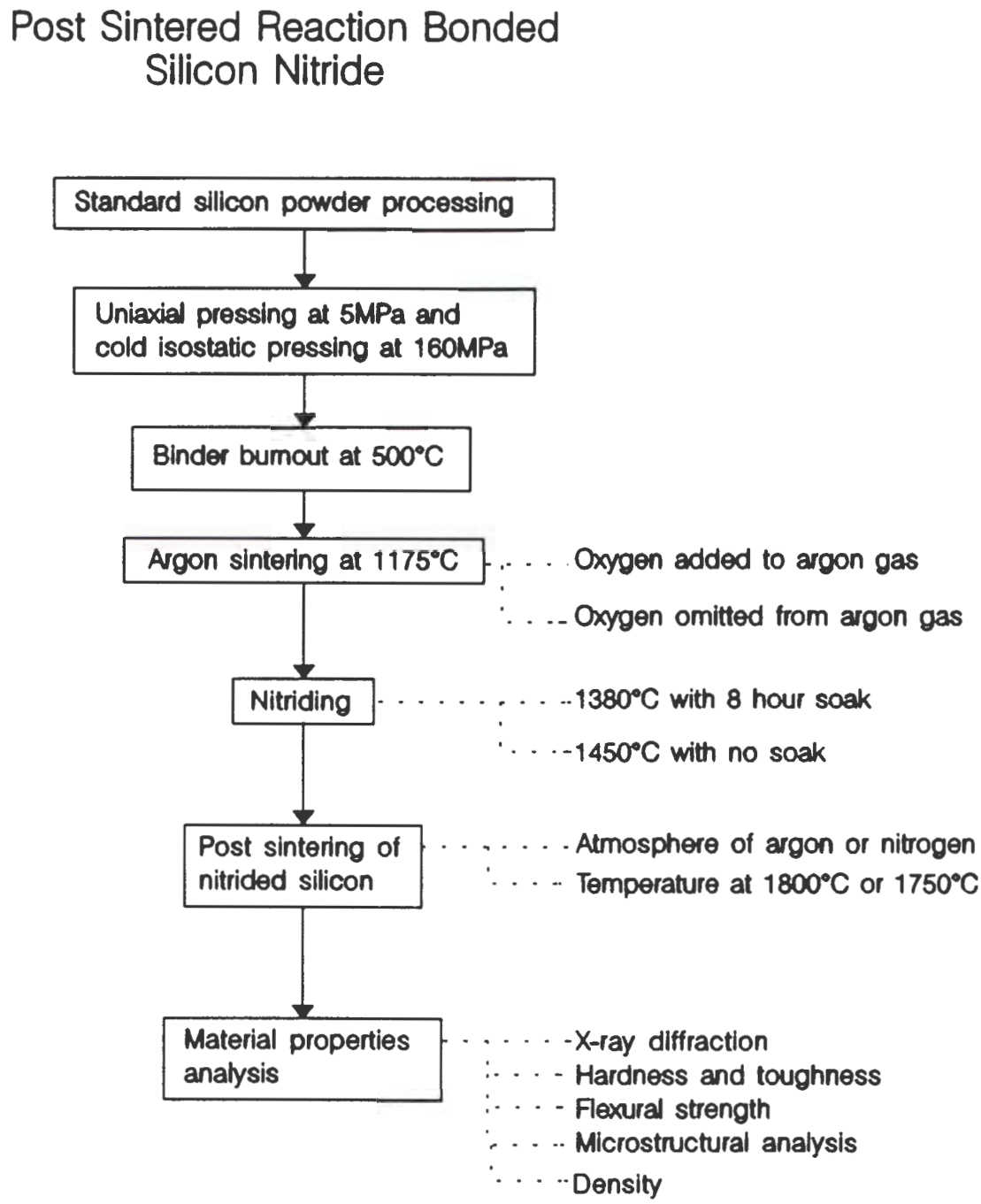

Figure 3.3: Flow diagram of the processing of post sintered reaction bonded silicon nitride.

3.1.3 Sintered Silicon Nitride

The processing routes used for sintered silicon nitride are shown in Figure 3.4.

3.1.3.1 Powder Processing

The grade E10 Si_3N_4 powder obtained from UBE, Japan, was synthesised via the diimide precipitation method from $SiCl_4$ and NH_6. The mean particle size of this powder was $\sim 1\ \mu m$. The effect of milling on the powder and the final materials were studied. A batch of powder was made up and attrition milled for 5 hours using Si_3N_4 milling media. Si_3N_4 milling media was used to prevent contamination of the powder by the ZrO_2 media (Barnett and Nel(1989)). Samples were taken every ½ hour for particle size analysis. It was found that after 1½ hours there was no significant reduction in particle size. A further two batches of powder, having the same composition were produced. The first powder batch was attrition milled for 1½ hours in iso-propanol. A second powder batch was mixed dry on a ball mill for 6 hours with no milling media.

The composition of the powder used is given in Table 3.2. The amount of additive is higher than in the RBSN materials (assuming full conversion of Si to Si_3N_4). After milling the powder slurries were dried, either in a conventional oven at 75°C overnight or in a domestic microwave oven, and sieved through a 125 μm sieve. The latter method was found to be much quicker than the conventional oven drying and no detrimental effects were observed on the powder or the final ceramic components. The powder did not seem to cake into as hard a mass when compared with conventional drying. No binder was used to process the silicon nitride powders.

Table 3.2: Composition of Powders used for Sintered Si_3N_4 materials

Composition - wt%			Si_3N_4 Milling Media	Iso-propanol	Polyethylene glycol
Si_3N_4	Y_2O_3	Al_2O_3			
87	10	3	160g/100g powder	150ml/100g powder	-

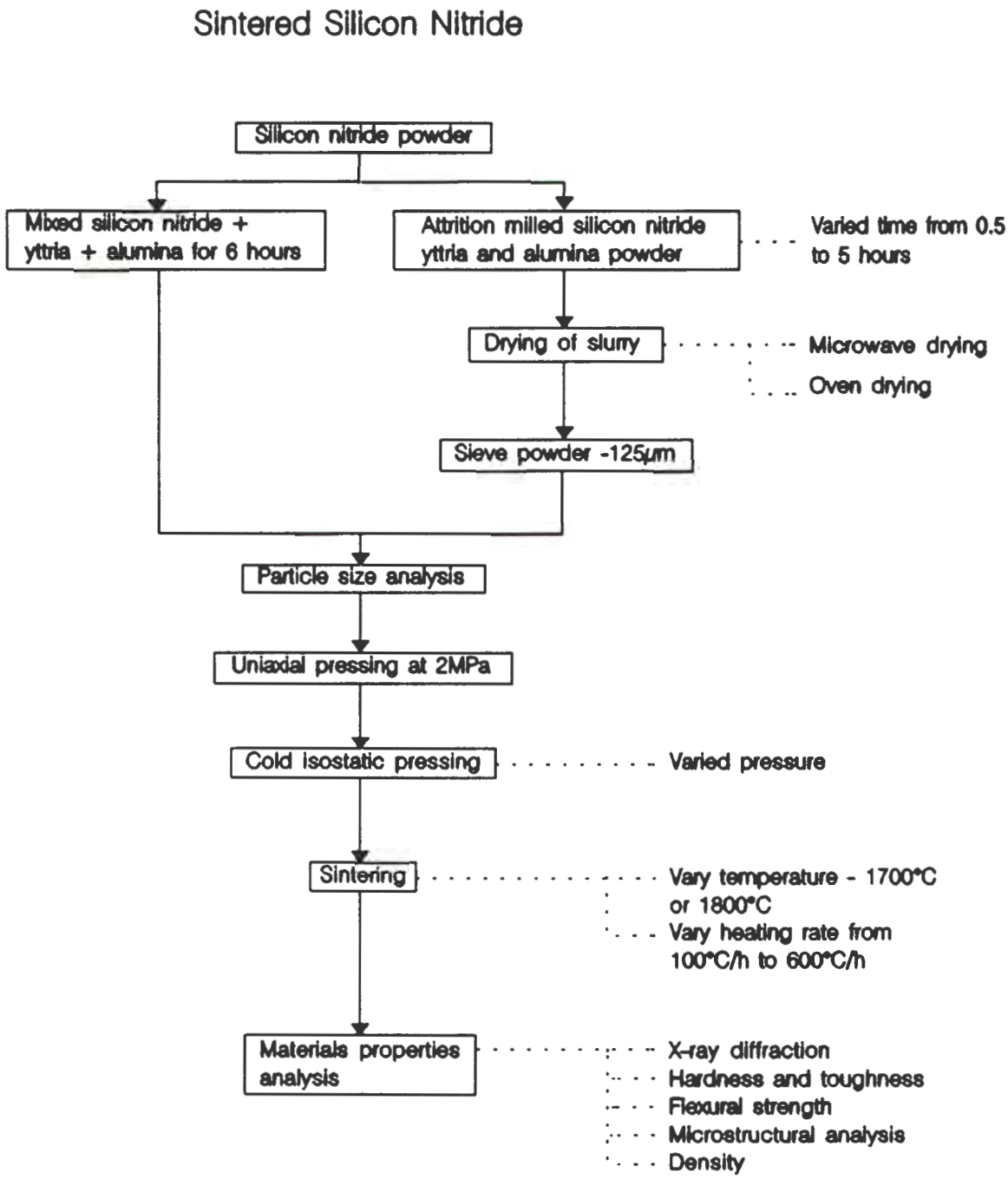

Figure 3.4: A flow diagram of showing the processing of sintered silicon nitride materials.

3.1.3.2 Formation Methods

The samples were also uniaxially pressed into 10mm discs, and 50mmx8mm bars of ~6mm thick. The Si_3N_4 discs and bars were pressed at 2MPa, lower than the silicon equivalents. This was necessary since higher pressures resulted in lamination of the compacts. A series of cold isostatic pressures were used, and it was found that the optimum pressure was just above 150MPa. All further Si_3N_4 compacts were pressed at 150MPa.

3.1.3.3 Heat Treatments

No binder was used during pressing and therefore the Si_3N_4 compacts were sintered directly. The compacts were sintered in a Centorr furnace at temperatures of 1700°C and 1800°C. The heating rate was varied between 100°Ch^{-1} and 600°Ch^{-1} from 1200°C to the maximum temperature in order to investigate the effect of heating rate on the final ceramic. From the phase diagrams it was estimated that this temperature was near the liquid phase formation temperature. Details of these sintering schedules are shown below:

	Heating/Cooling Rates - °Ch^{-1}		
	Schedule 1	Schedule 2	Schedule 3
Room Temperature - 1200°C	300	300	
1200°C - 1700°C	100	300	
1700°C soak	1hr	1hr	
1700°C - Room Temperature	300	300	
Room Temperature - 1200°C	300	300	300
1200°C - 1800°C	100	300	600
1800°C soak	1hr	1hr	1hr
1800°C - Room Temperature	300	300	300

3.2 ANALYSIS OF MATERIALS

3.2.1 Phase Analysis

Phase identification was obtained by x-ray diffraction. A Rigaku powder diffractometer with a Cu K_α radiation source with a monochromator was used. Because the Si_3N_4 is very hard, it is extremely difficult to grind down in order to obtain a powder diffraction pattern. A special sample holder was used to analyze the as-sintered and ground surfaces of the specimens. One disadvantage, when using this holder, was that the sample was not rotated and this led to poor counting statistics and the possibility of errors due to preferred orientation. Therefore, only semi-quantitative analyses can be made.

The semi-quantitative analysis of the Si_3N_4 phases was determined according to the method used by Gazzara and Messier (1977) who determined the ß:α ratio by using the (210) peak intensities in both α-Si_3N_4 and ß-Si_3N_4 as follows:

$$\beta:\alpha = \frac{I_\beta(210)}{I_\beta(210) + I_\alpha(210)}$$

3.2.2 Mechanical Properties

3.2.2.1 Hardness

A number of testing methods are available to determine the hardness of ceramics. Each technique measures the hardness in relation to the load applied by measuring either the contact area of the indentor, the projected area or the depth of penetration. Various shapes of indentors are also used, such as ball, cone or pyramid shapes.

Due to the high hardness values obtained for the Si_3N_4 ceramics, the Vickers hardness was determined. The indentor used has a pyramidal shape with an apex of 136°. The contact area is then used to determine the Vickers hardness:

$$H_v = \frac{P}{contact\ area} = 0.322\frac{P}{a^2 Sin136°} = 0.464\frac{P}{d^2}$$

where P is the load in Newtons, d the mean diagonal length of the indentation in meters and the hardness is given in GPa.

The load used was 15.625kg, and the indentation was measured on an optical microscope. A minimum of 5 random indentations were made on each sample. Prior to indentation the samples were mounted in resin and polished with a final polish using 1 μm diamond paste.

3.2.2.2 Strength

Flexural strength tests were used to evaluate the strength of the Si_3N_4 produced during this study. The rectangular beam configuration of the sample has a simple shape and it is relatively easy to apply the load.

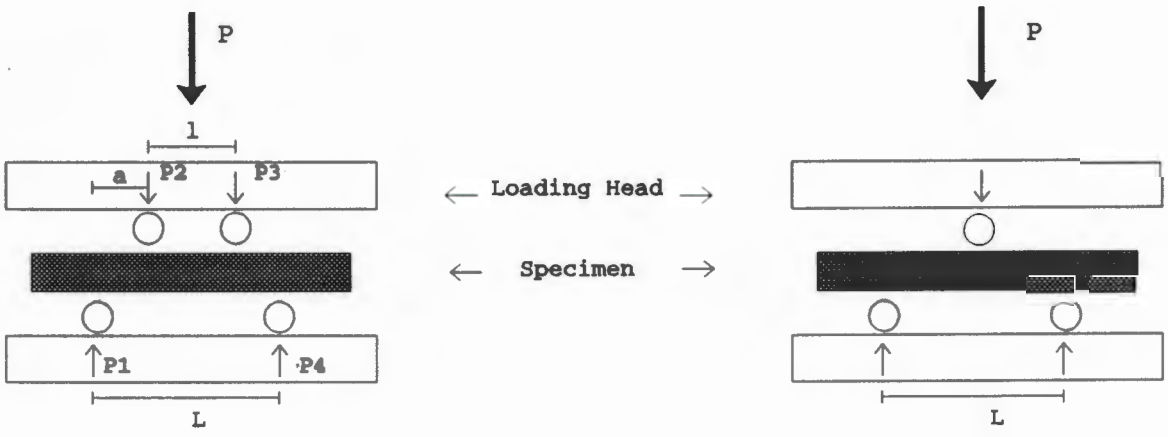

Figure 3.5: Loading configurations for the 4- and 3-point beam systems.

There are two basic configurations to the flexural testing, namely the 3-point beam system and the 4-point beam system. These are shown graphically in Figure 3.2 (Baratta (1984)).

The 3-point loading system is often used when investigating new materials or process developments, since smaller specimens are necessary, and fracture origins can easily be pin-pointed. The 4-point loading system, however, assures a simple uniaxial stress

state, compared to the complex biaxial stress state in the 3-point configuration (Baratta (1982)).

The ASTM C778-82 method of 4-point bend testing uses the following formula to determine the flexural strength, σ:

$$\sigma = \frac{3Pa}{bd^2}$$

where P is the load in newtons, b the width of the sample, d the height of the sample, and a the distance between adjacent loading and support edges as shown in Figure 3.2. When the upper and lower spans are kept to a constant ratio of l/L = ½, then the substitution for a in the above formula gives:

$$\sigma = \frac{3}{2}\frac{Pl}{bd^2}$$

This configuration is also known as the ¼-4-point loading system (Baratta (1984)). When comparing the values of 3-point and 4-point bend strengths of the same material, it has been found that the 4-point bend values are 25 to 40% lower than those determined by the 3-point configuration.

The strength of the materials produced during this study were determined by 4-point bend method on a 100kN electromechanical testing rig. The tests were carried out using a 5kN load cell and a cross-head speed of 0.1mm/min. The outer span on the rig was 25mm and the inner span 12.5mm, and therefore the formula for the ¼ 4-point bend configuration can be used. A minimum of 5 test pieces were used for each test.

3.2.2.3 Toughness

Numerous methods for the determination of toughness values are available (Lewis (1990)). In this study, a simple comparison was needed to determine the resistance

to fracture, and therefore the Vickers indentation crack method was chosen. This can be determined simultaneously with the hardness. An added advantage is that there are no restrictions on the size of the specimen used for the test.

This method of toughness determination has been studied by numerous researchers, and a number of empirical equations are used by various workers. The following equation determined by Anstis et al (1981) was selected:

$$\text{Anstis et al} \quad K_{Ic} = 0.023\ E^{0.5}\ P^{0.5}\ a^{-0.5}\ (c/a)^{-1.5}$$

The same indentations were used for both the fracture toughness and hardness determinations, and a load of 15.625kg was used. A minimum of 5 indentations were made per test piece. The crack lengths were measured together with the hardness indentations on a metallurgical optical microscope. An average Young's Modulus of 210GPa was used for RBSN and 260GPa for sintered Si_3N_4. The equation used by Anstis et al (1981) has been recommended by Paterson and Stevens (1986) and appears to give the most conservative fracture toughness values compared to other proposed equations.

3.2.3 Microstructural Analysis

Optical microscopy was carried out on a reflecting metallurgical microscope. The samples studied were polished with a final polish using 1 μm diamond paste. The magnification was calibrated using a 1mm graticule with 10 μm divisions.

SEM studies were carried out on fracture surfaces, polished surfaces and etched surfaces. The samples were usually coated with gold which was found to produce better images. This coating is necessary to prevent the insulating ceramic surface from charging while under investigation. For analytical work, the samples were carbon sputter coated, since this coating cannot be detected by an EDS system fitted with a beryllium window.

For good resolution at higher magnifications a working distance of between 10 and 15mm was used. An accelerating voltage of 25kV was also found to be necessary for good resolution images. An ISO-SX30-E SEM was used which was fitted with an Link EDS system with a beryllium window.

Transmission electron microscopy studies were undertaken to examine the microstructures of the sintered Si_3N_4 in more detail. Studies were undertaken on a Phillips 420 analytical TEM/STEM. The samples were prepared from 120 μm thick slices from which 3mm diameter discs were ultrasonically cut. The discs were dimple ground and polished to a thickness of $\sim 10\mu$m in the centre of the sample. In the final stage of preparation, argon ion beam thinning of the sample was carried out until a small hole had been made through the specimen providing a reasonable area of thin section. The samples were then carbon coated to prevent charging of the sample under examination.

3.2.4 Etching of Silicon Nitride

Polished surfaces of Si_3N_4 were etched using molten KOH at a temperature of $\sim 350°C$. The samples were etched for 10 to 15 minutes after which they were thoroughly washed in distilled water before being examined in the SEM.

4. Results

4.1 INTRODUCTION

The results presented in this chapter emphasise the two processing routes, namely the production of reaction bonded silicon nitride (RBSN) and post sintered RBSN from silicon powder, and the production of sintered silicon nitride from Si_3N_4 powder. The effects of processing techniques and parameters will be presented first with the resulting physical properties and phase analyses. The mechanical properties and microstructures will then be discussed.

4.2 REACTION BONDED SILICON NITRIDE

The attrition milling of the silicon powder reduced the mean particle size from $\sim 10\ \mu m$ to $\sim 3\ \mu m$. All particles were below 10 μm after milling compared to $\sim 50\ \mu m$ prior to milling.

4.2.1 Argon Sintering

4.2.1.1 Effect of Oxygen during Argon Sintering

The presence of oxygen in the reaction chamber during the argon sintering stage resulted in a 1 to 5% mass increase after this initial step, associated with the partial oxidation of the Si. It was also observed that the densities increased by 5-10% and the volume decreased by 2-6%.

During the subsequent cycles the introduction of O_2 into the reaction chamber during the argon sintering stage was omitted. It was found that the silicon compacts increased in density by almost 2% after argon sintering (conventional in Table 4.1). This was accompanied by a decrease in volume ($\sim 3\%$) and a decrease in mass of $\sim 1\%$.

Further experiments were performed on the silicon compacts using a closed crucible and a static argon atmosphere rather than a flowing atmosphere. This reduced the mass loss after argon sintering to less than 1%, Table 4.1 - (closed conventional).

4.2.2 Nitriding

The samples which were exposed to the oxygen-argon sintering were nitrided at a maximum temperature of 1380°C which was held for 8 hours (Si_2ON_2-rich material in Table 4.1). The mass increase due to nitriding ranged between 56 to 58% which is lower than the expected value of 60% for nitridation. This could be due to the oxidation of the silicon prior to nitridation, which resulted in the formation of Si_2ON_2 and $Y_2Si_2O_7$. The latter only has 23% mass increase from initial unreacted materials. Details of this nitriding cycle compared to subsequent ones where pure argon was used during argon sintered are given in Table 4.1.

Table 4.1: Summary of Nitriding details of RBSN

Iden-tity	Green Density	Ar Sinter. Density	Change in Density-%	Change in Mass-%	Nitrided Density	Change in Mass-%	% Nitri-dation
A	1.48±0.01	1.58±0.01	6.75±2.5	2.6±2.1	2.31±0.05	~56	~94
B	1.49±0.02	1.52±0.02	2.01±0.9	-1.3±0.6	2.23±0.06	57.9±0.2	96.6±0.3
C	1.48±0.02				2.27±0.05	49.6±3.8	82.6±6.3
D	1.46±0.03			-0.49±0.2	2.24±0.04	53.1±2.7	88.7±4.5

A - Si_2ON_2-rich material: O_2-Ar sintering - nitriding at 1380°C for 8 hours
B - Conventional material: Ar Sintering in pure argon - nitriding at 1450°C
C - No Ar sintering
D - Closed conventional material: Repeat of 2 with closed crucible during argon sintering

Although the mass increase of the conventional material showed a higher gain, the nitrided products had lower densities compared to Si_2ON_2-rich material (Table 4.1). The mass increase of the conventional material was calculated on the mass after Ar sintering, since mass loss occurred. Calculations of Si_2ON_2-rich materials were based on the green densities due to the oxidation that had taken place. This could have resulted in the estimated conversion of $Si \rightarrow Si_3N_4$ being lower than it actually is for the Si_2ON_2-rich material, since some silicon could have been lost during the argon sintering, as was the case in the conventional material.

Closed conventional materials were nitrided at 1450°C and the mass increase observed was lower than expected. These samples were, however, larger than those previously produced.

Materials produced without Ar sintering showed a lower mass gain than those which were Ar sintered, but the densities were slightly higher (Table 4.1).

4.2.3 Effect of Pressing

The effect of pressing on the final nitrided product was investigated. Nitriding the compacts which had been CIPped at various pressures resulted in mass increases between 55 and 58%, which is equivalent to 91 to 97% nitridation, Figure 4.1 (Messier and Croft (1982)). It was found that the optimum CIP pressure for compaction (Figure 3.1) and nitridation almost coincided and therefore 160MPa was used for all further studies.

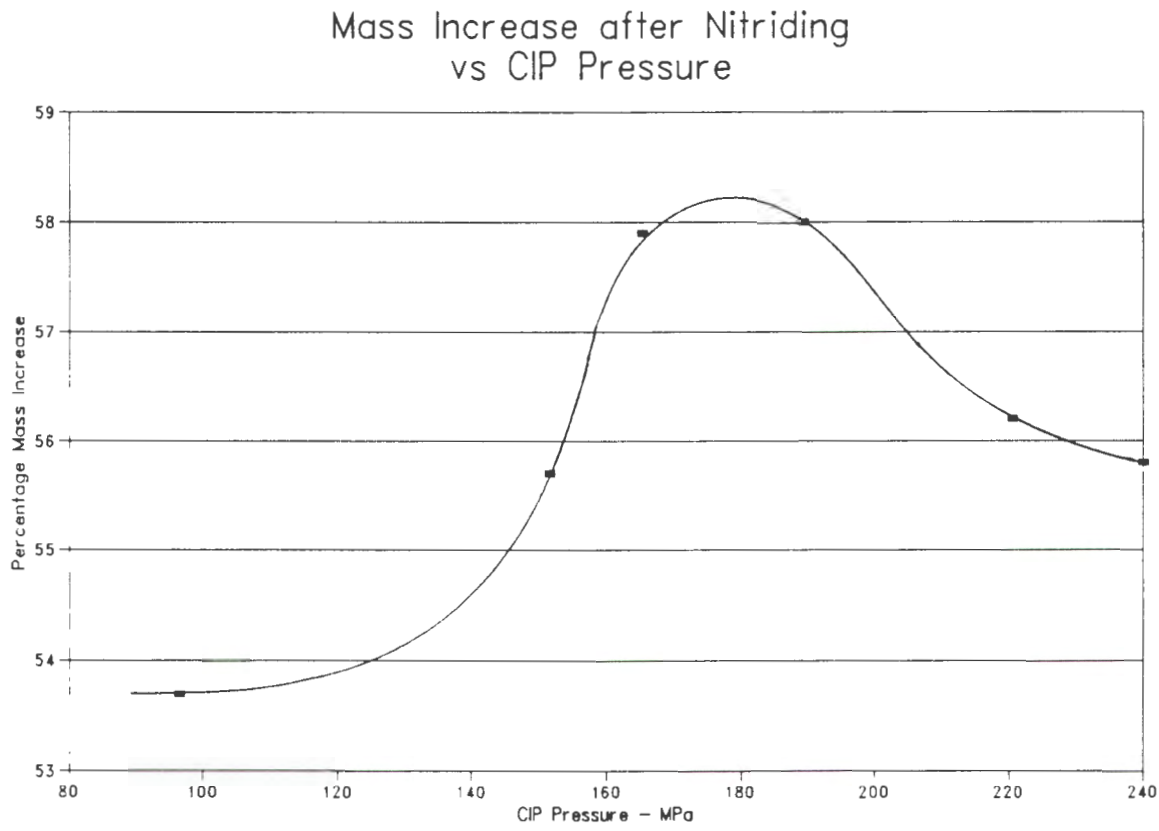

Figure 4.1: Effect of CIPped pressure on mass increase after nitriding.

4.2.4 Phase Analysis

Significant differences were observed in the phases present in Si_2ON_2-rich and conventional materials, as shown in Table 4.2.

Table 4.2: Phases present in the reaction bonded Si_3N_4 materials.

Material	Major Phases	Minor Phases	ß-Si_3N_4 fraction
Si_2ON_2-rich	Si_2ON_2	α-Si_3N_4, ß-Si_3N_4, $Y_2Si_2O_7$, SiO_2 (quartz)	0.64
Conventional	α-Si_3N_4	ß-Si_3N_4, $Y_2Si_2O_7$, SiO_2 (cristobalite) Si_2ON_2 on the surface	0.31

The major phase present after nitriding the Si_2ON_2-rich material was Si_2ON_2, with minor phases being α-Si_3N_4, ß-Si_3N_4, $Y_2Si_2O_7$ and SiO_2 (quartz), Figure 4.2. The fraction of ß-Si_3N_4 for these materials was 0.64. After nitriding the conventional material, Si_2ON_2 was present on the surface of the samples, but much less than in the previous cycle. In the bulk, the main phases present were α-Si_3N_4, ß-Si_3N_4 and $Y_2Si_2O_7$, Figure 4.3, with the fraction of ß-Si_3N_4 being lower at 0.31.

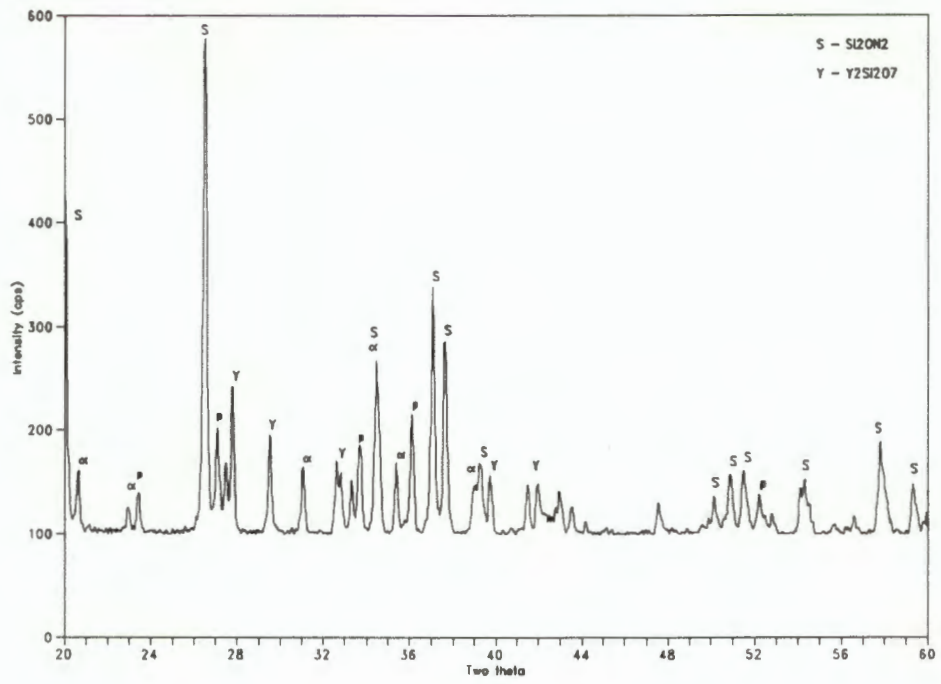

Figure 4.2: XRD trace of Si_2ON_2 rich material after nitridation.

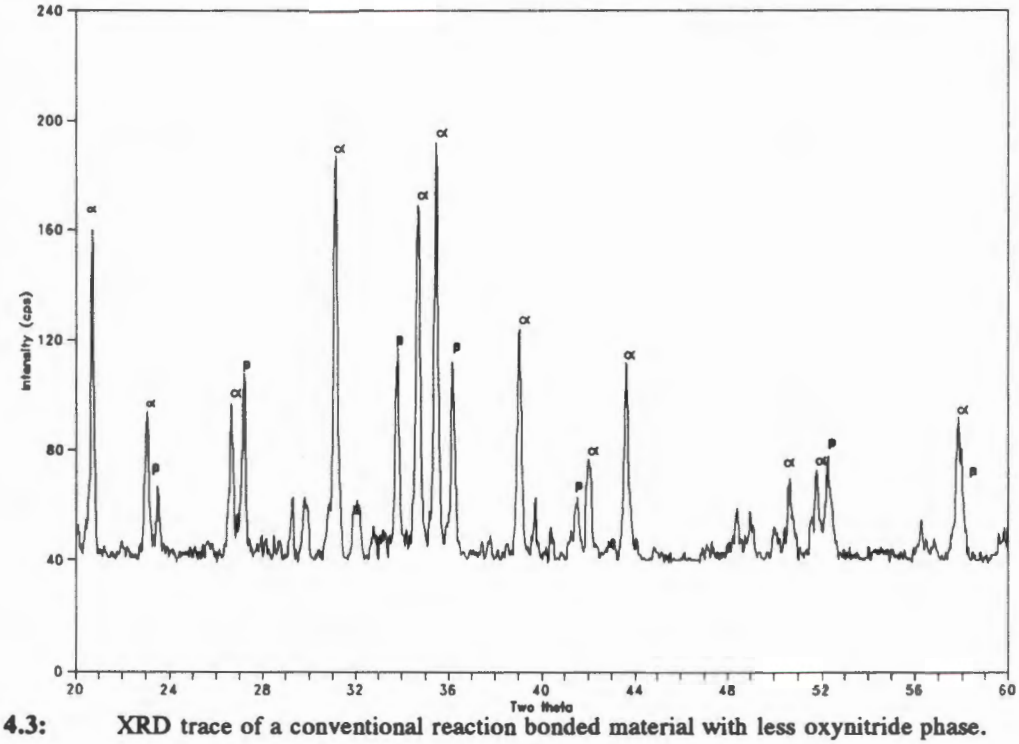

Figure 4.3: XRD trace of a conventional reaction bonded material with less oxynitride phase.

4.3 POST SINTERED REACTION BONDED Si_3N_4

4.3.1 Effect of Temperature and Atmosphere

Some of the RBSN samples produced during the nitriding runs discussed in section 4.2 were further processed by sintering in a Centorr furnace. The first sintering cycle had a maximum temperature of 1800°C. An argon atmosphere was used with a powder bed of Si_3N_4 and BN. All the samples had drops of silicon on the surface which had exuded out of the sample during sintering and only three samples at the bottom of the crucible could be analyzed. The other samples showed major deterioration due to the dissociation of the Si_3N_4 to silicon and nitrogen. These materials showed mass losses of up to 16%, indicating a large amount of material had evaporated.

The second sintering cycle had a maximum temperature of 1750°C. A nitrogen atmosphere and Si_3N_4-BN powder bed were used. The sintering lead to shrinkages of 10 to 15% resulting in densities of 3.1 to 3.2 g/cm^3.

A third sintering cycle with a maximum temperature of 1800°C produced materials with densities in the same range as those sintered at 1750°C. No silicon was observed on any of the surfaces after sintering when a nitrogen atmosphere was used.

4.3.2 Sintering of Si_2ON_2-rich Material

When sintered at 1750°C material rich in Si_2ON_2 had lower densities than material predominantly composed of α-Si_3N_4. However, after sintering at 1800°C Si_2ON_2-rich material had higher densities than the conventional α-Si_3N_4-rich material. The average densities were, however, lower than those obtained for α-Si_3N_4-rich material sintered at 1750°C. These results are shown in Table 4.3. The higher mass losses at 1800°C are ascribed to the sublimation of Si_3N_4 during sintering. This is confirmed as indicated above when argon is used in place of nitrogen, resulting in accelerated mass loss.

Table 4.3: Summary of densities and mass loss after sintering RBSN materials

Material	Density	Mass loss on sintering
Si_2ON_2-rich - after 1800°C	3.227±0.017	7.06±4.4
Si_2ON_2-rich - after 1750°C	3.182±0.018	4.01±0.3
Conventional - after 1800°C	3.168±0.046	8.84±2.2
Conventional - after 1750°C	3.252±0.006	4.04±0.4
Conventional - Ar atmosphere	3.207±0.011	12.2±4.67

4.3.3 Phase Analysis

An x-ray diffraction study showed that in all cases the major phase was ß-Si_3N_4. There was no sign of Si_2ON_2 in the post sintered RBSN, however, various minor phases were present in the samples. These phases were $Y_2Si_2O_7$, α-Si_3N_4 and various Sialons such as $Si_2Al_3O_7N$, Θ-$Si_3Al_{12}O_9N_{10}$ and $Si_3Y_{10}Al_2O_{18}N_4$. There did not seem to be a correlation between the initial RBSN phases and the post sintered RBSN phases, since the Θ-Sialon was present in samples from both batches, but not in all the samples. $Y_{10}Si_3Al_2O_{18}N_4$ was detected in many samples, but was present in higher concentrations in those materials which were originally Si_2ON_2-rich. Figure 4.4 shows a typical XRD pattern of the resulting post-sintered conventional material, while Table 4.4 gives more detail of the phases present after sintering Si_2ON_2-rich and conventional materials at 1750°C and 1800°C.

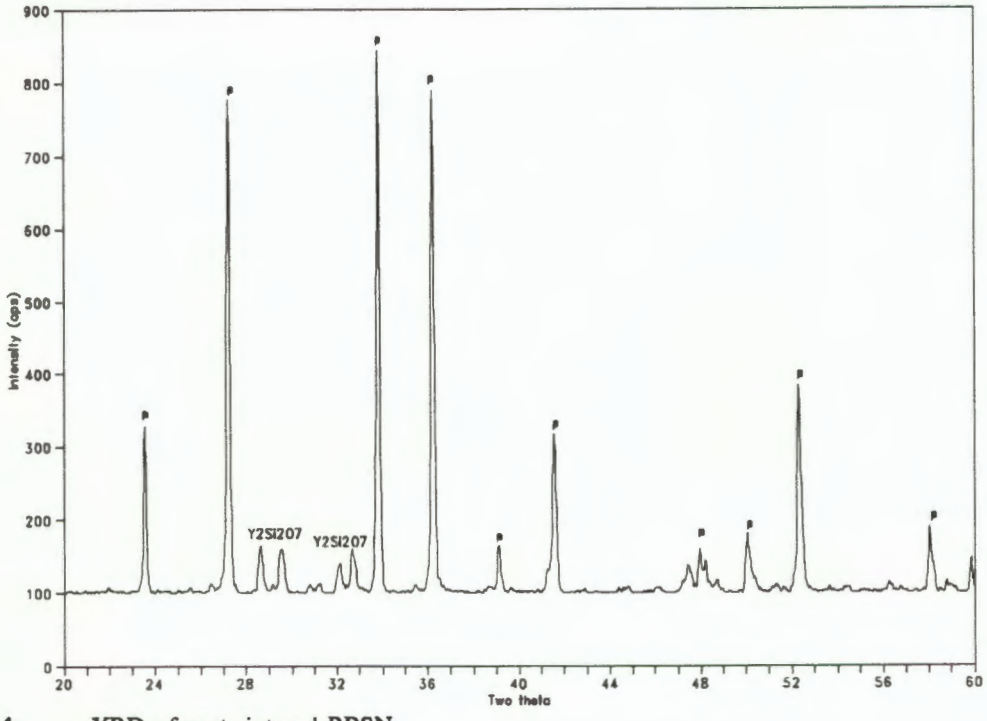

Figure 4.4: XRD of post sintered RBSN

Table 4.4: Phases present in the post sintered reaction bonded Si_3N_4 materials.

Material	Temperature	Major Phases	Minor Phases
Post sintered Si_2ON_2-rich material	1750°C	ß-Si_3N_4	$Y_2Si_2O_7$, $Y_{10}Si_3Al_2O_{18}N_4$, traces of α-Si_3N_4
Post sintered Si_2ON_2-rich material	1800°C	ß-Si_3N_4	$Y_{10}Si_3Al_2O_{18}N_4$, Θ-$Si_3Al_{12}O_9N_{10}$, $Si_3Al_{12}O_9N_{18}$, $Si_5Al_{12}O_8N_{10}$, traces of α-Si_3N_4
Post sintered conventional material	1750°C	ß-Si_3N_4	$Y_{10}Si_3Al_2O_{18}N_4$, Θ-$Si_3Al_{12}O_9N_{10}$, $Si_2Al_3O_9N_{10}$, traces of α-Si_3N_4
Post sintered conventional material	1800°C	ß-Si_3N_4	$Y_{10}Si_3Al_2O_{18}N_4$, Θ-$Si_3Al_{12}O_9N_{10}$, Si, other unidentified minor phases.

4.4 SINTERED SILICON NITRIDE

4.4.1 Effect of Milling on the Si_3N_4 Powder

Attrition milling the powders did not reduce the particle size significantly, but it was found to be an essential step in producing a dense sintered silicon nitride. XRD patterns of both the milled and mixed powders were studied (Figure 4.5). The major phases in both powders were α-Si_3N_4, ß-Si_3N_4 and Y_2O_3. The only observable difference was slight peak broadening in the areas of the major SiO_2 peaks in the milled powder, ie at 2Θ of 20.9 and 26.6. The powders were analyzed for oxygen content since it was thought that the milled powder could have oxidised during the milling process. The analysis was carried out on an Auger microscope fitted with an x-ray photoelectroscope, but no significant difference was observed between the two powders. The milled powder had a surface oxygen content of 23at% compared to 24at% in the mixed powder (including the oxygen content of the Y_2O_3 and Al_2O_3 additives), while the nitrogen contents were 30 and 29at% respectively.

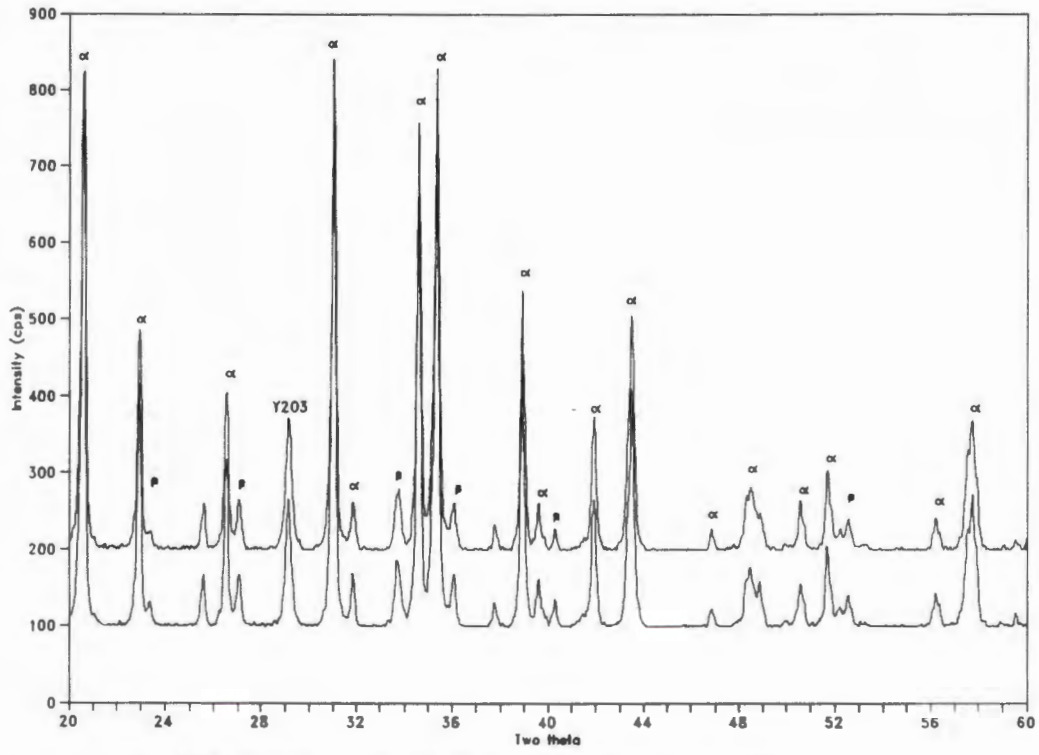

Figure 4.5: The XRD trace of milled (top trace) and mixed (bottom trace) powders.

4.4.2 Effect of Heating Rate and Sintering Temperature

Various temperatures and heating rates were used to sinter Si_3N_4 and their effect on the final densities and properties were studied. These results did not show definite trends, but generally the materials sintered at 1800°C were more dense than the material sintered at 1700°C at the same rate. It also seemed that the materials sintered at the faster rate, 300°Ch^{-1}, produced higher densities than the 100°Ch^{-1} cycles, Table 4.8. Faster rates of 600°Ch^{-1} were also used which resulted in slightly higher densities, but these materials did not produce the strengths obtained in the slower schedules.

4.4.3 Microwave Dried Powder

Some of the milled powder was dried in a conventional domestic microwave oven. The density of the materials produced from this powder was higher than the corresponding conventionally dried powder, but the strengths were significantly lower, as can be seen in Table 4.9.

4.4.4 Phase Analysis

X-ray diffraction patterns of the materials produced from the milled and mixed powders were studied after sintering. In all cases the major phase present after sintering was ß-Si_3N_4, but the minor phases depended on the temperature and heating rate used during sintering, as can be seen in Table 4.5.

The effect of temperature on the resulting material was studied using a constant heating rate of 300°Ch^{-1}. In the mixed powder materials, sintering at 1700°C resulted in 17% of the Si_3N_4 present being α-phase, while sintering at 1800°C resulted in only 7% residual α-Si_3N_4 (Figure 4.6). A significant amount of Y_2O_3 was also identified in these materials.

The effect of temperature on the milled powders is even greater. After sintering at 1700°C, 47% of the Si_3N_4 was present as α-Si_3N_4, while at 1800°C full transformation was observed (Figure 4.7). Other phases present after sintering the milled powder were Y_2O_3, Si-Al-O-N (at 1700°C) and Θ-$Si_3Al_2O_9N_{10}$ (at 1800°C).

Table 4.5: Phases present in the sintered Si_3N_4 materials.

Sintering conditions	Major Phases	Minor Phases	α-Si_3N_4 content
Mixed			
1700°C @ 100°Ch^{-1}	ß-Si_3N_4	Y_2O_3, Θ-$Si_3Al_2O_9N_{10}$	0
1700°C @ 300°Ch^{-1}	ß-Si_3N_4	α-Si_3N_4, Y_2O_3	17
1800°C @ 100°Ch^{-1}	ß-Si_3N_4	α-Si_3N_4, $Si_3Al_2O_3N_5$	0
1800°C @ 300°Ch^{-1}	ß-Si_3N_4	α-Si_3N_4, Y_2O_3	7
Milled			
1700°C @ 100°Ch^{-1}	ß-Si_3N_4	$Si_3Al_3O_3N_5$, Θ-$Si_3Al_2O_9N_{10}$	0
1700°C @ 300°Ch^{-1}	ß-Si_3N_4	Y_2O_3, Si-Al-O-N	47
1800°C @ 100°Ch^{-1}	ß-Si_3N_4	$Si_3Al_3O_3N_5$, Θ-$Si_3Al_2O_9N_{10}$, Y_2O_3	0
1800°C @ 300°Ch^{-1}	ß-Si_3N_4	Θ-$Si_3Al_2O_9N_{10}$, Y_2O_3	0

No α-Si_3N_4 was detected in any of the materials sintered at a heating rate of 100°Ch^{-1}. Figure 4.8 shows the x-ray diffraction pattern of a mixed powder material sintered at 1800°C using the slower heating rate of 100°Ch^{-1}. This pattern is significantly different from Figure 4.6(b) which was sintered at 1800°C using the faster heating rate of 300°Ch^{-1}. The other phases present were Y_2O_3 and Θ-$Si_3Al_2O_9N_{10}$. In the milled powder materials a similar trend was observed and the minor phases present were $Si_3Al_3O_3N_5$ and Θ-$Si_3Al_2O_9N_{10}$.

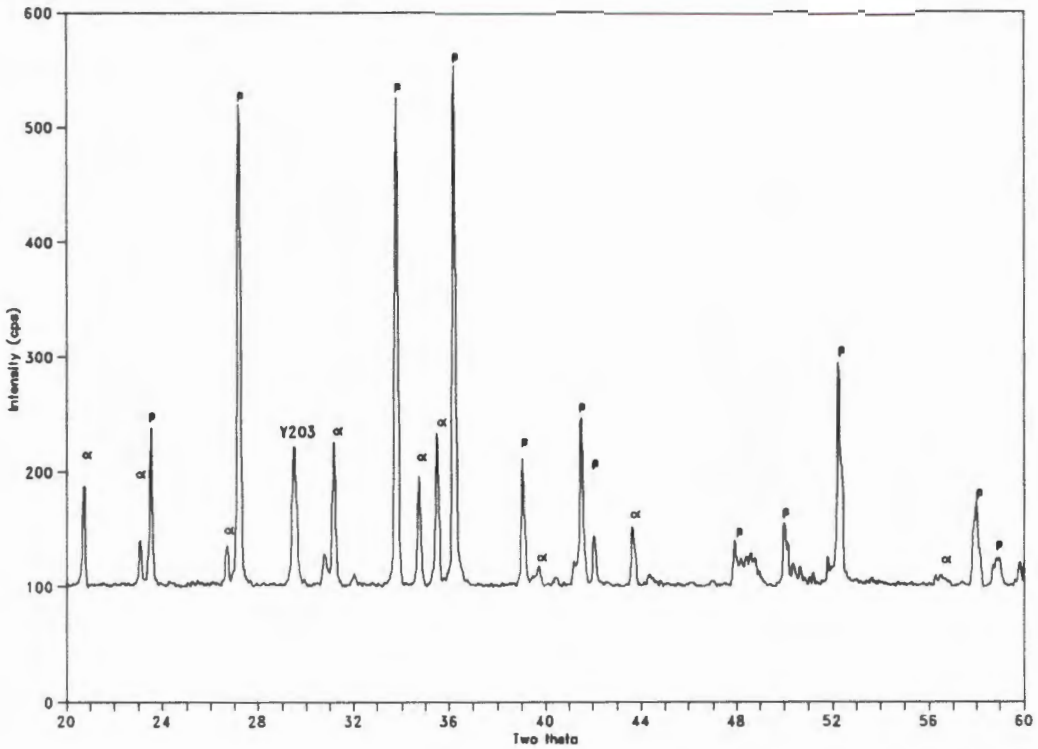

(a)

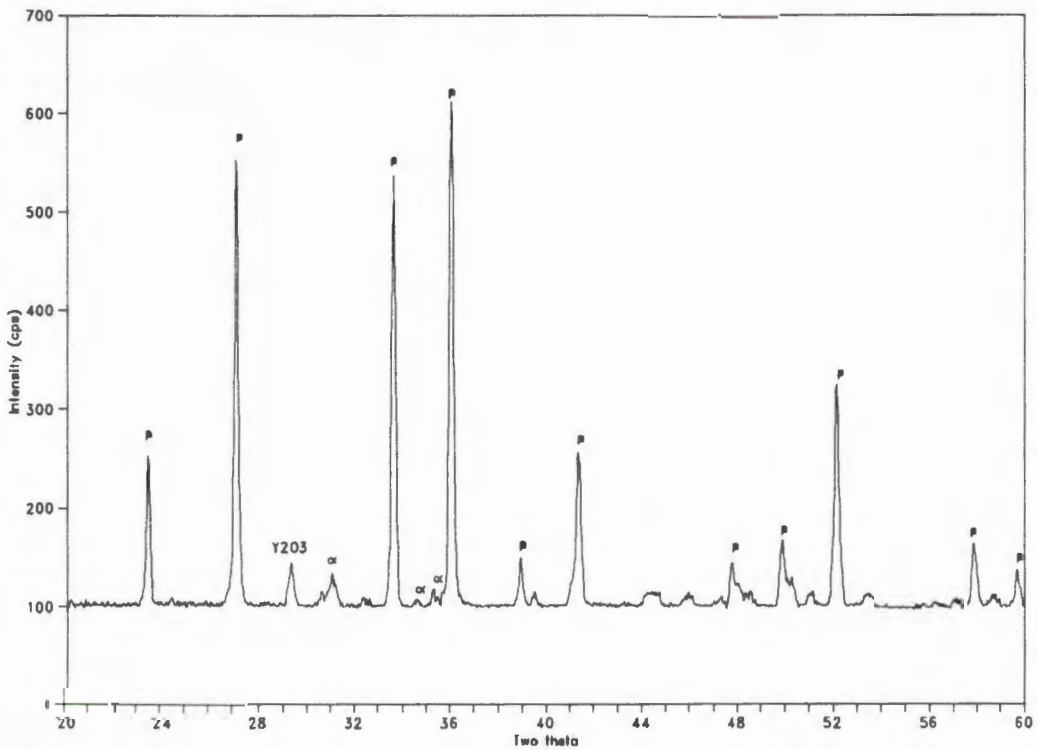

(b)

Figure 4.6: XRD trace of sintered materials produced from mixed powders after sintering at (a) 1700°C and (b) 1800°C at 300°Ch^{-1}.

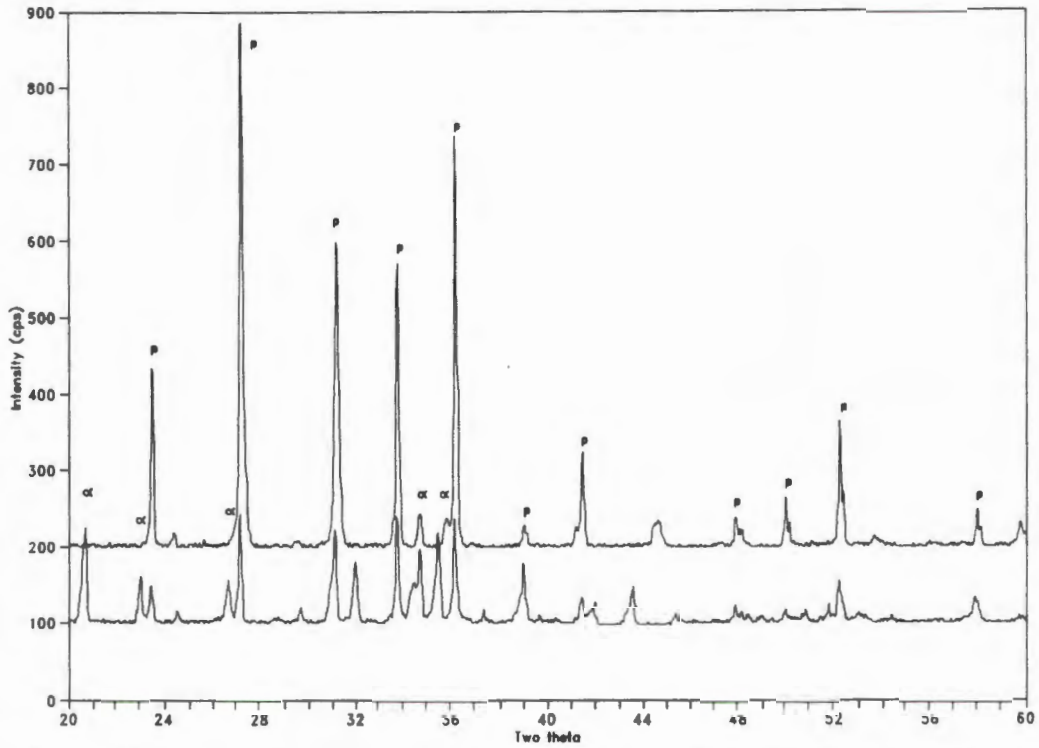

Figure 4.7: XRD trace of sintered material produced from milled powder after sintering at 1700°C (bottom) and 1800°C (top) at a rate of 300°Ch^{-1}.

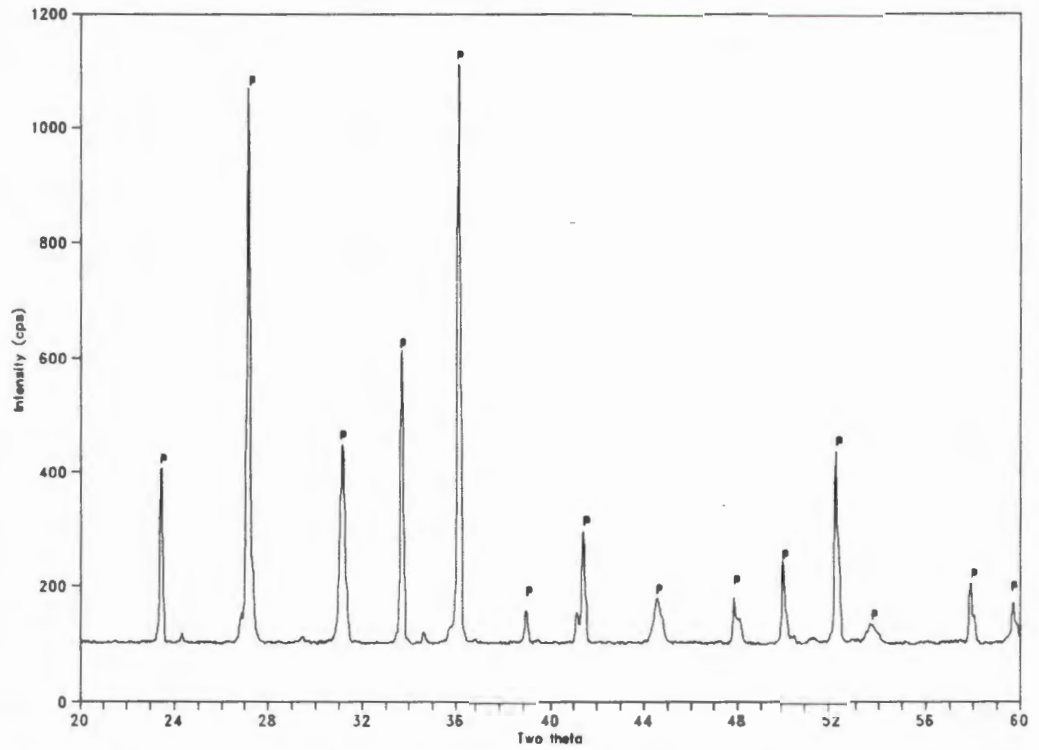

Figure 4.8: XRD trace of mixed material sintered with the slower heating rate at 1800°C.

4.5 MECHANICAL PROPERTIES

Table 4.6 summarizes the mechanical properties of all the materials produced during this study. Generally the hardness increased with density, while the toughness decreased. The sintered silicon nitride materials were sintered at different temperatures and heating rates which affected the properties to a great extent, and details are shown in Tables 4.8 and 4.9.

4.5.1 Reaction Bonded Silicon Nitride

4.5.1.1 Effect of Argon Sintering

Billy et al (1981) reported that Si_2ON_2 had higher hardness values than Si_3N_4. The higher Si_2ON_2 content in the reaction bonded Si_3N_4 (Si_2ON_2-rich material) resulted in hardness values of up to 1.5 times higher than those with less Si_2ON_2 (conventional material) (Table 4.6). This higher Si_2ON_2 content was accompanied by a higher density which could also have affected the hardness values. The toughness values of the Si_2ON_2-rich ceramics, however, were lower than the conventional RBSN.

There was a general trend of an increase in hardness with an increase in density. The toughness decreased as the hardness increased. These trends were observed in both reaction bonded materials.

When argon sintering was omitted, the hardness was lower than both reaction bonded materials which were argon sintered, while the toughness values were the highest of the three materials. This is a striking result as both materials had similar densities.

The strengths of conventional argon sintered RBSN was higher than the material which was not argon sintered (Table 4.7), indicating the necessity of the Ar sintering in processing RBSN.

4.5.2 Post Sintered Reaction Bonded Si_3N_4

4.5.2.1 Effect of Si_2ON_2 in RBSN

The Si_2ON_2-rich material had lower hardness values compared to the conventional material for both the 1750°C and 1800°C sintering cycles. The toughness values of

Table 4.6: A summary of the hardness, toughness and density values of all the silicon nitride materials.

Material	Hardness GPa	Toughness $MPa.m^{½}$	Density $g.cm^{-3}$
Reaction Bonded Materials			
Si_2ON_2-rich Material	6.29±0.8	3.93±0.7	2.31±0.05
Conventional Material	4.29±0.1	4.35±0.6	2.23±0.06
No Ar sintering	2.13±0.1	5.30±0.4	2.27±0.05
Post Sintered Reaction Bonded Materials			
Si_2ON_2-rich Material - 1800°C	14.36±0.9	4.75±0.4	3.22±0.07
Si_2ON_2-rich Material - 1750°C	14.27±0.3	4.45±0.1	3.18±0.04
Conventional Material - 1800°C	15.06±0.5	4.33±0.3	3.17±0.05
Conventional Material - 1750°C	14.48±0.4	4.00±0.5	3.52±0.06
Conventional Material - Ar atmosphere	14.60±0.2	4.41±0.4	3.21±0.01
Sintered Si_3N_4			
Si_3N_4 from Mixed Powder	9.4-10.6	6.1-7.5	2.93-3.04
Si_3N_4 from Milled Powder	9.1-11.7	5.2-6.9	2.97-3.15

Table 4.7: A summary of the strengths and densities of all the silicon nitride materials.

Material	Strength MPa	Density $g.cm^{-3}$
Reaction Bonded Materials		
Conventional Material B	94±18	2.23±0.06
No argon sintering	68±26	2.27±0.05
Post Sintered Reaction Bonded Materials		
Conventional Material - 1750°C	184±42	3.25±0.06
Sintered Si_3N_4		
Si_3N_4 from Mixed Powder	277-362	2.93-3.04
Si_3N_4 from Milled Powder	311-521	2.97-3.15

the post sintered Si_2ON_2-rich material were higher than the corresponding conventional RBSN values, Table 4.6. There was no clear relationship between the hardness, toughness and density values, and the usual trend of an increasing hardness and decreasing toughness was not observed.

4.5.2.2 Effect of Sintering Temperature

Sintering at 1800°C produced higher hardness and toughness values for both the Si_2ON_2 rich material and the conventional material, compared to those sintered at 1750°C. Although the post sintered conventional material sintered at 1800°C had the lowest density of the reaction bonded materials after sintering, it produced the highest hardness, 15.06GPa, while the post sintered Si_2ON_2-rich material had the highest toughness, 4.75MPa.$m^{½}$.

The strength of the post sintered reaction bonded materials were almost twice as high as those of the reaction bonded materials. The strength of the conventional material increased from 94MPa after nitriding to 184MPa after sintering at 1750°C.

4.5.2.3 Effect of Atmosphere During Sintering

The materials produced by sintering in an argon atmosphere with the samples embedded in a Si_3N_4-BN powder bed had a hardness of 14.6GPa. This was higher than those of the Si_2ON_2-rich material after sintering, but lower than the hardness values obtain for the conventional RBSN after sintering at 1800°C. The toughness values were in the same range as those of the other reaction bonded materials after sintering in nitrogen atmospheres.

4.5.3 Sintered Silicon Nitride

4.5.3.1 Effect of Milling

When comparing the hardness and toughness values of the sintered Si_3N_4 materials produced from the mixed and milled powders there was no significant difference for materials produced under the same conditions, Table 4.8.

Table 4.8: Average hardness, toughness and densities of the silicon nitride materials sintered at the various temperatures and heating rates.

Sintering conditions	Hardness GPa	Toughness $MPa.m^{½}$	Density g/cm^3
Mixed			
1700°C @ 100°Ch^{-1}	10.0±0.3	7.1±0.6	2.98±0.04
1700°C @ 300°Ch^{-1}	9.4±0.4	6.8±0.5	2.99±0.02
1800°C @ 100°Ch^{-1}	10.3±0.4	6.1±0.7	2.93±0.04
1800°C @ 300°Ch^{-1}	10.6±0.5	7.5±0.3	3.04±0.01
Milled			
1700°C @ 100°Ch^{-1}	9.1±0.2	6.7±0.8	2.98±0.06
1700°C @ 300°Ch^{-1}	11.7±0.1	5.2±0.6	3.02±0.03
1800°C @ 100°Ch^{-1}	10.2±0.3	6.9±0.4	3.15±0.01
1800°C @ 300°Ch^{-1}	9.9±0.2	6.5±0.4	3.11±0.01
1800°C @ 600°Ch^{-1}	12.1±0.2	5.3±0.3	3.21±0.02
1800°C @ 300°Ch^{-1} (microwave dried)	14.4±0.1	5.7±0.2	3.29±0.01

The milling, however, had a marked effect on the strengths of the ceramics, Table 4.9. The milled powder produced ceramics with higher strengths than the mixed powder. This corresponds to the higher densities for the materials produced from the milled powders.

4.5.3.2 Effect of Temperature and Heating Rate

Ceramics produced from the mixed powder did not show much dependence on temperature or heating rate. The hardness and toughness values did not follow any trend, Table 4.8. The strengths decreased with an increase in temperature from 1700°C to 1800°C for both heating rates. The increase in heating rate decreased the final strength of the materials both at 1700°C and 1800°C, despite the fact that the higher heating rate produced the higher densities. Thus, the sintering cycle with a maximum temperature of 1700°C and a heating rate of 100°Ch^{-1} produced the highest strengths for the mixed Si_3N_4 powders, Table 4.9.

Table 4.9: Average strengths and densities of the silicon nitride materials sintered at the various temperatures and heating rates.

Sintering conditions	Strength MPa	Density g/cm^3
Mixed		
1700°C @ 100°Ch^{-1}	362±40	2.98±0.04
1700°C @ 300°Ch^{-1}	295±49	2.99±0.02
1800°C @ 100°Ch^{-1}	311±45	2.93±0.04
1800°C @ 300°Ch^{-1}	277±57	3.04±0.01
Milled		
1700°C @ 100°Ch^{-1}	372±32	2.98±0.06
1700°C @ 300°Ch^{-1}	433±34	3.02±0.03
1800°C @ 100°Ch^{-1}	363±26	3.15±0.01
1800°C @300°Ch^{-1}	521±48	3.11±0.01
1800°C @600°Ch^{-1}	273±55	3.21±0.02
1800°C @ 300°Ch^{-1} (microwave dried)	362±34	3.29±0.01

The milled powder resulted in materials with strengths which increased with an increase in the heating rate from 100°Ch^{-1} to 300°Ch^{-1} for both 1700°C and 1800°C sintering temperatures. At a heating rate of 600°Ch^{-1}, however, the average strength was slightly lower than at 100°Ch^{-1}. A dependence on temperature was only found when using the faster heating rate of 300°Ch^{-1}. The strength increased form 433MPa to 521MPa as the temperature increased from 1700°C to 1800°C. A heating rate of 100°Ch^{-1} resulted in no significant difference in the strengths after 1700°C and 1800°C, Table 4.9.

The toughness values tended to decrease with an increase in hardness for a specific temperature used, Table 4.8. The hardness values generally increased with an increase in density. No significant differences in hardness and toughness values were observed when sintering with the heating rates of 100°Ch^{-1} and 300°Ch^{-1}. Only the ceramics sintered at 1700°C at a heating rate of 300°Ch^{-1} showed a slightly higher

hardness of 11.7GPa. Increasing the heating to 600°Ch^{-1} and using a maximum temperature of 1800°C increased the hardness to 12.1GPa.

4.5.3.3 Conventional Drying vs Microwave Drying

The effect of microwave drying the milled slurry appears to have been advantageous in that the final density and the hardness values were higher than the corresponding conventionally dried material. Although the toughness is lower than for those obtained with conventionally dried powder, it was only 10% lower compared to almost 50% increase in hardness, Table 4.8.

The strengths of the microwave dried material was, however, significantly lower than those of the materials produced from the conventionally dried powder, despite the higher densities, Table 4.9. Since the densities were higher, it could indicate the possibility that the critical flaws were larger, and therefore responsible for these lower strength values.

4.6 MICROSTRUCTURE

4.6.1 Argon Sintered Silicon

Fracture surfaces of pressed silicon and argon sintered silicon compacts were examined under the scanning electron microscope. The pressed silicon compact consisted primarily of grains of less than 1 μm in diameter with a few larger grains of up to 4 μm (Figure 4.9). After argon sintering, the grains were larger, generally 1-5 μm in cross-section, and a thread-like network was observed in the compact (Figure 4.10). A number of pores were observed in both the pressed and argon sintered compacts, indicating less than optimal packing during forming.

Figure 4.9: Scanning electron micrograph of the pressed silicon compact, showing grains of less than 1 μm in diameter with occasional larger grains of ~4 μm.

4.6.2 Reaction Bonded Si_3N_4

After nitriding and post sintering a number of representative samples were mounted and polished to a 1 μm diamond finish. These surfaces were studied using both optical and scanning electron microscopy.

The RBSN samples were characterised by a high porosity which varied from very fine pores to larger pores of up to 20-30 μm in diameter (Figure 4.11). Although the pores were not

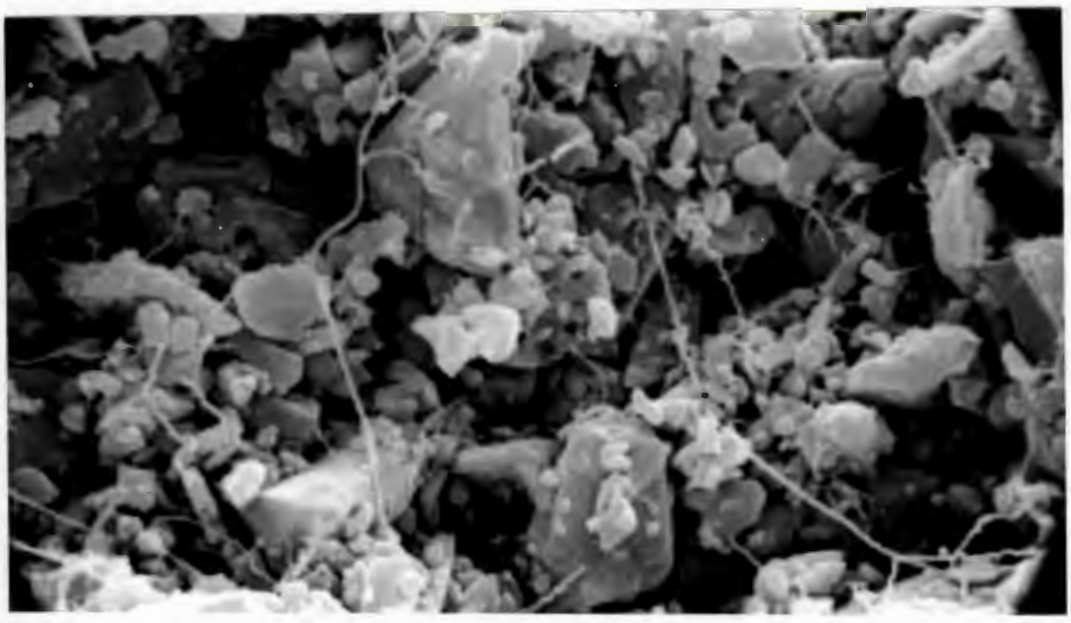

Figure 4.10: Scanning electron micrograph of an argon sintered silicon compact. The grains were larger than those in the pressed compact (1-5 μm in diameter), and a thread-like network was observed.

always spherical in shape, the term "diameter" used in this study will denote the maximum cross-sectional dimension of the pores. The edges of the samples had lower porosity than the bulk material (Figure 4.12). This was the case for both the Si_2ON_2-rich and conventional reaction bonded materials. When inspecting the polished surfaces with the naked eye, a darker area was observed around the edge of the specimen with a lighter coloured core. This colour variation appeared to coincide with the porosity variation. There were also areas of low porosity around residual silicon (Figure 4.13). These areas were not observed very frequently since there was not copious amounts of residual silicon present, but where the silicon was found, it was usually accompanied by an area of lower porosity. There were also areas in the bulk material which had lower porosity, but no residual silicon was present (Figure 4.11).

The polished reaction bonded materials were studied in the SEM using the backscattered imaging mode. The RBSN materials showed occasional areas where the surface looked more glassy or molten. It is thought that these could have been areas of residual silicon. During the later stages of nitriding, the silicon would have been molten. Since no large areas of residual silicon were observed during the optical microscopy study of the materials, this area

probably reacted with nitrogen whilst in a liquid state, forming Si_3N_4. Only silicon was detected in these areas using the EDS analysis, thus eliminating it as a glassy intergranular phase of Y_2O_3, Al_2O_3 and SiO_2 (Figure 4.14). The lighter areas in the micrograph indicated regions of high Y_2O_3 concentration, which were distributed throughout the material. The bright rings around the pores are caused by charging of the specimen. This charging could not be totally eliminated since more gold coating masks the Y_2O_3-rich phases and at lower accelerating voltage the image clarity deteriorates.

4.6.3 Post Sintered Reaction Bonded Materials

The polished surfaces of the post sintered RBSN (Figure 4.15) were different from the RBSN materials (Figures 4.11 - 4.13), and also differed from each other depending on the original Si_2ON_2 content (Figure 4.16 (Si_2ON_2-rich material) vs 4.17 (conventional material)) and the sintering temperature (Figure 4.20). All the optical micrographs of PSRBSN samples showed a concentration of bright phase near the edge of the samples. This phase was not the same bright phase as the residual silicon in the RBSN. The extreme edge of most of the samples had a lower porosity and this bright phase was absent (Figure 4.15). It is thought that this is an Y-rich phase formed during sintering.

Figure 4.11: Typical optical micrograph of the nitrided surfaces showing the fine porosity and occasional large pores. There were also fairly large areas of lower porosity present.

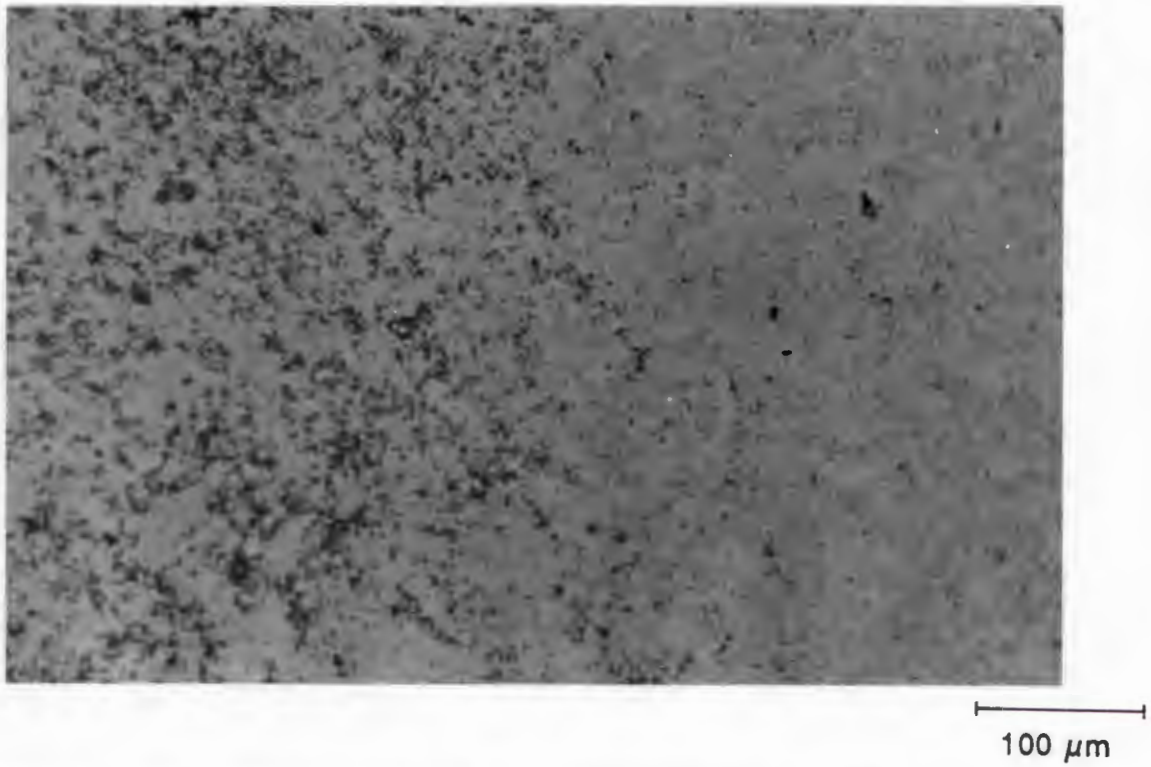

Figure 4.12: Optical micrograph showing the low porosity at the edge of the RBSN materials compared to the bulk material.

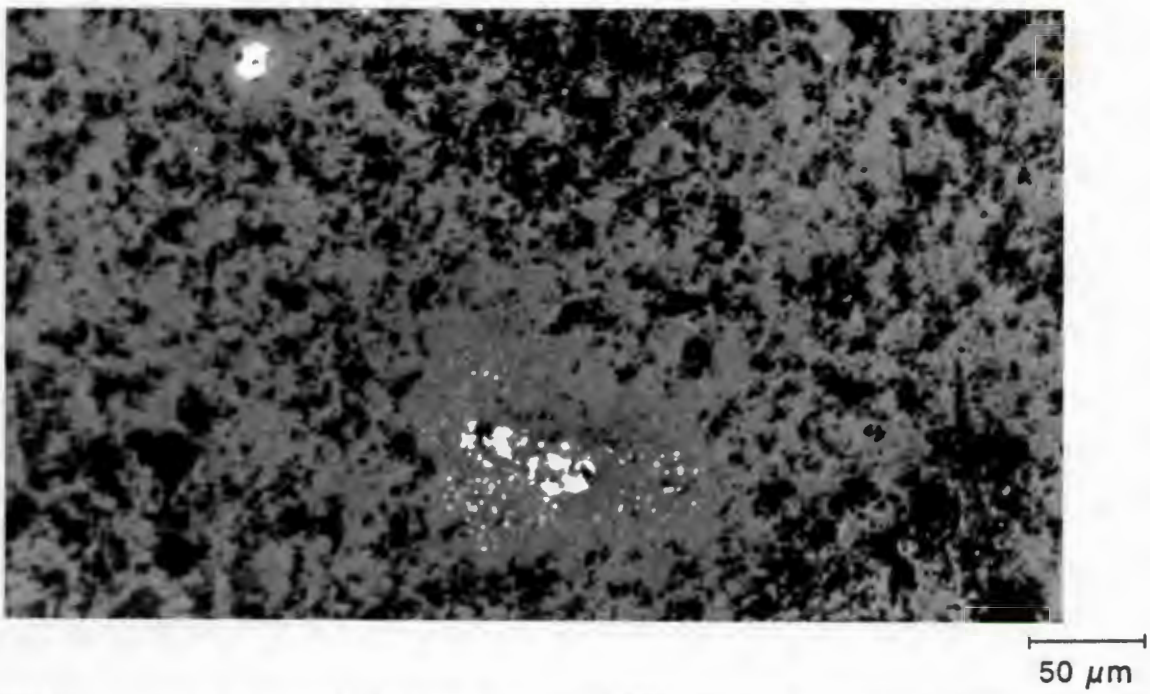

Figure 4.13: Optical micrograph of an area on a polished RBSN sample where residual silicon (bright phase) is present. The area immediately surrounding the silicon has lower porosity than the bulk material.

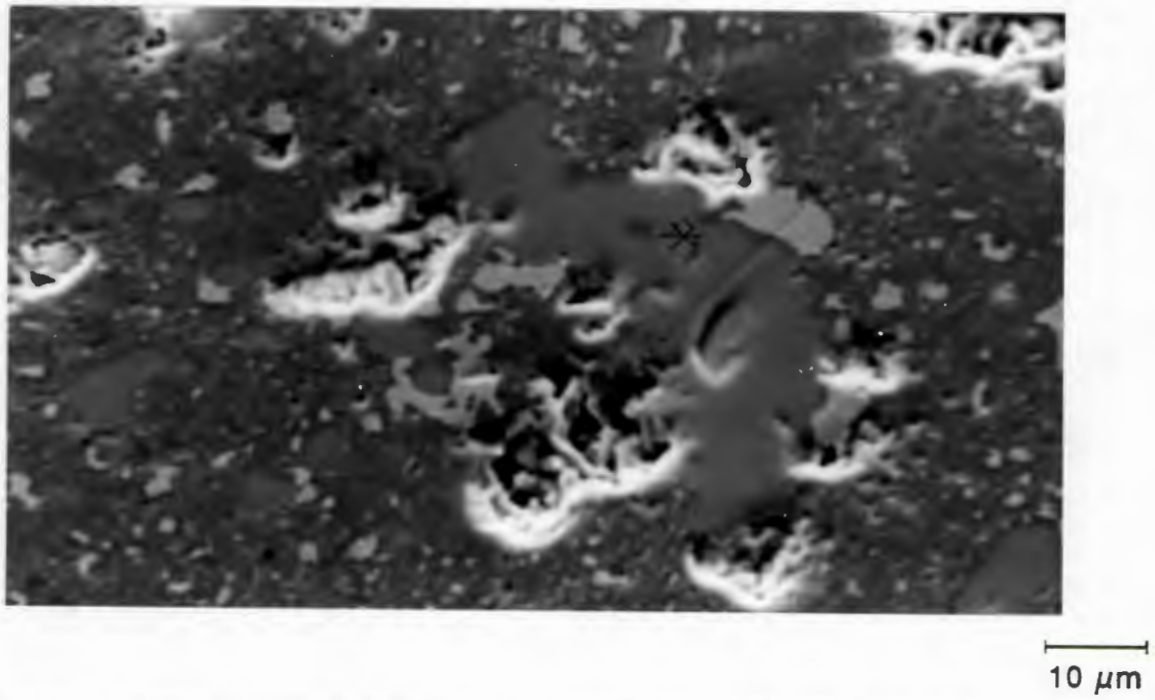

Figure 4.14: SEM micrograph of a polished RBSN material showing an area which has a much smoother, glass-like inclusion. The lighter phase is an Y-rich phase.

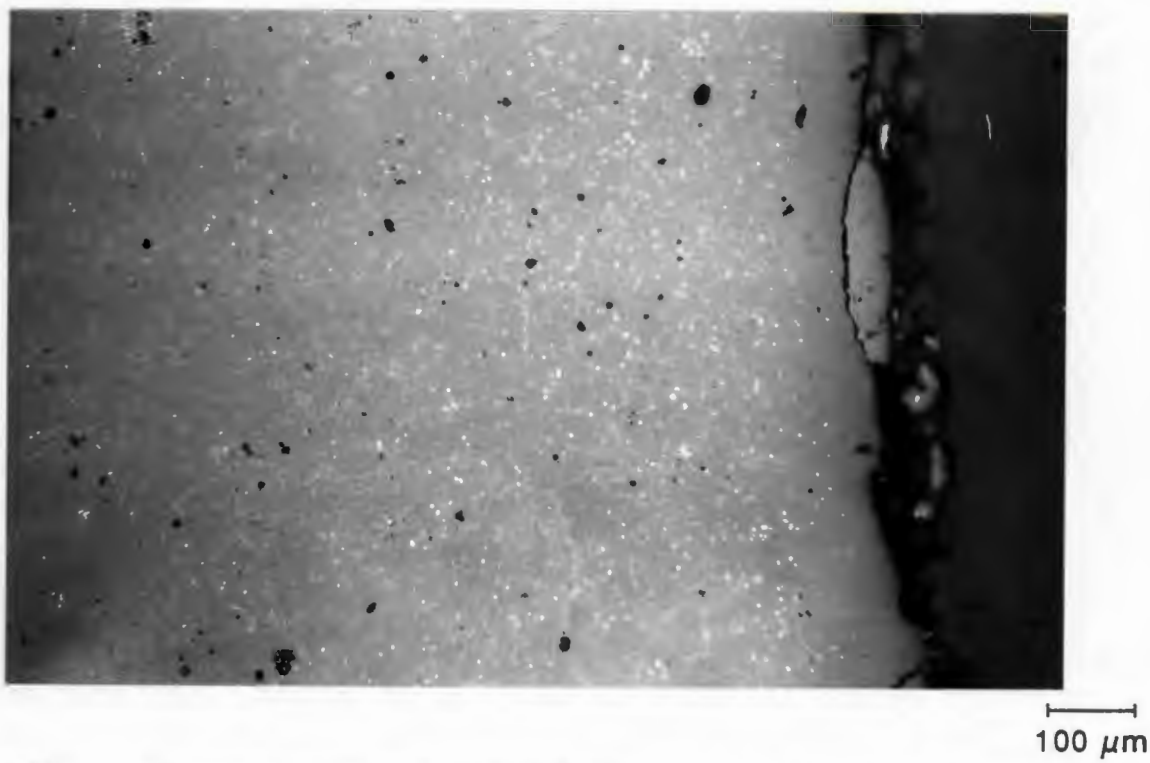

Figure 4.15: An optical micrograph of a post sintered conventional RBSN polished surface showing a bright phase near the edge and the less porous area, free of the bright phase on the edge of the sample after 1750°C.

4.6.3.1 *Effect of Presence of Si_2ON_2 on Sintering*

The originally Si_2ON_2-rich material had a fine distribution of pores in the bulk of the material after sintering, with occasional larger pores of up to 40 μm in diameter (Figure 4.16). There were no other distinguishing features on these surfaces when studied on the optical microscope.

The conventional material had less Si_2ON_2 present initially, and after sintering there were fewer pores remaining compared to the Si_2ON_2-rich material (Figure 4.17). After sintering at 1800°C these pores, however, were larger, 10 - 15 μm in diameter, than those in the Si_2ON_2 rich material.

At higher magnification a third phase could be discerned throughout the conventional material. Apart from the bright phase seen at the lower magnifications (Figure 4.15) there was also a lighter phase present (Figure 4.18). This phase was observed after sintering at both 1750°C and 1800°C, but was not seen in the Si_2ON_2-rich material after sintering.

4.6.3.2 *Effect of Sintering Temperature*

Si_2ON_2-rich material sintered at 1750°C and 1800°C did not show significant differences when polished surfaces were studied on the optical microscope. In the conventional material, however, those ceramics sintered at 1750°C had smaller pores, 5 - 10 μm in diameter, compared to those sintered at 1800°C, where the pores were 10 - 15 μm in diameter. This could be an indication of over-sintering in the latter materials.

Studying these surfaces in the SEM using backscatter imaging, the Y_2O_3 distribution could be clearly seen.

It appears that the materials sintered at 1800°C (Figure 4.19 (b)), have larger areas which are Y-depleted than those sintered at 1750°C (Figure 4.19 (a)). This was observed on polished surfaces of both post sintered materials. This phenomenon could be due to the grain growth occurring at the higher temperature.

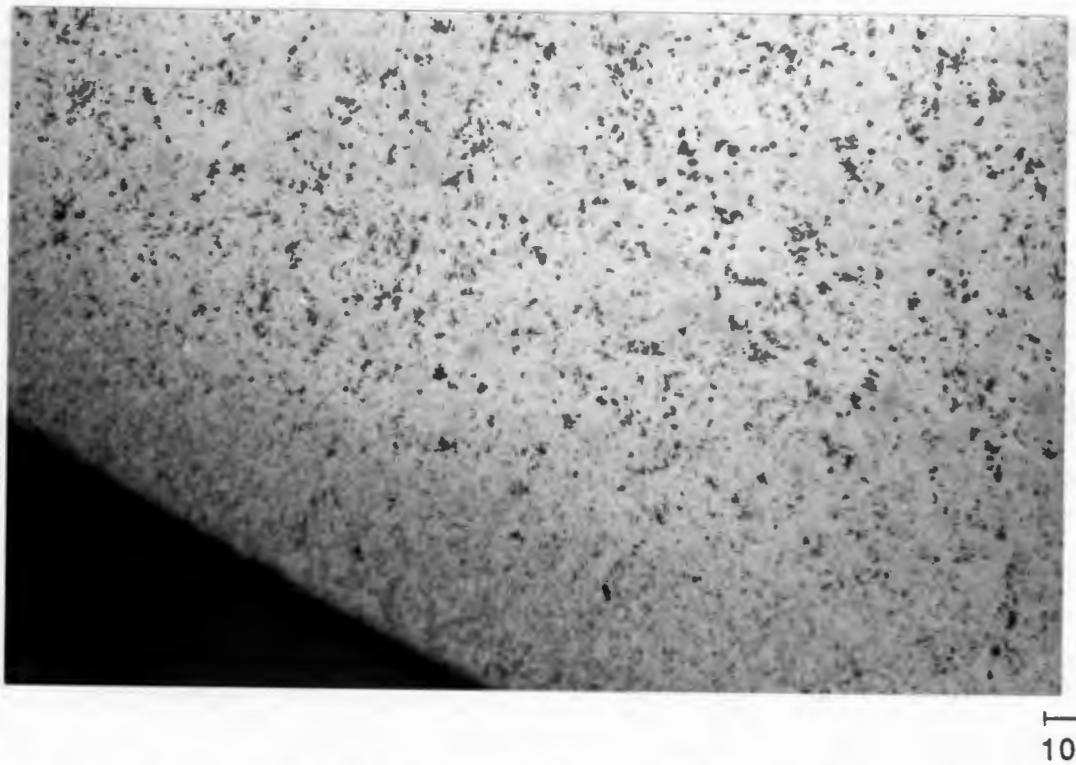

Figure 4.16: The polished surface of the Si_2ON_2-rich material had fine pores throughout the bulk material after sintering at 1800°C.

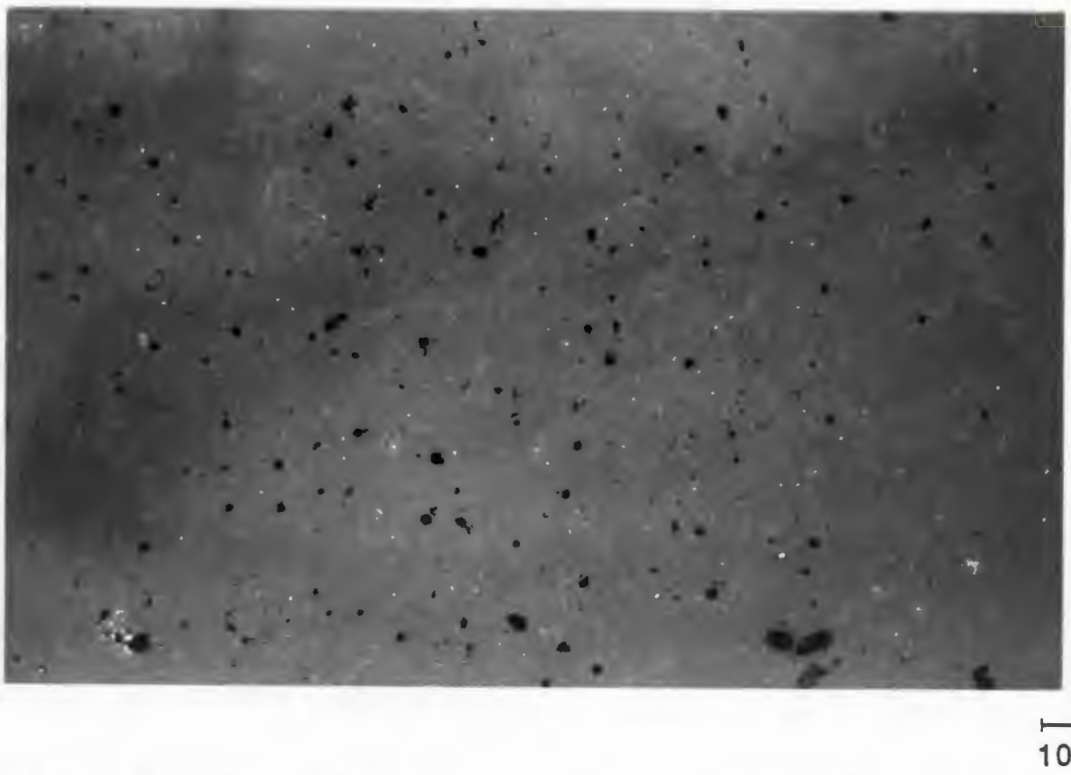

Figure 4.17: Polished surface of a sintered conventional reaction bonded material (after 1800°C). The pores were generally larger than those observed in Si_2ON_2-rich material after sintering at 1800°C.

Figure 4.18: Optical micrograph of post sintered conventional material showing a second light phase present throughout the structure. This phase was not as bright as the other light phase present near the edge of the specimens.

To confirm this, the polished surfaces were studied after etching in molten KOH. The etching removed the grain boundary phases which contained the bulk of the Y_2O_3 and Al_2O_3 additives, leaving the grains clearly visible. The materials sintered at 1800°C had larger grains than those sintered at 1750°C. This was found in both materials after sintering (Figures 4.20 and 4.21). The Si_2ON_2-rich material sintered at 1800°C had the largest grains, generally 2 -5 μm in length with an aspect ratio of 1 - 2. Occasional excessive grain growth was observed with grains as long as 10 μm (Figure 4.20(b)). After sintering at 1750°C this material had grain sizes varying between 1 - 2 μm in length, with a few grains of up to 5 μm in length (Figure 4.20(a)). The aspect ratio of the grains ranged from 1.5 to 5. The conventional material had grains of approximately the same size as the Si_2ON_2-rich material after sintering for both sintering temperatures (Figure 4.21). After 1800°C, however, grains of the conventional material were more elongated, with aspect ratios of between 3 and 4, and grain sizes of 2 -6 μm in length (Figure 4.21(b)). Some larger grains of up to 10 μm in length were also observed. Sintering at 1750°C tended to produce more equiaxed grains with aspect ratios of 1-2 and grains of between 0.5 μm and 4 μm in length (Figure 4.21(a)).

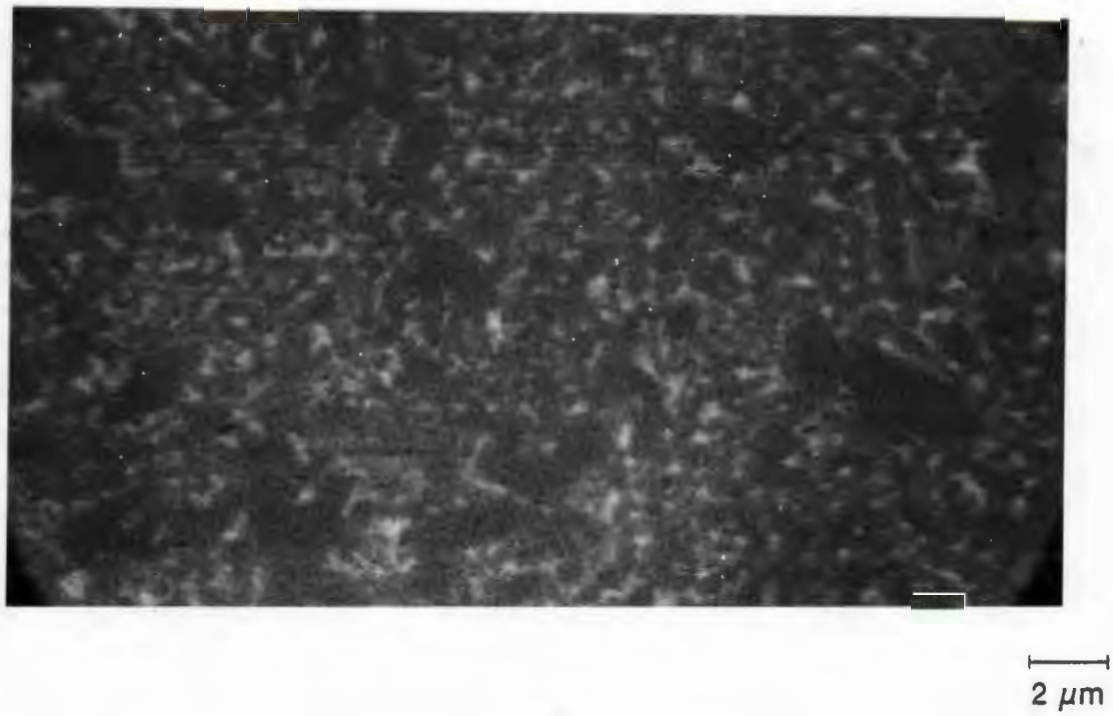

(a)

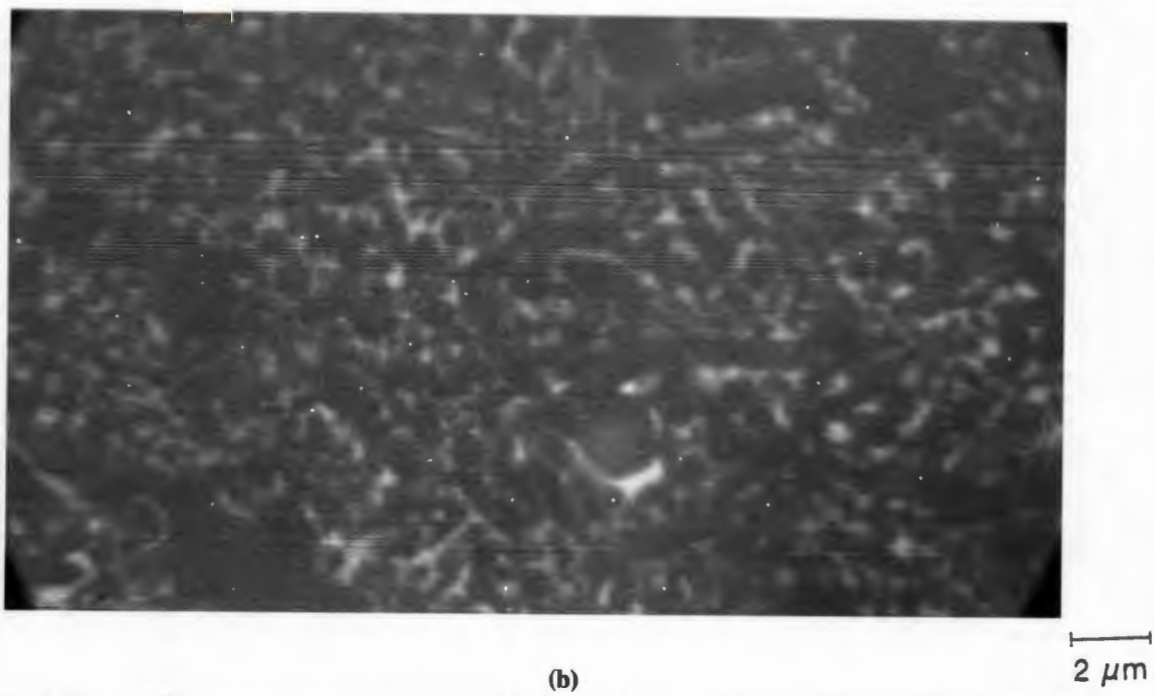

(b)

Figure 4.19: SEM micrographs of post sintered Si_2ON_2-rich material in backscatter imaging mode, showing the lighter Y_2O_3 distribution a) after 1750°C, b) after 1800°C.

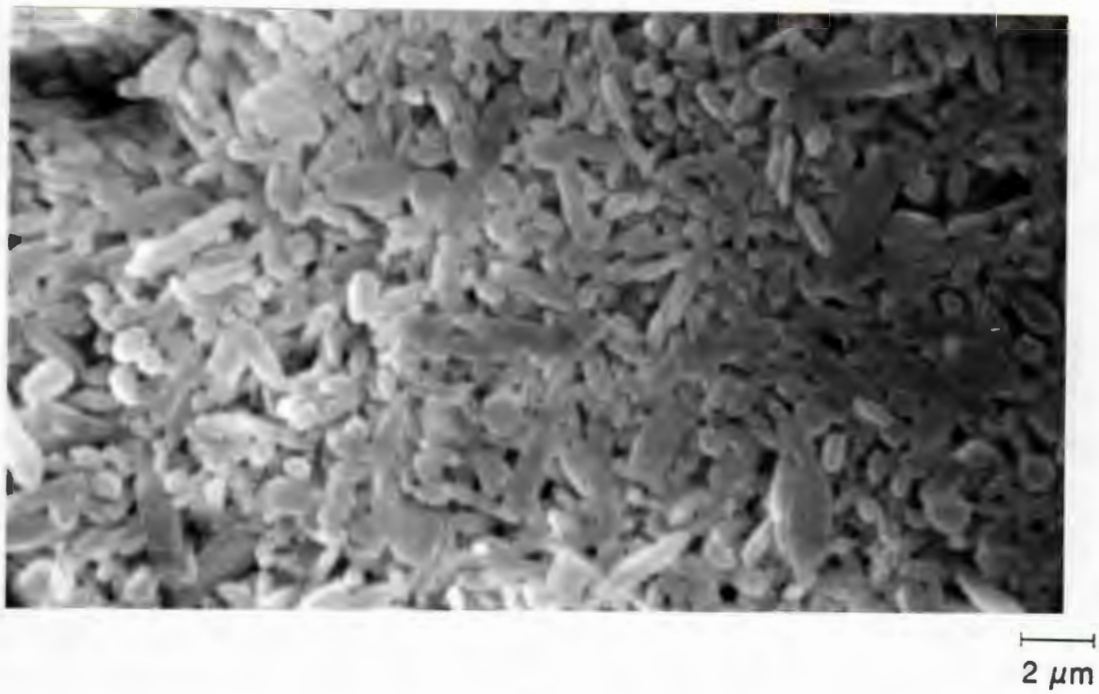

(a)

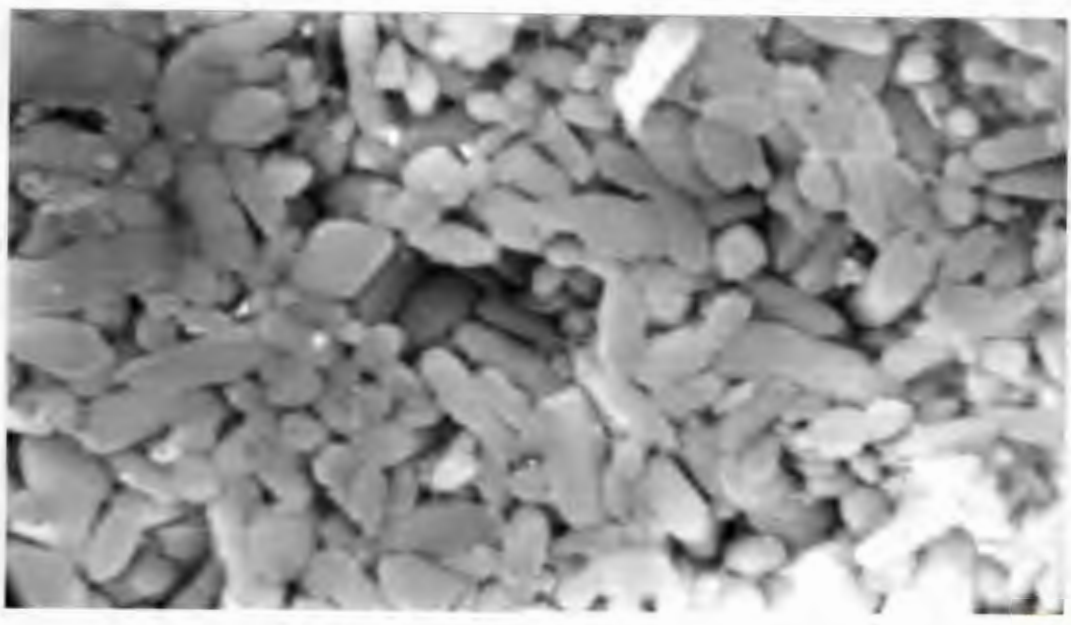

(b)

Figure 4.20: Etched samples of Si_2ON_2-rich material sintered at a) 1750°C and b) 1800°C. Those sintered at the higher temperature have larger grains than those sintered at 1750°C.

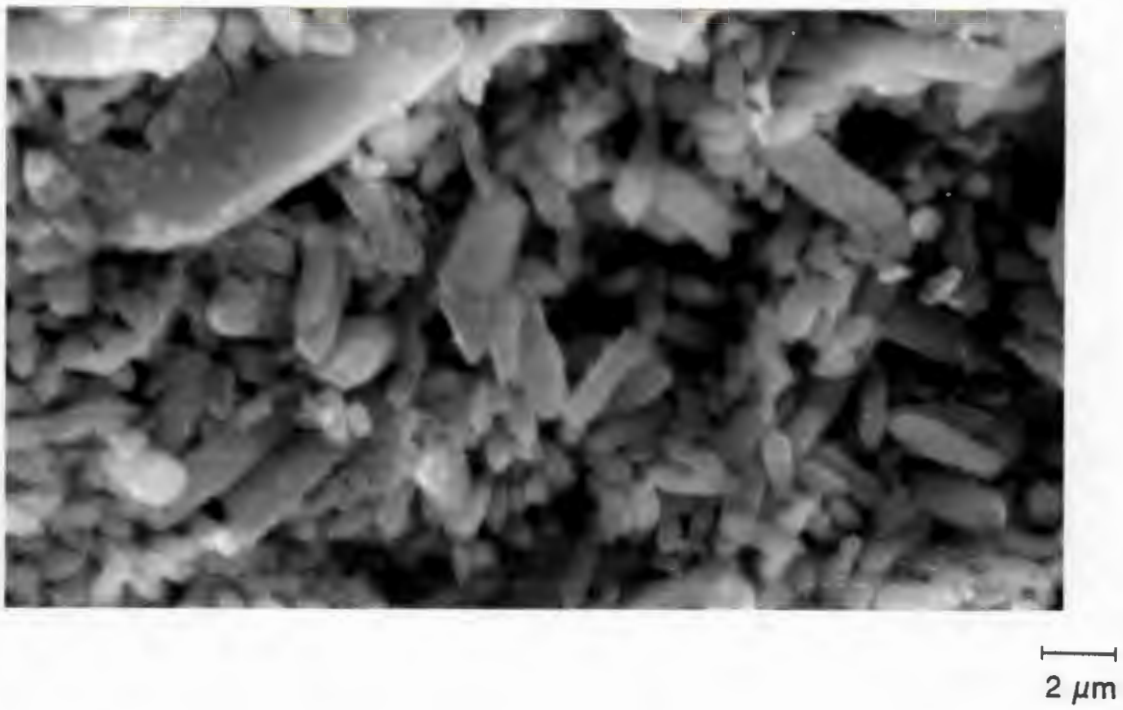

(a)

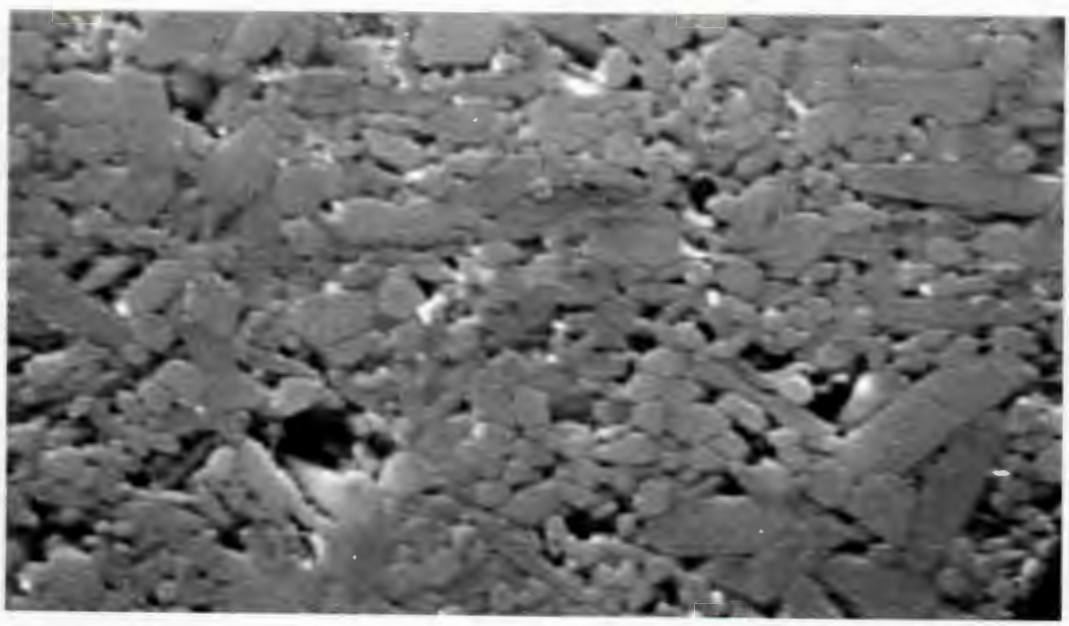

(b)

Figure 4.21: The etched surfaces of the conventional material after sintering at a)1750°C (over-etched) and b) 1800°C. The materials sintered at 1800°C have larger grains than those sintered at 1750°C.

4.6.3.3 Reaction Bonded vs Post Sintered Microstructures

Studying the fracture surfaces of the materials gives a better idea of the morphology of the grains in three-dimensions. The shape of the grains are clearly visible in Figure 4.22, compared to the etched surfaces where the grains often have a rounded appearance in Figure 4.21 (b). The fine grain structure of the RBSN is shown in Figure 4.22. This structure is not conducive to crack deflection due to the small size of the grains, $< 1\ \mu m$. The fracture path is dominated by the pores and other flaws present in the material, resulting in the low strength values which were obtained.

During sintering the Si_3N_4 undergoes transformation from $\alpha \rightarrow$ß-Si_3N_4 and grain growth takes place (Figure 4.23). The larger grains deflect the crack to a greater extent. This coupled with the higher density resulted in higher strength values for these materials compared to the RBSN (Table 4.7). The fracture surfaces of the two reaction bonded materials after sintering were very similar, with both materials exhibiting intergranular fracture. The grains were generally a combination of elongated and equiaxed grains. Figure 4.23 shows many areas where the fracture travelled around the grain, either leaving the grain exposed or areas where grain pulled-out was observed.

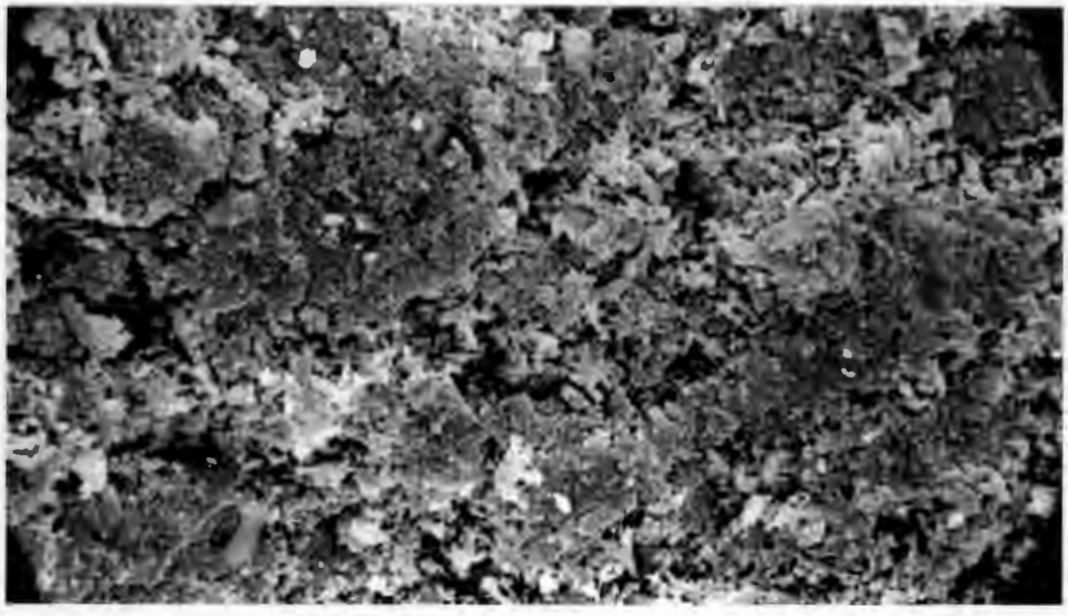

(a)

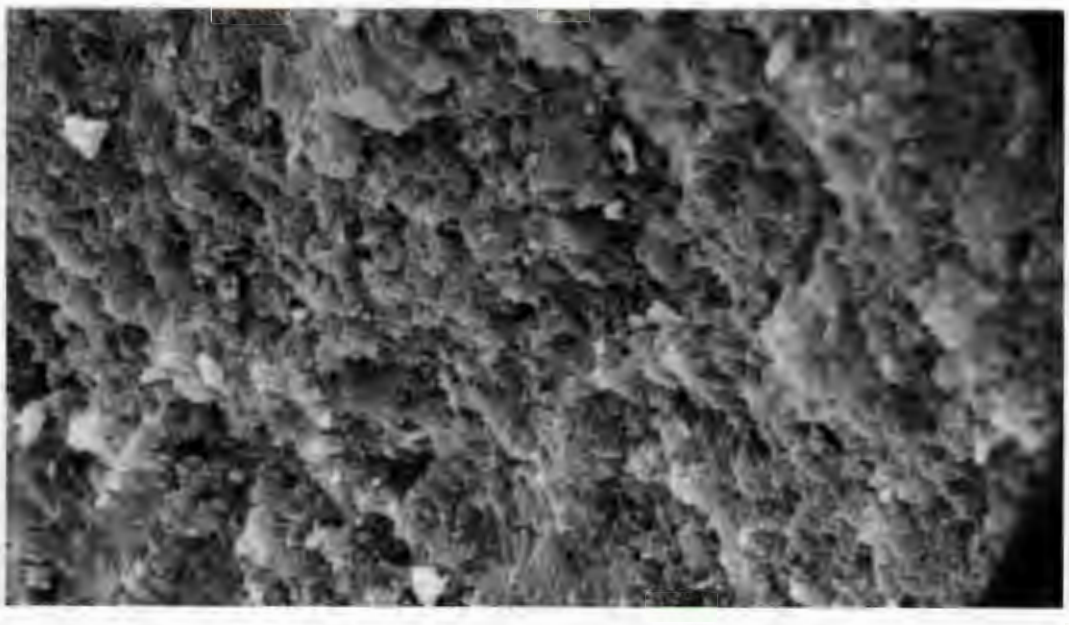

(b)

Figure 4.22: The fracture surfaces of the fine grained reaction bonded (a) Si_2ON_2-rich material and (b) conventional material.

Figure 4.23: A fracture surface of post sintered conventional reaction bonded material showing larger grains than the RBSN materials in Figure 4.22.

4.6.4 Sintered Si_3N_4

4.6.4.1 Effect of Milling the Si_3N_4 Powder

Polished surfaces of materials produced from the mixed and milled Si_3N_4 powders were studied on an optical microscope after the various sintering cycles. It was found that the materials produced from the mixed powders had a large amount of porosity with occasional areas of lower porosity (Figure 4.24(a)). The pores were observed to be up to 100 μm in diameter on occasions, but generally 10 - 30 μm. Finer porosity of <10 μm diameter was also present. The microstructures of the milled material after sintering at the same temperature and rate differed significantly from materials produced from mixed powders. Although porosity was still present (Figure 4.24(b)), it was distributed evenly throughout the material, and it was finer than in the materials produced from the mixed powders.

4.6.4.2 Effect of Temperature and Heating Rate

The microstructures of the materials produced from the mixed powder were not studied as extensively as the milled materials, since they did not perform as well, probably due to the large pores present in the structure (Figure 4.24(a)). The materials produced from the milled powder using various sintering schedules produced high density materials with high strength and hardness and good toughness values. Samples from various sintering schedules of the milled powder compacts (Table 4.8) were polished and etched. Grain growth occurred as the temperature was increased from 1700°C to 1800°C for both heating rates of $100°Ch^{-1}$ and $300°Ch^{-1}$ (Figure 4.25).

The materials sintered at 1700°C differed significantly when sintered at the two heating rates. The slower heating rate of $100°Ch^{-1}$ produced elongated grains of up to 10 μm in length with small grains between the larger ones (Figure 4.25(a)), while those sintered with a heating rate of $300°Ch^{-1}$ were more equiaxed, <5 μm in diameter, (Figure 4.25(b)).

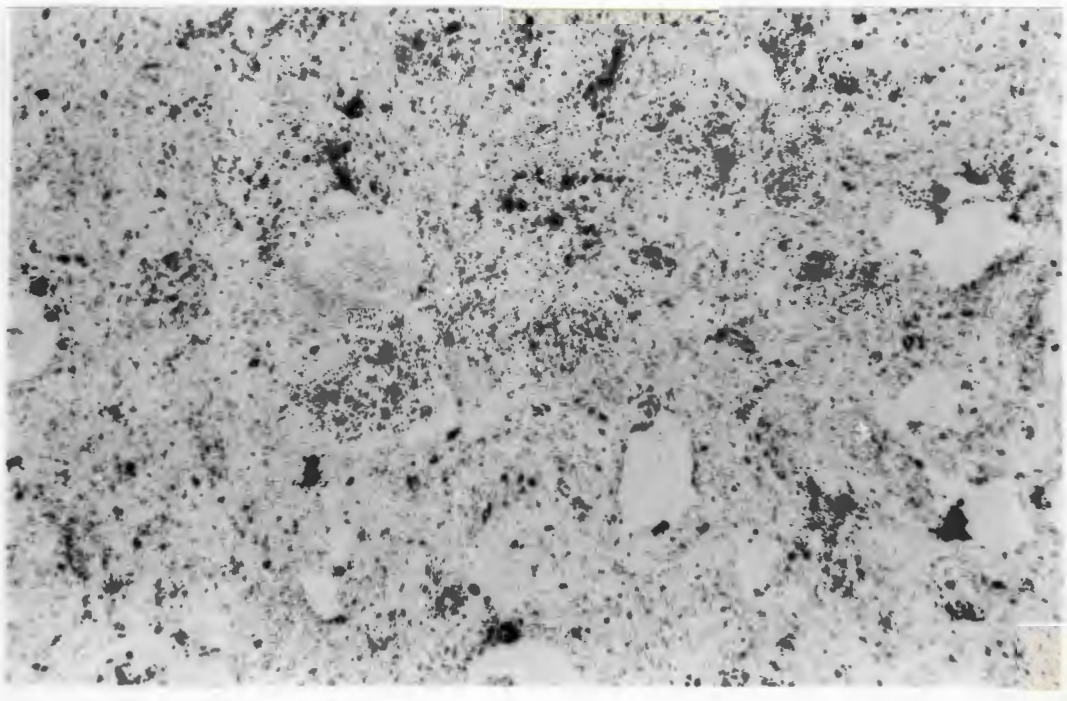

200 μm

(a)

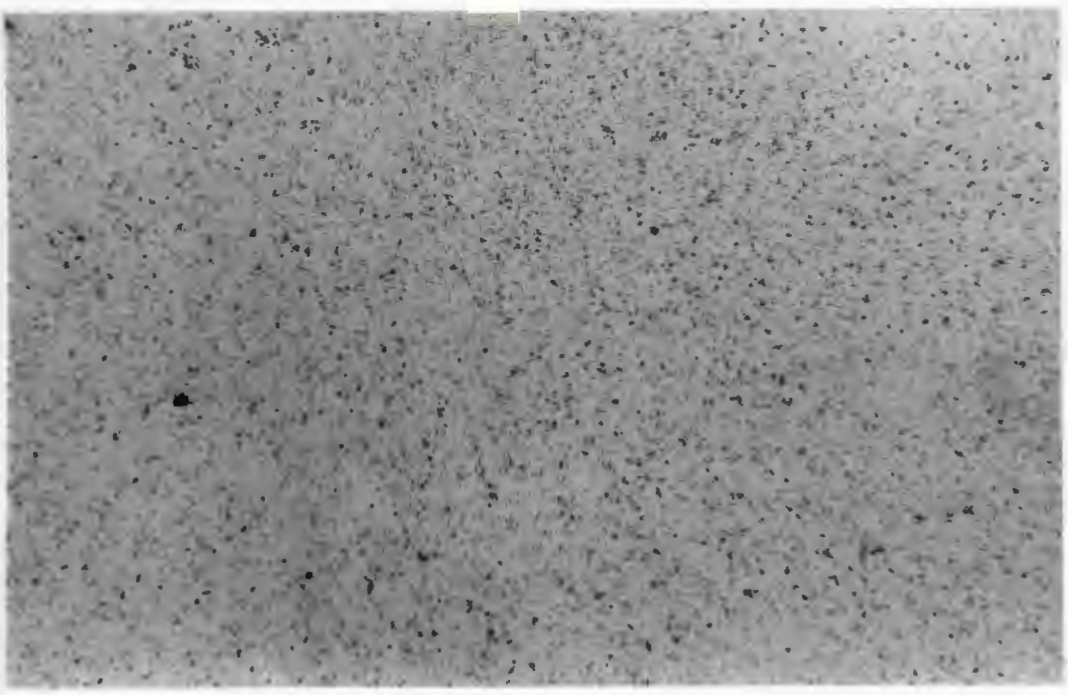

200 μm

(b)

Figure 4.24: Optical micrographs of the polished surfaces of Si_3N_4 materials produced from a) the mixed powder and b) the milled powder after sintering at 1700°C at a rate of 100°Ch^{-1}.

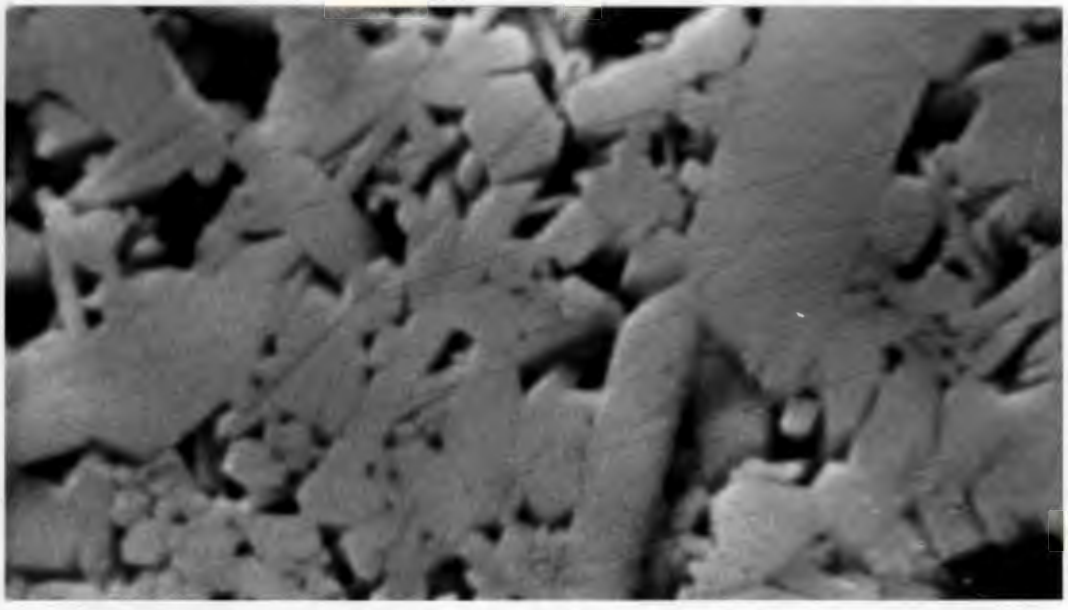

1 μm

(a)

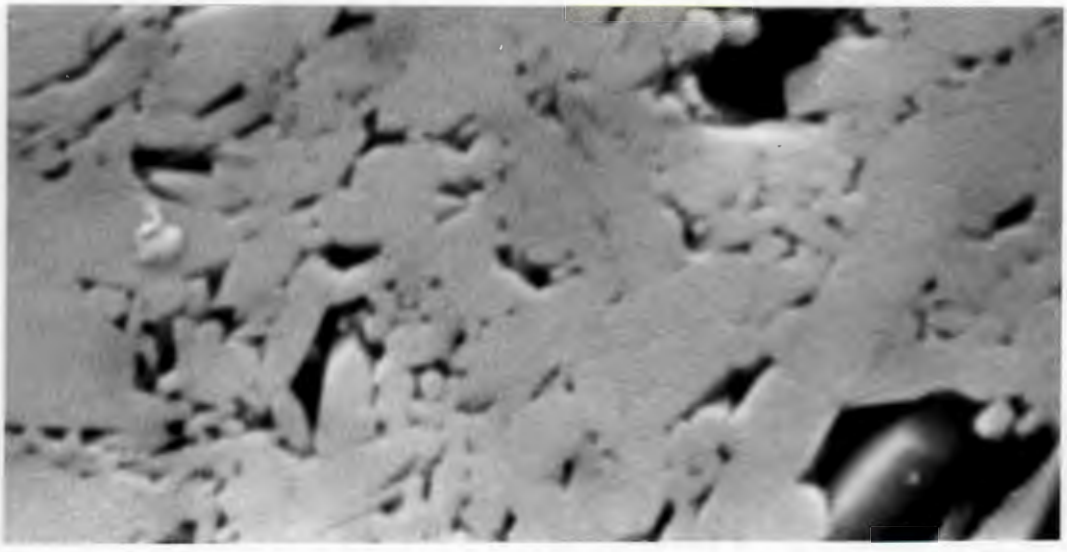

1 μm

(b)

Figure 4.25: Etched surfaces of materials produced from the milled Si_3N_4 powder showing the increase in grain size with an increase in temperature and decrease in heating rate - (a) 1700°C at 100°Ch^{-1}, (b) 1700°C at 300°Ch^{-1}.

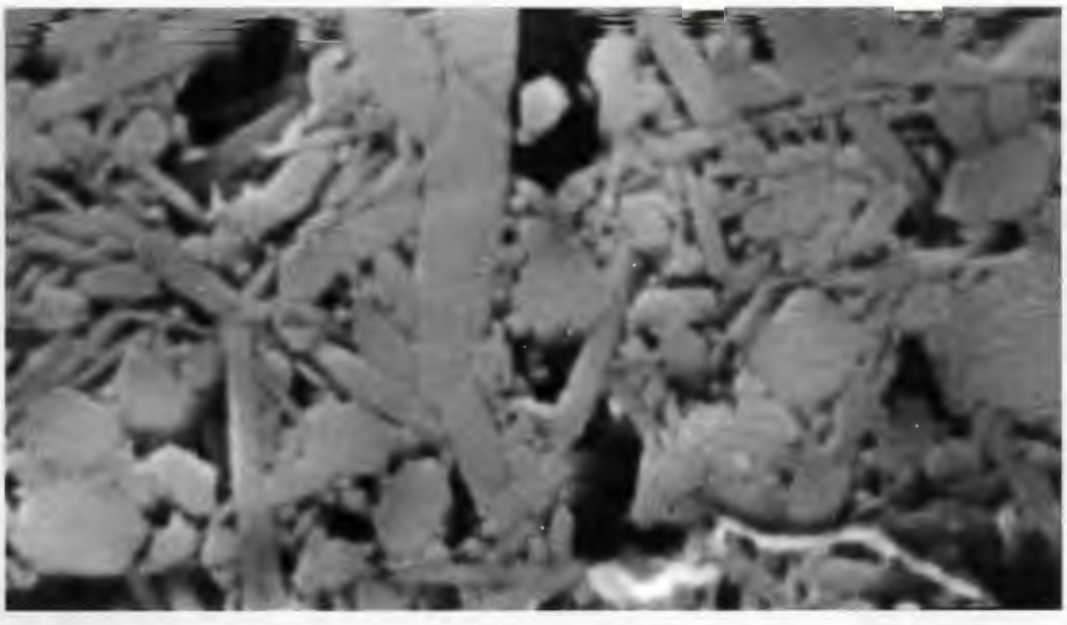

1 μm

(c)

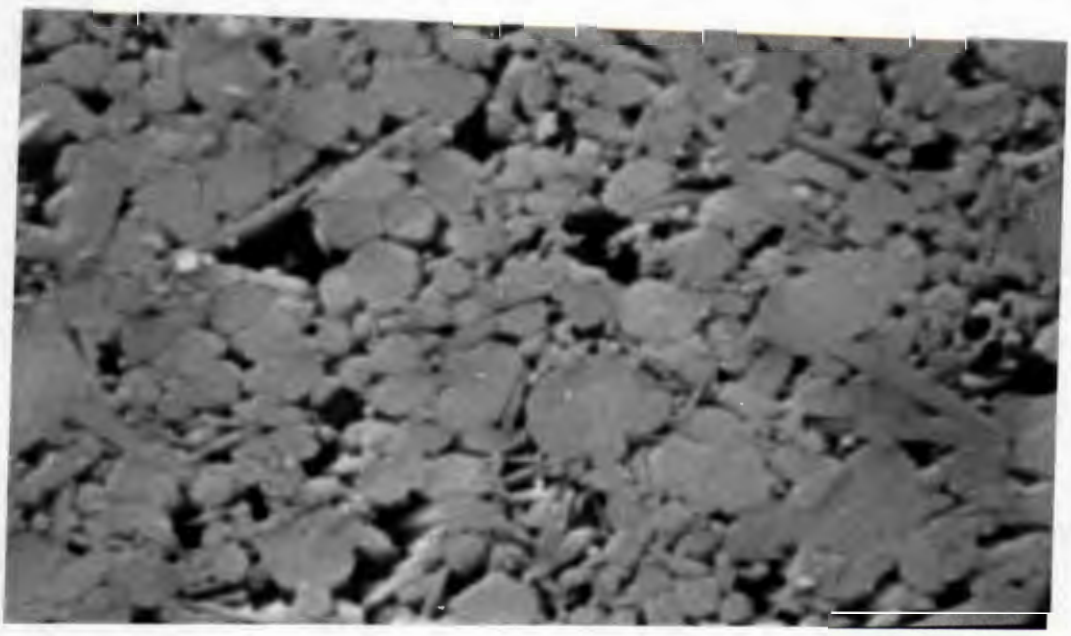

1 μm

(d)

Figure 4.25: Etched surfaces of materials produced from the milled Si_3N_4 powder showing the increase in grain size with an increase in temperature and decrease in heating rate - (c) 1800°C at 100°Ch^{-1}, and (d) 1800°C at 300°Ch^{-1}.

The microstructure of materials sintered at 1800°C at a rate of 100°Ch^{-1} had a wide distribution of grain sizes from submicron equiaxed grains to elongated grains of 10 μm in length (Figure 4.25(c)). The material produced at 300°Ch^{-1} also had a varying grain size distribution, but had fewer elongated grains and the sizes ranged from 0.2 μm to 2 μm in diameter (Figure 4.25(d)).

Figure 4.26 depicts two typical fracture surfaces of materials produced from the milled powders. In all cases studied, the fracture mechanism was found to be intergranular. The shape of the grains of the materials sintered at 1700°C with a heating rate of 100°Ch^{-1} were predominantly elongated (Figure 4.26(a)), which was also observed on the etched surfaces (Figure 4.25(a)). The fracture surface showed the interlocking nature of these grains. When the grains were predominantly equiaxed, as in Figure 4.26(b) (after 1700°C with a heating rate of 300°Ch^{-1}) the grains were found not to interlock.

The fracture surfaces of the materials sintered at 1800°C with a heating rate of 600°Ch^{-1} consisted of a combination of small equiaxed grains of 2 μm and less in diameter, and elongated grains of up to 5 μm in length (Figure 4.27). These grains were slightly smaller than in those materials sintered at 1800°C with the slower heating rates (Figure 4.25).

4.6.4.3 Causes of Failure

The fracture surfaces were also studied to determine the cause of failure. It was found that in most cases the failure was due to processing defects such as inclusions, large grains, or large pores. The most common were large pores which often contained numerous needle-like ß-Si_3N_4 grains with high aspect ratios (Figure 4.28).

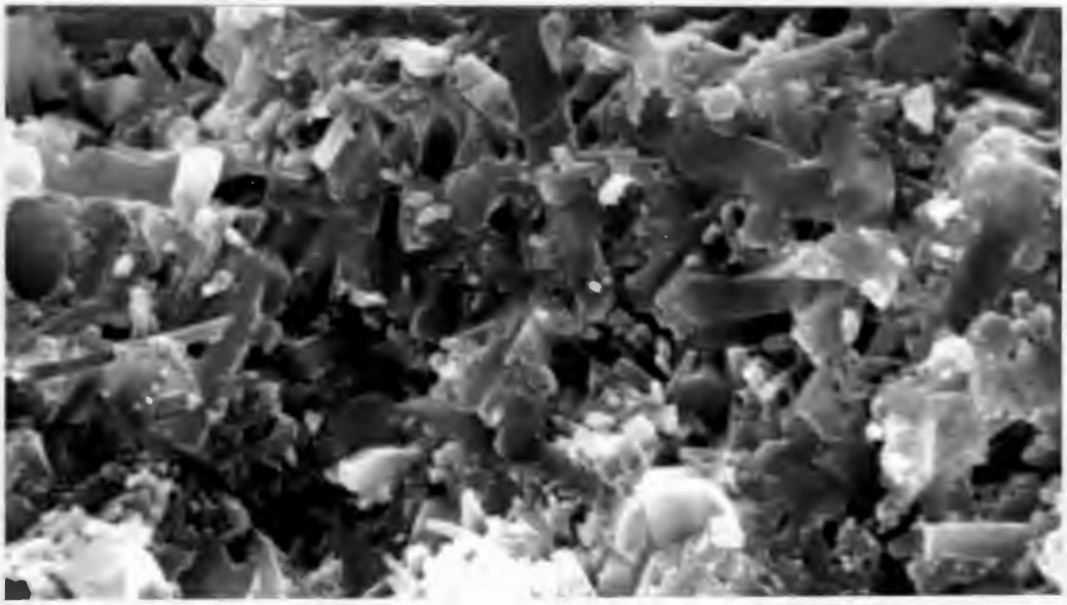

2 μm

(a)

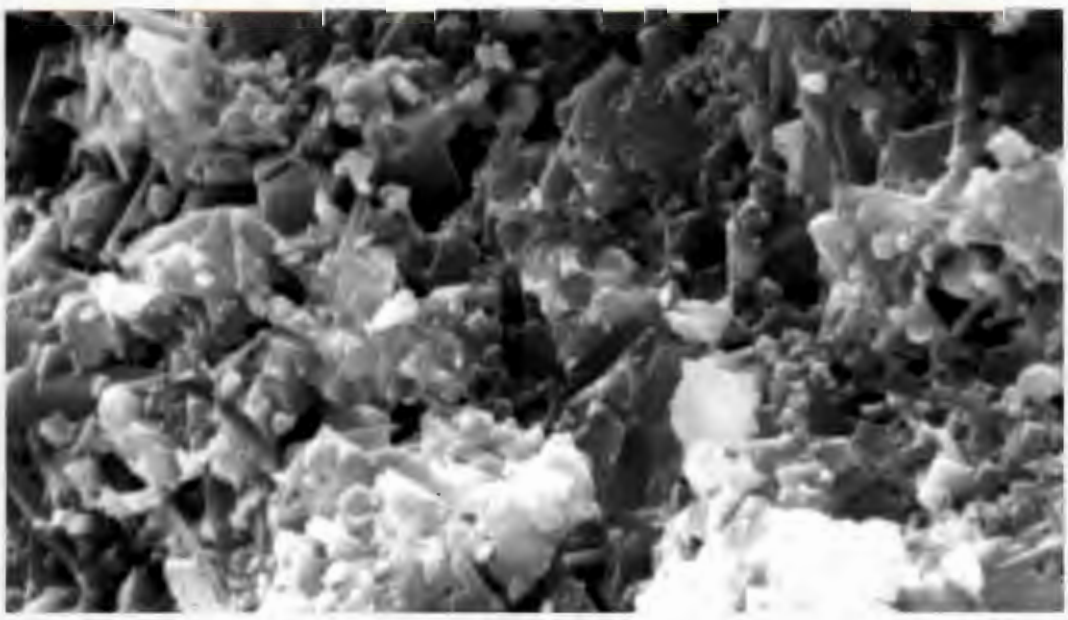

2 μm

(b)

Figure 4.26: Fracture surfaces of materials produced from the milled powder showing the shape of the grains and (a) the interlocking of the elongated ß-Si_3N_4 grains 1700°C at 100°Ch^{-1}, and (b) the lack of interlocking grains after 1700°C at 300°Ch^{-1}.

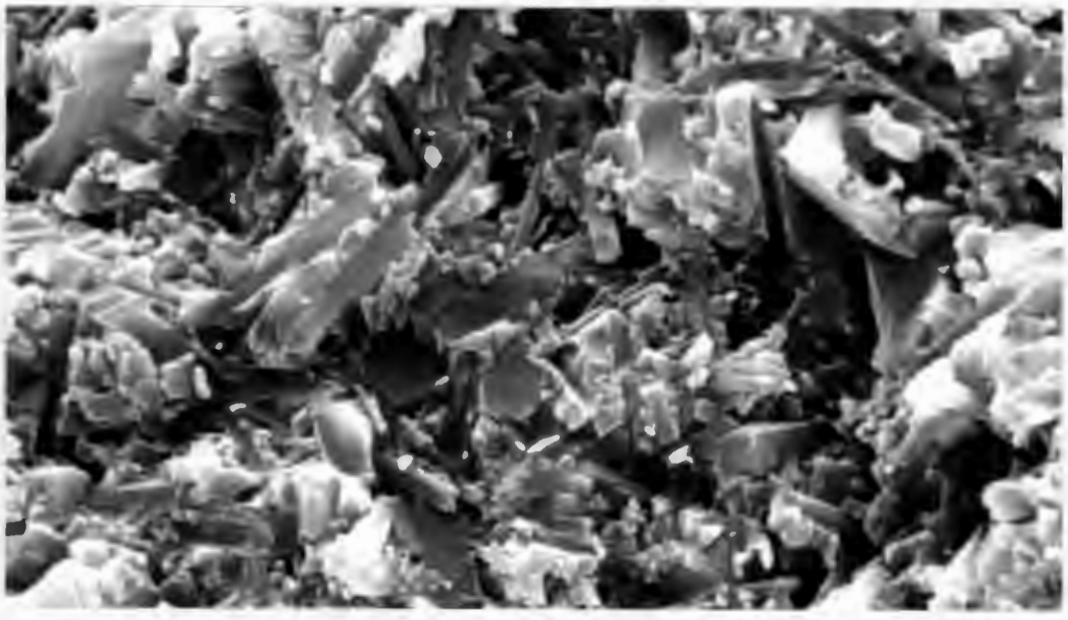

Figure 4.27: Fracture surface of a material sintered at 1800°C with a heating rate of 600°Ch^{-1} showing a combination of small equiaxed grains and larger elongated grains.

Figure 4.28: An example of a common fracture initiating defects in Si_3N_4 materials, showing a large pore with needle-like grains growing inside the pore.

4.6.4.4 Grain Composition - Mixed vs Milled Powder

Transmission electron microscopy was employed to determine what the differences were between the mixed and the milled materials after sintering in order to understand why the former did not densify. A number of samples from the various sintering cycles were studied using the EDS to analyze the grain and grain boundary compositions of these two types of materials.

The mixed powder produced microstructures with large Y_2O_3-rich grains. These grains were often found to be crystalline, but areas of non-crystalline yttrium-silicate glassy phases were also found (Figure 4.29). Table 4.10 summarizes the results of the EDS analyses for the various crystalline and non-crystalline regions in these materials. Distinction was made between large non-crystalline areas and triple-junctions.

The materials produced from the milled powders exhibited fewer large Y-rich areas, and these areas were generally smaller than in the mixed powder materials. The Y_2O_3 was generally found in the triple junctions and grain boundary areas (Figure 4.30). The central grain in this micrograph showed dark areas, and it was found to have a higher Y-content than the two neighbouring grains. Figure 4.31 shows a higher magnification micrograph of a Si_3N_4 material produced from the milled powder. The yttrium was found predominantly in the triple junctions and the grain boundaries, leaving the Si_3N_4 generally free of Y and Al, but there were occasions were the Si-rich grains contained significant amount of Y and/or Al, resulting in a SiYAlON or SiAlON phases, as summarized in Table 4.10 and shown in Figure 4.30. These phases were identified by x-ray diffraction in some of the materials after sintering, but no correlation was found between the phases and the processing routes.

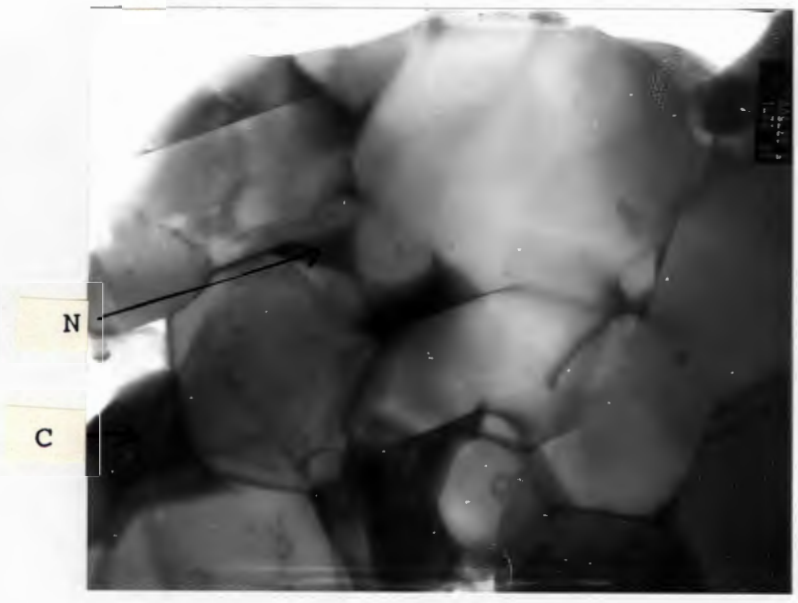

Figure 4.29: A transmission electron micrograph of sintered Si_3N_4 produced from mixed powders. Large areas of Y-rich phases were present, C indicating a crystalline phase and N an yttrium-silicate non-crystalline phase.

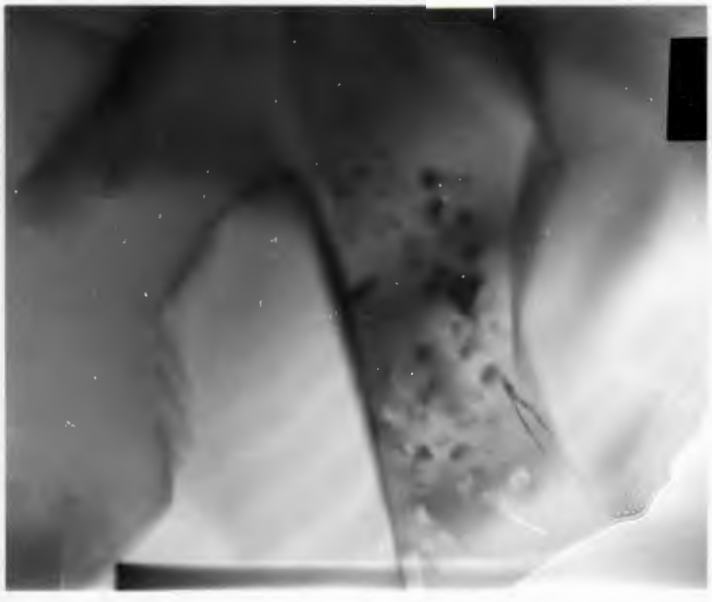

Figure 4.30: TEM micrograph of a sintered Si_3N_4 material produced from milled Si_3N_4 showing the Si-rich (Si_3N_4) grains with darker, Y-rich triple junctions and grain boundaries.

Table 4.10: Summary of the range of compositions found in Si_3N_4 materials produced from both the mixed and milled powders using the EDS system on the TEM.

	Weight %		
	Si	Y	Al
Mixed Powders			
Si-rich Grains	85 - 99	0 - 11	0 - 4
Y-rich Grains	35 - 53	46 - 62	~2
Y-rich non-crystalline	10 - 30	70 - 90	0.5 - 5
Triple Junctions	13 - 18	80 - 85	~2
Milled Powder			
Si-rich Grains	90 - 99	0 - 7	0 - 4
Y-rich Grains	21 - 45	52 - 76	~3
Y-rich non-crystalline	11 - 23	75 - 88	1 - 5
Triple Junctions	6 - 17	83 - 90	1 - 5

Figure 4.31: TEM micrograph showing typical Si_3N_4 grains and yttrium and aluminium rich triple junctions and grain boundaries.

5. Discussion

5.1 REACTION BONDED SILICON NITRIDE

5.1.1 Attrition Milling of Silicon

The attrition milling of the silicon powder was very effective in reducing the particle size. Comparing the time used in attrition milling, 2½ hours, to those quoted for ball milling in the literature, up to 72 hours (Giachello et al (1980)) this is a quick and efficient way of reducing the particle size. Although ZrO_2 milling media was used to mill the silicon powder, no trace of contamination was found. By contrast it has been reported previously that when milling Si_3N_4 powder using ZrO_2 milling media, the ZrO_2 contamination was significant and after sintering a ZrN layer was present on all the Si_3N_4 samples (Barnet and Nel (1989)). The relatively soft silicon powder does not appear to result in such high wear of the ZrO_2 media as the Si_3N_4 since contamination was not detected.

5.1.2 Argon Sintering

5.1.2.1 Effect of Oxygen Addition on Sintering of Silicon

During the first argon sintering cycle, an argon/oxygen atmosphere was used which produced partial oxidation of the silicon powder compacts. These compacts increased in mass and density, but decreased in volume. The increase in density is thought to be primarily due to consolidation of the powder compact and not the oxidation of silicon, since such consolidation was also observed in sintering cycles where pure argon was used.

When using a pure argon atmosphere during sintering, significant mass losses were observed. Such mass losses probably also occurred when oxygen was present, but due to the oxidation it cannot be quantified. The mass gain during the nitriding therefore, cannot be accurately determined for argon/oxygen sintering. There was, however, still sufficient oxygen present in the material and the atmosphere during nitriding to facilitate the formation of Si_2ON_2. Barta and Manella (1985) reported that an oxygen partial pressure of $3.6x10^{-17}$ to $1.2x10^{-24}$ atmospheres is necessary to form Si_2ON_2.

The conventional sintering of silicon in pure argon resulted in a decrease in mass and volume, while the density increased. This loss of mass is attributed to the sublimation of Si at the temperatures which are used, 1175°C. The flowing argon atmosphere through the system removes most of the silicon vapour which forms to establish equilibrium conditions between Si (s) and Si (g). The increase in density is due to partial sintering of the compact and this step appears to influence the nitriding of the Si-compact significantly. In the literature it is noted that the argon sintering also results in the coarsening of the silicon grains, which increases the permeability of the compact due to the formation of large pores (Arundle and Moulson (1977)). This was confirmed during studies of the green silicon and argon sintered silicon microstructures. When argon sintering was eliminated from the processing of RBSN, the mass increase of green silicon compacts was lower than those which had been argon sintered, but the densities were not significantly different. This could be due to the elimination of the sublimation of silicon and the absence of the consolidation of pores during argon sintering. Although the reaction of silicon with impurities such as iron will result in a liquid phase being formed, the grain coarsening and the large pore formation do not take place when the argon sintering is omitted.

When the silicon compact was contained in a smaller vessel, such as a crucible with a lid, and the argon atmosphere is static, the mass loss was reduced to less than 1 % compared to 1-3% when an open crucible was used.

5.1.3 Nitriding

5.1.3.1 Effect of Oxygen During Argon Sintering

Moulson (1979) reported that deliberately oxidised silicon could not be successfully nitrided, but that the addition of 10wt% of iron restored the reactivity. This was not the case with the Si_2ON_2-rich material used in this study, since no iron was added to the system to facilitate the reaction, and a mass gain of ~56% was observed, it is assumed that the reaction proceeded to near completion since very little residual

silicon was observed on the polished surfaces and XRD did not detect unreacted silicon.

The formation of Si_2ON_2 has not previously been reported with the reaction of Si, O_2 and N_2 at atmospheric pressure. Previous methods used in the production of Si_2ON_2 employed hot pressing methods and mixtures of powder consisting of Si + SiO_2 + N_2 (Billy et al (1981)) or SiO_2 + Si_3N_4 (Huang et al (1984)). The method applied during the above experiment was different to that used by Billy and co-workers (1981), since SiO_2 was formed in-situ, and not added separately by mixing powders.

The lower mass increase in the Si_2ON_2-rich material after nitriding can be attributed to a number of things. Firstly, the oxidation of the silicon prior to nitriding made it possible for the Y_2O_3 to react with the SiO_2 to form $Y_2Si_2O_7$ during the nitriding stage. This reaction has a total mass gain of only 23% when formed from Y_2O_3, silicon and oxygen. This could account for part of the discrepancy between the expected mass gain and the actual mass gain after nitriding. Silicon volatilization could account for up to 5% of the mass discrepancy after nitriding. The lower nitriding temperature of 1380°C is not thought to have played a major role in the low of mass gain, since the temperature was held at 1380°C for 8 hours, and no unreacted silicon was detected by x-ray diffraction. It is assumed therefore that the mass gain is mainly related to the phase composition rather than incomplete reaction.

The lower densities found in conventionally argon sintered reaction bonded materials can be attributed primarily to the lower densities after argon sintering. Sample size also had an influence - the larger samples had significantly lower mass increases and more unreacted silicon after nitriding. This in turn influences the final density and the properties of these materials.

5.1.3.2 Effect of Pressing

The mass increase due to nitriding is related to the density of the compact after cold isostatic pressing. An optimum green density is required, which will be sufficiently

dense to result in a high density RBSN compact after nitriding, but also permeable enough to allow gas to enter and react before pore closure takes place (Riley (1977)). Higher pressing pressures resulted in the compact being more dense. The pore structure is finer and therefore pore closure occurs before the nitriding reaction is complete. The mass gain of materials pressed at the higher pressures therefore is less than those pressed at the optimum pressure found in this study of 160MPa. At lower pressures, the compact is less dense and therefore the initial green density will not be high enough to produce high density RBSN due to significantly more residual porosity. This results in lower densities. The lower mass increase of these materials can also be attributed to the higher porosity, resulting in a higher surface area from which the silicon could sublime.

5.1.3.3 Phase Analysis

The phases present in the argon sintered reaction bonded material were mainly α-Si_3N_4, formed by a vapour phase reaction between silicon and nitrogen; ß-Si_3N_4, formed by direct nitridation of the liquid silicon (Riley (1977)); and $Y_2Si_2O_7$, a reaction between Y_2O_3 and surface SiO_2. Si_2ON_2 was also present, but it was confined to the surface. No oxynitride was detected in the bulk material. The Si_2ON_2-rich material was nitrided below the melting point of silicon. This should reduce the formation of ß-Si_3N_4 which forms mainly from the nitridation of liquid silicon. ß-Si_3N_4, however, was present and it would seem that the presence of oxygen enhanced the formation of the ß-phase. By contrast conventional argon sintered RBSN had a smaller fraction of ß-Si_3N_4.

5.2 POST SINTERED RBSN

5.2.1 Effect of Temperature and Atmosphere

Post-sintering runs of the RBSN materials in argon gas confers no benefits compared to nitrogen atmospheres. The Si_3N_4 starts to dissociate in the sintering temperature range, ~1800°C. Without the presence of N_2 in the atmosphere the reaction

$$Si_3N_4\ (s) \rightarrow 3Si\ (l) + 2N_2\ (g)$$

will tend to the right of the equation. The use of a powder bed of Si_3N_4-BN provided a nitrogen partial pressure in the crucible, and therefore the dissociation of the Si_3N_4 was partially inhibited.

Sintering reaction bonded Si_3N_4 (both Si_2ON_2-rich and conventional materials) resulted in densities ranging from 3.15g/cm^3 to 3.25g/cm^3. The post sintered conventional RBSN had the highest densities after sintering at 1750°C (3.25g/cm^3). Sintering these materials at 1800°C produced the lowest densities, 3.17g/cm^3. This could be due to the dissociation of the Si_3N_4 or oversintering. Sintering the Si_2ON_2-rich material at 1800°C produced the higher density materials, 3.22g/cm^3 compared to 3.18g/cm^3 after 1750°C. The densities of the post sintered materials were also higher than most of those obtained for sintered Si_3N_4 which had a higher concentration of additives to facilitate sintering. It was thus demonstrated that it is possible to reduce the liquid phase content of silicon nitride by pursuing a post-sintering route.

Mass losses were observed after sintering at all temperatures above 1700°C. At 1750°C the mass loss was virtually the same for both the conventional RBSN and the Si_2ON_2-rich materials, ~4%. This can be attributed to the dissociation/evaporation in conventional RBSN while in the Si_2ON_2-rich material the mass loss could be due to the loss of oxygen in the $Si_2ON_2 \rightarrow Si_3N_4$ reaction and dissociation/evaporation of Si_3N_4.

Sintering at 1800°C resulted in a mass loss of ~7% for the Si_2ON_2-rich material, while the conventional material lost an average of 8.8% of the presintered mass. It would seem that the higher temperature enhanced the dissociation/evaporation of the Si_3N_4 considerably. The high mass loss in conventional RBSN material after sintering can only be attributed to the dissociation of Si_3N_4. The Si_2ON_2-rich material appeared to be relatively more stable since the mass loss of ~7% was a combination of the loss of O_2 when converting Si_2ON_2 to Si_3N_4 (7wt%/mol of silicon) and the dissociation/evaporation of Si_3N_4. Since a quantitative analysis of the phases was not possible, the exact mass loss due to the loss of oxygen could not be determined, but the maximum oxygen content was ~2% of the compact mass, when taking into account the mass gained on argon sintering and nitriding, and assuming that no oxygen

was lost during nitriding. Not all the oxygen in the system was lost, since $Si_3Al_2Y_{10}O_{18}N_4$ and $Y_2Si_2O_7$ were still present after sintering.

5.2.2 Phase Analysis

After the post sintering cycles the major phase present was ß-Si_3N_4, which is expected since the sintering took place at more than 150°C above than the transformation temperature (1500 - 1600°C). No Si_2ON_2 was detected in the sintered samples. It would seem that the oxygen is easily displaced by the nitrogen when using a nitrogen atmosphere and sintering at 1750°C or higher. A partial pressure of oxygen would be necessary to retain the Si_2ON_2 phase. Some of the oxygen is, however, retained in the structure in the form of $Y_{10}Si_2Al_3O_{18}N_4$ and $Y_2Si_2O_7$ after sintering, which results from the reaction of either Si_3N_4 or Si_2ON_2 with Al_2O_3 or Y_2O_3 additives.

The minor phases present in the post sintered materials seem to be influenced by additive concentrations in specific areas, which determine the liquid phase composition and the phases which crystallize from this liquid. There was no correlation between the initial phases present and the final composition of the material.

5.3 SINTERED Si_3N_4

5.3.1 Effect of Milling Si_3N_4 Powder

The importance of milling the Si_3N_4 powder mixtures before using them to produce components can be seen in the resulting densities and strengths of the two batches of sintered Si_3N_4 produced from milled and mixed powders. The other properties appear to be less sensitive to this step. The particle size was not significantly reduced during milling, and it was initially thought that the milling might increase the amount of oxygen present by further oxidising the surface of the Si_3N_4. This, however, was not the case, since the oxygen levels in both powders were not found to be significantly different using Auger spectroscopy. The x-ray diffraction analysis did not show any major differences either. Some of the minor peaks were not as well defined in the milled powder diffraction pattern, but there were no significant differences which could have indicated more oxide being present in the milled powder. The attrition milling appears to result in better mixing of the additives in the Si_3N_4

powder, resulting in a more evenly distributed additive. This will be discussed in more detail in section 5.5.3.

5.3.2 Effect of Sintering Temperature and Heating Rate

The heating rate and final sintering temperature played an important part in the sintering of milled and mixed Si_3N_4. The milled powders produced ceramics of higher density than the mixed powders for all sintering schedules except 1700°C at a rate of 100°Ch^{-1}, where the densities were the same.

In contrast to the RBSN materials, the materials sintered at the higher temperature, 1800°C, produced the higher densities and better properties.

Most of the powder compacts sintered to higher densities when the faster heating rate was used. This is contrary to what was expected and what was reported by Campbell and Dutta (1982), since at the slower rate more rearrangement and solution precipitation can take place before the maximum temperature is reached, when the grain growth and solid state sintering takes place. The exception to this trend was seen when the milled powder compact was sintered at 1800°C. The slower rate produced the higher density, but the strength was not as high as those sintered with heating rates of 300°Ch^{-1}. When an even higher rate of 600°Ch^{-1} was used, this again gave higher densities than both the slower rates, and although the strengths were lower, the hardness values were higher and the toughness values were in the same range as those of the slower sintering cycles.

5.3.3 Phase Analysis

The extent of phase transformation on sintering depended on the temperature and rate of sintering. The fast heating rate at 1700°C did not seem to allow sufficient time for full transformation to take place. When sintering at 1700°C with the slower rate, no α-Si_3N_4 was observed and therefore it is assumed that complete transformation took place. Sintering at 1700°C with the slower heating rate appears to be necessary to facilitate complete transformation, which is expected when using Y_2O_3 as an additive (Hampshire and Pomeroy

(1985)). This was true for the mixed and the milled powders. No α-Si_3N_4 was detected in any of the materials after sintering at 1800°C.

The mixed powders showed less residual α-Si_3N_4 than the milled powders after sintering at 1700°C with a heating rate of 300°Ch^{-1}. Significant amounts of Y_2O_3 were also present in these materials. This was not anticipated since the Y_2O_3, Al_2O_3 and surface SiO_2 were expected to react to form the liquid phase via which sintering should have taken place. The presence of Y_2O_3 in the sintered material suggests that not all the Y_2O_3 was used to form the liquid phase. This could be the reason for the low density. The less liquid phase present, the more difficult it would be to sinter the Si_3N_4 when external pressure is not applied.

The transformation of α-Si_3N_4 to ß-Si_3N_4 on sintering appeared to be slower for milled compared to mixed powder compacts. More α-phase relative to ß-phase was present after sintering at 1700°C with a rate of 300°Ch^{-1} compared to the mixed powder materials. Only half of the Si_3N_4 was present in the ß-phase. Sintering at 1800°C did not leave any residual α-Si_3N_4, but there was significant amounts of Θ-$Si_3Al_3O_9N_{10}$, which is formed by the reaction of α-Si_3N_4 and Al_2O_3 (Jack (1991)). The major phase present was ß-Si_3N_4 and traces of Y_2O_3 were also present. When the heating rate was slowed down to 100°Ch^{-1}, the major phase was again ß-Si_3N_4 for both temperatures. It is also thought that in these materials, as with the PSRBSN, the local additive content in a specific areas during sintering influences the final composition of the minor phases.

5.4 MECHANICAL PROPERTIES

5.4.1 Reaction Bonded Si_3N_4

5.4.1.1 Effect of Argon Sintering

The properties of RBSN materials are seen to be dependent on the density and phases present. The presence the harder of Si_2ON_2 (Billy et al (1981)) positively influenced the hardness of the nitrided material with a slight reduction in toughness. The Si_2ON_2-rich reaction bonded material had higher densities which can also improve the hardness, but it is believed that the presence of Si_2ON_2 is the main contributor to this higher hardness. This is in keeping with the results reported by Paterson (1988).

The materials which were not argon sintered had lower strengths and hardness values compared to the RBSN materials which were argon sintered. The toughness of these materials appears to be much higher than the other reaction bonded materials, but it was difficult to measure these crack lengths due to the high porosity, and therefore these values could be slightly inflated.

The strength of the RBSN materials is relatively low, due to the large number of pores and areas where localised melting of the silicon took place as these act as fracture initiation sights. The RBSN materials' strengths were even lower when the argon sintering step was omitted from the processing route. This is thought to be related to the lower mass increase observed after nitriding, which indicates that residual silicon could be present. The residual silicon metal produces flaws in the ceramic matrix as it melts during sintering, and these could cause premature failure of the material.

5.4.2 Post Sintered Reaction Bonded Si_3N_4

5.4.2.1 Effect of Si_2ON_2 in Reaction Bonded Si_3N_4

On sintering, the hardness values increased dramatically from ~5GPa to >14GPa. This was accompanied by an increase in the density, but no direct correlation between density and hardness was observed. The originally Si_2ON_2-rich material exhibited lower hardness values after sintering than the conventional RBSN material, while the toughness values were in the same range.

5.4.2.2 Effect of Sintering Temperature

Sintering the reaction bonded materials at 1800°C produced ceramics with higher hardness and toughness values than those sintered at 1750°C. This result was contrary to the generally accepted trend that an increase in hardness is accompanied by a decrease in the toughness of a material. The lowest density material of the post sintered materials had the highest hardness values, which was not expected. The materials sintered in the argon atmosphere at 1800°C also had higher hardness than

the materials sintered at 1750°C in nitrogen. The densities of these materials were, however, relatively high.

5.4.3 Sintered Si_3N_4

The sintered Si_3N_4 materials did not exhibit such clear cut trends as the post sintered RBSN materials. There was no obvious relationship between density, toughness and strength as was found in the RBSN materials. It is thought that the mechanical properties are influenced more by the resulting microstructures than the densities of the materials. Various sintering schedules were used to manipulate the microstructure and in so doing the properties were influenced. This will be discussed further in the next section, but it would seem that the strength is influenced positively by a wider distribution of grain sizes with both large elongated grains and smaller equiaxed grains situated between the large grains.

5.4.3.1 Effect of Milling

The density and strength of the milled materials were generally higher than the mixed materials. The hardness and toughness, however, did not seem to be influenced as significantly by the milling process. The strengths were generally significantly higher for the milled materials, and this is probably due to the fact that the strength is highly dependent on the flaw size in the material. The lower densities imply more porosity in the material produced from the mixed powder, which results in more of fracture initiation sites in the sintered body. The average pore size in these materials was observably larger than those of the material produced from the milled powder.

5.4.3.2 Effect of Sintering Temperature and Heating Rate

The hardness was related to the density when sintering at a specific temperature. At 1800°C, it was seen that the hardness increased with an increase in density for the materials produced from the milled powder. Although there were only two sintering runs at 1700°C, this trend was also followed for these materials produced from the milled powder. It was expected that the α-content would play a role in the hardness of the materials, since it has been found that the α-Si_3N_4 has a higher hardness than ß-Si_3N_4 (Greskovich and Gazza (1985)). This was not confirmed in the results

obtained, since the α-rich Si_3N_4 had lower hardness values in some cases. This cannot necessarily be taken as a contradiction of the results of Greskovich and Gazza (1985), since in this study there was a mixture of both ß-Si_3N_4 and α-Si_3N_4, and the microstructure of the materials differed in each sintering schedule. It does indicate however, that microstructural variation has a significant influence on hardness and that relative hardness of phases may be masked by microstructural differences.

Sintering at the faster rate of 600°Ch^{-1} resulted in higher densities and hardness values for the Si_3N_4. The strength, however, was much lower than those obtained at the slower heating rates, and the toughness was also very low. The smaller grains of these materials cannot deflect the cracks as much as the larger grains obtained with the slower heating rates, resulting in the lower toughness values.

5.4.3.3 Effect of Microwave Drying

Microwave drying of the powder after milling resulted in the highest densities and hardness values for the study. The strength was, however, lower and the toughness was in the same range as those obtained with the slower heating rates with conventional oven dried powders. The lower strengths are attributed to flaws in the sintered compacts. The high density and hardness values indicate that microwave drying of the slurry has no detrimental effect on the sintering process.

5.5 MICROSTRUCTURE

5.5.1 Argon Sintered Silicon

Argon sintering had a pronounced effect on the microstructure of the silicon compact. Coarsening of the silicon grains was observed and is reported to improve the permeability of the compact (Popper (1978)). This appears to be an important step in the processing of RBSN, since the mass gain after nitriding was considerably higher than when the argon sintering step was omitted.

A number of pores were observed on the fracture surfaces of both the pressed and the argon sintered silicon compacts. These pores are thought to be due to poor packing of the powder

on forming. It is not thought that these pores were due to grain pullout from the matrix on fracture, since in the pressed compact, the grains were generally smaller than the pores, which were ~2 μm and larger, while in the argon sintered compacts a thread-like network was observed to pass over many of the pores. If a grain had been pulled out to form the pore, it would not have left these "threads" intact.

5.5.2 Reaction Bonded Si_3N_4

The large pores observed in the argon sintered compacts cannot be completely filled in by the 22% volume change which occurs when the silicon reacts with the nitrogen to form Si_3N_4, and they therefore influence the properties of the RBSN and PSRBSN materials. They result in lower densities and lower strength values in these materials.

Evidence of these pores were clearly visible on the polished surfaces of both the reaction bonded materials. There was, however, a noticeable difference in porosity between the bulk material and the surface layers. The surface layers were less porous, and the pores were much smaller than in the bulk material.

The lower porosity observed around the residual silicon can be attributed to the silicon melting in the later stages of nitriding, and then reacting with nitrogen in the liquid phase. The molten silicon would then have filled in the pores in the vicinity, resulting in lower porosity. The residual silicon present in these materials after nitriding can be attributed to pore closure due to the formation of the Si_3N_4, which prevented the nitrogen from reaching the silicon. It is very likely that other lower porosity areas on the RBSN polished surfaces in Figure 4.12 were formed in a similar manner, with the exception that the molten silicon reacted completely before pore closure could take place.

Examining these RBSN surfaces in the scanning electron microscope revealed an evenly distributed Y-rich phase throughout the material. This is probably the Y_2O_3 additive which was mixed in with the silicon powder prior to forming, and the distribution is ideal for the post-sintering of the RBSN. This even distribution of the Y_2O_3 can better facilitate sintering relative to less well distributed oxide phases.

The small grains observed on the fracture surfaces of the RBSN materials, however, did not allow for much crack deflection and resulted in the low toughness values for these materials. The large pores present in the material were also seen on the fracture surfaces, and resulted in the low strengths. These pores can be minimized by spray drying the silicon powder after milling, which will result in a powder with better flow properties, and the particles will be more uniform in size than those obtained by conventional drying and sieving.

5.5.3 Post Sintered Reaction Bonded Si_3N_4

Although the microstructures of the reaction bonded Si_2ON_2-rich and conventional RBSN materials were not significantly different, the microstructures obtained after post sintering were found to be dependent on the original composition and the temperature at which the sintering took place.

A bright phase observed on the optical microscope near the edge of the polished surfaces was present in all sintered materials. This phase was not silicon, which was seen in the reaction bonded materials. The phase is thought to be an Y-rich phase. The fact that it is not present along the edges of the samples can be attributed to the migration of the additive to the powder bed. Since the powder bed did not contain additives as recommended by Mangles and Tennenhouse (1981), the additive could have migrated into the bed in order to establish an equilibrium between the bed and the ceramic.

5.5.3.1 Effect of Si_2ON_2 or its Absence on Phase Distribution

The finer porosity found in Si_2ON_2-rich material after sintering confirms that this material sintered to a fairly high density at both 1750°C and 1800°C. No other phases or significant features were seen.

A distinguishing factor of conventional RBSN after post sintering was a third phase which was observed at high magnification on the optical microscope. This is assumed to be an Y-rich phase. When studying both the Si_2ON_2-rich and conventional materials in the scanning electron microscope after post sintering, the Y_2O_3 distribution could clearly be seen when using the back-scatter imaging mode.

5.5.3.2 *Effect of Sintering Temperature*

The polished sections made visible the Y_2O_3 distribution after sintering. Grain size can be inferred, since the larger the grains, the larger the areas between the Y_2O_3-rich regions. The materials sintered at the higher temperature had larger grains, and the Y_2O_3-rich regions were further apart than those of the smaller grained material sintered at 1750°C.

This was confirmed by etching the polished surfaces in molten KOH. During the etching process, the intergranular Y-rich phase was removed, leaving the Si_3N_4 grains clearly visible. The larger grains in the materials sintered at the higher temperatures can be partly attributed to the longer time spend in the sintering temperature region, thus giving more time for grain growth which takes place in the final stage of sintering. Another contributing factor is the fact that the higher temperature lowered the viscosity of the liquid phase, and thus facilitated quicker mass transport in the solution-reprecipitation stage of sintering. This increased the rate of precipitation of the grains from the liquid phase, and the growth rate of these grains.

5.5.3.3 *Reaction Bonded Si_3N_4 vs Post Sintered RBSN*

The grains in the sintered reaction bonded materials were much larger than those of the reaction bonded materials, and this along with the increased density and lower porosity resulted in the improved strength values for these materials. The shape of the grains after sintering was found to be generally elongated and needle-like, with some grains being more equiaxed. The elongated grains tend to form interlocking networks which act as a reinforcement in the ceramic matrix, and thus improving the strengths. The needle-like grains are typical of ß-Si_3N_4 grains after sintering a material which had a high α-Si_3N_4 content. The presence of α-Al_2O_3 promotes the growth of elongated ß-Si_3N_4 grains (Lange (1980), Wötting and Ziegler (1986(a))). α-Si_3N_4 grains are generally equiaxed, as was seen in the fracture surfaces of the reaction bonded materials.

5.5.4 Sintered Si_3N_4

5.5.4.1 Effect of Milling the Si_3N_4 Powder

The milling of the Si_3N_4 powder played a significant role in the production of the final sintered ceramic product. Although the attrition milling did not significantly reduce the particle size of the Si_3N_4 powder, the final microstructures of the materials produced from these powders showed a much more uniform structure compared to those produced from the mixed powder. The lower porosity areas in the mixed powder materials were thought to be the result of agglomeration of the powder particles which were not broken down during the mixing process. These agglomerates would have been broken during the milling process, and thus these areas of lower porosity are absent in the materials produced from the milled powder. It would also appear that milling the powder resulted in better packing efficiency compared to mixed powder. Although porosity was still present in the materials produced from the milled powder, the porosity was finer and distributed uniformly throughout the material. This fine porosity reduces the critical flaw size in the material, and therefore has a positive effect on the strengths.

5.5.4.2 Effect of Sintering Temperature and Heating Rate

As with the post sintered reaction bonded Si_3N_4, the sintered Si_3N_4 materials were influenced by the temperature at which the sintering took place. It was also observed that the heating rate also influenced the final microstructure. The increase in grain size when increasing the temperature is due to the same factors as discussed for the post sintered RBSN, namely the increased time spent in the sintering temperature region, and the lower viscosity of the liquid phase, which facilitates the mass transfer during sintering.

The elongated grains present in the Si_3N_4 materials after sintering at 1700°C with a heating rate of $100°Ch^{-1}$ can be attributed to the length of time spend in the sintering region, which is three times longer than those materials sintered at the faster heating rate. This allows more time for the mass transport of the Si_3N_4 via the liquid phase to the ends of the grains where the grain growth is preferential in the ß-Si_3N_4.

Sintering at 1800°C reduced differences in the microstructures. Grains were much larger than those found in materials sintered at 1700°C. At 1800°C the viscosity of the liquid phase is lower and therefore the mass transport is faster for both heating rates. The grains in the materials sintered with the slower heating rate were, however, larger and there were more elongated grains than those sintered at a rate of $300°Ch^{-1}$, due to the longer time spent in the sintering temperature range. Those materials sintered at a heating rate of $600°Ch^{-1}$ exhibited even smaller grains, thus confirming that the grain size is dependent on the processing conditions as reported by Tajima et al (1988).

The interlocking nature of the ß-Si_3N_4, as discussed previously, was also observed in the sintered Si_3N_4 materials and it was expected that the materials with the high concentration of elongated Si_3N_4 grains would exhibit the higher strengths due to the reinforcement, but this was not the case since at both temperatures the materials sintered at the faster heating rate, $300°Ch^{-1}$, exhibited the higher strengths. The slightly higher density of the materials sintered at 1700°C with the heating rate of $300°Ch^{-1}$ can be a contributing factor to the higher strengths, but this trend was not observed when sintering the Si_3N_4 at 1800°C. The strengths were higher when using the faster heating rate, despite the slightly lower density compared to sintering with the slower heating rate. This may be due to grain coarsening which reduces the strength (Campbell and Dutta (1982)) despite the interlocking character of the grains.

5.5.4.3 Grain Composition

In order to determine the reason why the mixed powders did not produce dense ceramics with good microstructures and properties, transmission electron microscopy was used to investigate the grains, grain boundaries, and triple junctions in the sintered materials.

These results supported the proposal discussed earlier that the mixing of the powder did not break down the agglomerates in the powder, since the Y_2O_3 was also found in discrete large grains, and was not confined to the intergranular regions. These

large areas which were rich in yttrium were found to be both crystalline and non-crystalline, and usually contained significant amounts of silicon. The concentration of Y_2O_3 in these areas would prevent the effective sintering via the liquid phase since the liquid phase would not surround all the grains and sintering could only take place in areas where the liquid phase was present. This might also be an alternative explanation for the presence of lower porosity regions observed on the polished surfaces of the mixed powder materials. These regions could have had a higher concentration of Y_2O_3 present and therefore sintering could have been better facilitated in these regions.

In the materials produced from the milled powders, there were also Y-rich regions, but these areas were generally smaller than those discussed above, and they were not as numerous. The observation of Y and Al in some of the predominantly Si-rich grains gives and indication of the formation of SiAlON and SiYAlON phases in the sintered Si_3N_4. These phases were identified in some of the materials by X-ray diffraction.

5.5.4.4 Causes of Failure

When studying the fracture surfaces, it was found that the main causes for failure in the Si_3N_4 ceramics produced during the study were large pores and inclusions in the structure. Both these defects are introduced during the early stages of processing, such as powder preparation and pressing of the compact. Agglomeration of the powder and the introduction of impurities during the powder preparation could result in the inclusions observed. The larger pores which were found could be due to poor packing during forming or due to an uneven distribution of the binder used to facilitate pressing in the RBSN materials.

6. Conclusions

6.1 GENERAL CONCLUSIONS

Post sintering reaction bonded Si_3N_4 materials and sintering Si_3N_4 powders produced high density Si_3N_4 materials with comparable densities.

Sintering conditions influenced the physical and mechanical properties of all the materials studied. Higher sintering temperature produced higher densities for the sintered Si_3N_4 and post sintered RBSN materials which were rich in Si_2ON_2. The higher sintering temperature, however, resulted in lower densities for the conventional RBSN.

An increase in the density was generally accompanied by an increase in the hardness and the strength, but there were exceptions to this trend in both the post sintered conventional RBSN and the sintered Si_3N_4.

Although the densities of the post sintered RBSN materials and the sintered Si_3N_4 materials were comparable after sintering, the post sintered RBSN materials had higher hardness values compared to the sintered Si_3N_4, while the latter had the higher strengths. The lower strength in the post sintered RBSN was probably due to the large pores present in material which decreases the strength of the material.

The microstructures showed that sintering at the higher temperatures resulted in larger grains. In some cases excessive grain growth was observed, which has a detrimental effect on mechanical properties. The higher sintering temperature also resulted in lower densities in the conventional RBSN which was ascribed to oversintering, since larger pores were observed in these materials after sintering at the higher temperatures.

Finally, dense Si_3N_4 materials were produced using two processing methods. The sintered Si_3N_4 materials exhibited higher strength and toughness values, while the post sintered RBSN had higher hardness values. The sintered Si_3N_4 materials, however, utilized a higher concentration of additive which results in a more costly starting material, but the sintering schedules were much shorter than those used for the post sintered RBSN.

A number of specific conclusions regarding the conditions used and materials produced will be discussed in more detail below.

6.2 ARGON SINTERING AND RBSN

1. Argon sintering produced a coarsening in the silicon grains and was also observed to produce a thread-like network throughout the structure.

2. Eliminating the argon sintering step resulted in a lower mass increase on nitriding, and more residual silicon being present after nitriding.

3. A mass loss of up to 3% occurs during argon sintering. This can be minimized by enclosing the samples in a crucible.

4. A Si_2ON_2-rich material was readily formed below 1400°C during the nitriding of a pre-oxidised silicon compact. This has not been demonstrated previously and was not considered possible at atmospheric pressure in nitrogen.

5. The Si_2ON_2-rich materials also had a higher ß-Si_3N_4:α-Si_3N_4 ratio compared to the Si_2ON_2-deficient materials.

6. Si_2ON_2-rich reaction bonded materials exhibit higher hardness values than the conventional reaction bonded materials, but the toughness values were lower.

7. The strengths of the reaction bonded materials were relatively low, but when eliminating the argon sintering step, these strengths decreased even further. This was due to the large pores and pressing defects present in the microstructure.

8. The mass increase and final density of the silicon compact during nitriding is dependent on the density obtained on forming. The optimum pressing pressure was found to coincide with the optimum density for a higher percentage conversion of Si to Si_3N_4 on nitriding.

9. Silicon compacts of larger volume were more difficult to nitride fully, and resulted in more residual silicon being present.

10. Lower porosity areas were found around residual silicon indicating melting may be a factor.

6.3 POST SINTERED REACTION BONDED SILICON NITRIDE

1. Si_2ON_2-rich reaction bonded materials were more stable during sintering and exhibited lower mass losses than the Si_2ON_2-deficient reaction bonded materials after sintering at 1800°C. This is believed to be the first recorded post sintering of these materials.

2. After sintering at 1750°C, the conventional reaction bonded materials produced the highest densities. The densities of the PSRBSN materials were generally higher than the sintered Si_3N_4 materials.

3. All the PSRBSN materials exhibited higher hardness values than the sintered Si_3N_4, while the toughness values were lower.

4. No Si_2ON_2 was detected in the post sintered reaction bonded materials. This results is believed to be the first record of the transformation of an oxynitride rich material under these conditions.

5. The conventional RBSN materials had a third phase visible (optical microscopy) after sintering. This phase was exclusive to the Si_2ON_2-deficient RBSN materials after sintering, and was not conclusively identified.

6. The higher the temperature during sintering, the larger the size of the grains were in the sintered body. The conventional RBSN showed more elongated grains after sintering at the higher temperature while the lower sintering temperature produced more equiaxed grains. The opposite was true for the Si_2ON_2-rich materials, where the elongated grains were observed after sintering at the lower temperature.

6.4 SINTERED Si_3N_4

1. Milling is an essential step in the Si_3N_4 powder processing route, not to reduce the particle size distribution but, rather, to facilitate intimate mixing of the Si_3N_4 powder and the additives, and to break up agglomerates in the powders.

2. Milling the Si_3N_4 powder appears to improve the flow properties and packing properties of the powder.

3. The incomplete mixing of the Si_3N_4 and additive powders in the mixed powders produced microstructures with large Y-rich areas among the Si_3N_4 grains. The milled powder also produced Y-rich areas, but these were smaller and confined mainly to grain boundaries and triple junctions.

4. Faster heating rates during sintering produced high densities and generally produced higher strength materials.

5. The slower heating rate produced a structure with larger grains and more of these grains were elongated compared to when a faster heating rate was used.

6. For full transformation of α-Si_3N_4 to ß-Si_3N_4 at the lower sintering temperature (1700°C) it was necessary to use a slower heating rate of $100°Ch^{-1}$.

7. The $\alpha \rightarrow$ß transformation was influenced by the powder processing method, since the milled powder produced Si_3N_4 materials with a higher α-Si_3N_4 content after 1700°C compared to the mixed powders.

8. There was no correlation between the density of the sintered Si_3N_4 and the strength and toughness values, and therefore it must be concluded that these mechanical properties are dependent on the resulting microstructures and inherent defects which differed depending on the sintering schedules.

9. The hardness increased with an increase in density for materials sintered at a specific temperature.

10. The hardness was not dependent on the α-Si_3N_4 content.

11. The hardness and toughness values were not influenced by the milling process.

12. Milling the Si_3N_4 powder in water and drying the slurry in a microwave oven had no detrimental effect on the sintered materials, and this process dried the slurry much faster than conventional oven drying.

13. As with the post sintered RBSN materials, the grain size increased with an increase in sintering temperature.

14. The main causes of fracture in all the strength tests were large pores, inclusions and large grains in the structures.

6.5 POST SINTERED RBSN AND SINTERED Si_3N_4

1. Although the raw material for RBSN is cheaper and locally available, the processing route is longer - Argon sintering (15 hours), nitriding (52 hours) and post sintering (12 hours) - a total of 79 hours, compared to a maximum of 29 hours for sintered Si_3N_4. In each of these stages processing is complex and defects can be introduced.

2. Post sintered RBSN uses less additives to produce a dense ceramic compared to sintered Si_3N_4.

3. PSRBSN produces ceramics with higher hardness values and densities than sintered Si_3N_4.

4. The strengths of the sintered Si_3N_4 are higher than those of the PSRBSN.

5. The toughness values of the materials via the two routes were of the same order, but the sintered Si_3N_4 generally showed slightly higher values than the PSRBSN.

7. Recommendations

By spray drying the powders, the particles would be more or less uniform in size and spherical. This would improve the flow properties of the powder, which would result in better packing and thus minimize the large pores found in the both the RBSN and sintered Si_3N_4 materials during this study. The better flow properties of the powder would also make it possible to use more uniform forming methods such as an automatic press.

Full rate controlled sintering of the reaction bonded Si_3N_4 would control the temperature according to the rate of the nitriding reaction, and this would result in a more uniform reaction rate, which would possibly minimize the amount of residual silicon after nitriding. This would be essential when larger components are produced.

To further improve the hardness of the RBSN, it would be beneficial to retain the Si_2ON_2 in the structure after sintering, since the Si_2ON_2 has a higher hardness than the Si_3N_4. In order for this to be accomplished, a partial pressure of oxygen would be necessary in the reaction chamber where the sintering is performed. Further work on silicon oxynitride materials may result in materials with excellent sinterability and properties.

The addition of the additives via chemical routes would ensure a more even distribution of the additive throughout the ceramic compact. This would also eliminate the necessity for the milling step in the processing of the Si_3N_4 powders, and this could be replaced by a shorter, more effective mixing step.

8. Acknowledgements

I would like to thank the following people for their help during this study. Without their help, this study would not have been possible.

The Ceramics Programme of the Division of Materials Science and Technology, CSIR, for the use of their facilities and financial support of the research in Si_3N_4.

Alfred Mathenjwa for his help in the preparation of the powders for processing, the pressing of the samples, mounting and polishing of the sintered samples and many other tasks.

Julian Stander for determining the particle size distributions of all the powders.

Detlef Basel for the printing of the photographs used in this manuscript.

Loukie Aldem and Dr Herbert Schmid for their help on the SEM and TEM respectively.

The late Prof Martin Shaw for his encouragement and guidance during the writing up of much of this manuscript.

Dr Adrian Paterson for making time in his busy schedule to be my supervisor, advising and encouraging me throughout the study.

Prof Colin Allen for agreeing to take over as my supervisor on short notice after the untimely death of Prof. Shaw.

Sandra Everitt for proof reading the manuscript.

9. References

Anon (1990): Testing - for materials selection, Advanced Materials and Processes, Guide to Selecting Engineered Materials, Vol 137, No 6, pp 5-16.

Anstis G.R., Chantikul P, Lawn B.R. and Marshall D.B. (1981): A critical evaluation of indentation techniques for measuring fracture toughness: I, Direct crack measurements, J. Am. Ceram. Soc, Vol 64, No 9, pp 533-8.

Arundale P. and Moulson A. J. (1977): Microstructural changes during argon sintering of silicon powder compacts, J. Mat. Sci. Letters, Vol 12, pp 138-40.

Atkinson A., Moulson A.J. and Roberts E.W., (1976): Nitriding high-purity silicon, J. Am. Ceram. Soc., Vol 59, No 7-8, pp 285-9.

Barratta F.I. (1982): Requirements for flexure testing of brittle materials, Army Materials and Mechanics Research Centre Report, No AMMRC TR 82-20.

Barratta F.I. (1984): Requirements for flexure testing of brittle materials, in Methods for assessing the structural reliability of brittle materials, ASTM special technical publication 844, pp 194-222.

Barnett N.O. and Nel J.M. (1989): Sintered silicon nitride using MgO-ZrO_2 and Y_2O_3 Additions, CSIR Report MST(89)SC29.

Barta J., Manella M. (1981): Pressureless sintering of silicon nitride, Science of Ceramics, Vol 11, pp 219-24.

Barta J., Manella M. and Fisher R. (1985): Si_3N_4 and Si_2N_2O for high performance radomes, Mat. Sci. Eng., Vol 71, pp 265-72.

Bonnel D.A. (1989): Structure of grain boundary phases in silicon nitride, Materials Science Forum, Vol 47, pp 132-42.

Billy M., Boch P., Dumazeau C., Glandus J. C. and Goursat P. (1981): Preparation and properties of new silicon oxynitride-based ceramics, Ceram. Int., Vol 7, No 1, pp 13-8.

Boskovic S., Gauckler L.J., Petzow G. and Tein T.Y. (1978): Reaction sintering forming ß-Si_3N_4 solid solutions in the system Si, Al/N,O II. Sintering of Si_3N_4-SiO_2-AlN mixtures, Powder Metal. Int. Vol 10, No 4, pp 184-5.

Bowen L.J., Weston R.J., Carruthers T.G. and Brook R.J. (1978): Hot pressing and the α-ß phase transformation in silicon nitride, J. Mat. Sci., No 13, pp 341-50.

Bradley S.A. and Karasek K.R. (1987): Analysis of grain boundaries for reaction-bonded silicon nitride with yttria additions, J. Mat. Sci. Letters, Vol 6, pp 791-4.

Braue W., Wötting G. and Ziegler G. (1986): The impact of compositional variations and processing conditions on secondary phase characteristics in sintered silicon nitride materials, Cermic Microstructures '86, Mat. Sci. Res Vol 21, pp 883-96.

Braun G., Baden G., Henkel K. and Rossbach H. (1988): Thermal analysis of the direct nitridation of silicon to Si_3N_4, J. Them. Anal., Vol 33, pp 479-85.

Brook R.J., Carruthers T.G., Bowen L.J. and Weston R.J. (1977): Mass transport in the hot pressing of α-silicon nitride, in Nitrogen Ceramics (F.L. Riley ed) Noordhoff, Leyden, The Hague, The Netherlands, pp 383-92.

Chakraborty D and Mukerji J. (1986): Effect of Si and Fe on $\alpha \rightarrow \beta$ phase transformation in Si_3N_4, Indian Journal of Technology, Vol 24, pp 231-2.

Cinibulk M.K., Thomas G. and Johnson S.M. (1990): Grain-boundary phase crystallization and strength of silicon nitride sintered with a YSiAlON glass, J. Am. Ceram. Soc., Vol 73, No 6, pp 1606-12.

Danforth S.C., Jennings H.M. and Richman M.C. (1979): Influence of microstructure on the strength of reaction bonded silicon nitride (RBSN), Acta Metallurgia, Vol 27, pp 123-30.

Dutta S. and Buzek B. (1984): Microstructure, strength and oxidation of a 10wt% zyttrite-Si_3N_4 ceramic, J. Am. Ceram. Soc. Vol 67, No 2, pp 89-92.

Evans A.G. and Davidge R.W. (1970): The strength and oxidation of reaction bonded silicon nitride, J. Mat. Sci., No 5, pp 314-25.

Gazzara C.P. and Messier D.R. (1977): Determination of phase content of Si_3N_4 by x-ray diffraction analysis, Am. Ceram. Soc. Bull., Vol 56, No 9, pp 777-80.

Galasco F.S. and Veltri R.D. (1981): Sintering of Si_3N_4 under nitrogen pressure, Army Materials and Mechanics Research Centre, Report AMMRC TR-81-28.

German R.M. (1985): Liquid Phase Sintering, Plenum Press, New York.

Giachello A. and Popper P. (1979(a)): Post-sintering of reaction-bonded silicon nitride, Ceramurgia International, Vol 6, No 3, pp 110-4.

Giachello A., Martinego P.C., Tommasini G. and Popper P. (1979(b)): Sintering of Silicon Nitride in a Powder Bed, J. Mat. Sci., No 14, pp 2825.

Giachello A., Martinego P.C., Tommasini G. and Popper P. (1980): Sintering and properties of silicon nitride containing Y_2O_3 and MgO, Am Ceram. Soc. Bull. Vol 59, No 12, pp 1212-5.

Govila R.K., Mangles J.A. and Baer J.R. (1985): Fracture of yttria-doped sintered reaction bonded silicon nitride, J. Am. Ceram. Soc., Vol 68, No 7, pp 413-8.

Greskovich C.D., Prochazka S. and Roslowski J.H. (1976): Basic research on technology development for sintered ceramics, ARPA report # SRD-76-036.

Greskovich C (1981): Preparation of high density Si_3N_4 by a gas-pressure sintering process, J. Am. Ceram. Soc, Vol 65, No 12, pp 725-30.

Greskovich C.D., Palm J.A. and Prochazka S (1983): Sintering of silicon nitride to high density, US Patent #4 379 110, 5 April 1983.

Greskovich C.D. and Yeh H.C. (1983): Hardness of dense beta silicon nitride, J. Mat. Sci. Letters, Vol 2, pp 657-9.

Greskovich C.D. and Gazza G.E. (1985): Hardness of dense α- and ß-Si_3N_4 ceramics, J. Mat. Sci. Letters, Vol 4, pp 195-6.

Griel P. (1989): Processing of silicon nitride ceramics, Mat. Sci. Eng., Vol A109, pp 27-35.

Grieveson P., Jack K.H. and Wild S. (1968): The crystal structures of alpha and beta silicon and gernamium nitrides, Special Ceramics 4, pp 237-8.

Hamasaki T., Ishizaki K. and Tanaka K. (1990): Influencing factors on fracture toughness of HIP sintered silicon nitride, J. Ceram. Soc. Japan, Int. Edition, Vol 98, pp 48-53.

Hampshire S. and Jack K.H. (1983): Densification of transformation mechanisms in nitrogen ceramics, in Progess in Nitrogen Ceramics (F.L. Riley Ed.) Martinus Nijhoff Publishers, The Hague, The Netherlands, pp 225-30.

Hampshire S. (1984): The role of additives in the pressureless sintering of nitrogen ceramics for engine applications, Metals Forum, Vol 7, No 3, pp 162-70.

Hampshire S. and Pomeroy M. (1985): Pressureless sintering of silicon nitride with mixed oxide additives, Ann. Chem. Fr., Vol 10, pp 65-72.

Heinrich J. (1980): Influence of processing conditions on the microstructure and mechanical properties of reaction sintered silicon nitride, Translation of "Der Einfluss von Herstellungsbedingungen auf das Gefuege und die mechnischen Eigenschften von reaktiongesintertem silicuimnitrid", Report DFVLR-FB-79-32.

Heinrich J. (1983): Contribuiton of the strength-porosity relationship of reaction bonded silicon nitride, in Progress in Nitrogen Ceramics, Ed F.L. Riley, Published by Martinus Nijhoff Publishers, The Hague, The Netherlands, pp 393-99.

Heinrich J. (1985): Contribution to the technology of hot-isostatic pressing of some non-oxide ceramics, CFI/Ber., DKG 4/5, pp 222-8.

Heinrich J., Munz D. and Ziegler G. (1982): Influence of microstructural variables on mechanical properties, creep and thermal shock behaviour of reaction bonded silicon nitride, Powder Metal. Int., Vol 14, No 3, pp 153-59.

Heinrich J., Backer E. and Böhmer M. (1988): Hot isostatic pressing of Si_3N_4 powder compacts and reaction-bonded Si_3N_4, J. Am. Ceram. Soc. Vol 71, No 1, pp C28-31.

Hirosaki N., Okada A. and Matoba K. (1988): Sintering of Si_3N_4 with additions of rare-earth oxides, Comm. Am. Ceram. Soc., March 1988, pp C144-7.

Hirosaki N., Okada A. and Mitomo M. (1990): Effect of oxide addition on the sintering and high temperature strength of Si_3N_4 containing Y_2O_3, J. Mat. Sci., No 25, pp 1872-6.

Huang Z.K., Griel P. and Petzow G. (1984): Formation of silicon oxynitride from Si_3N_4 and SiO_2 in the presence of Al_2O_3, Ceram. Int., Vol 10, No 1, pp 14-7.

Hwang C.M. and Tein T.Y. (1983): Sintering and grain growth of silicon nitride in presence of reactive liquid, Report No DE 86003865/WMS, University of Michigan.

Jack K.H. (1979): The role of additives in the densification of nitrogen ceramics, Report prepared for U.S. Army, European Research Office.

Jack K. H. (1991): Sialons: Ceramic alloys for engineering application, J. Mat. Educ., Vol 13, pp 1-40.

Jennings H.M. and Richman M.C. (1976): Structure, formation mechanisms and kinetics of reaction-bonded silicon nitride, J. Mat. Sci, No 11, pp 2087-98.

Jennings H.M., Edwards J.O. and Richman M.C. (1976(b)): Molecular structure, microstructure, macrostructure and properties of silicon nitride, Inorganica Chimica Acta, Vol 20, pp 167-81.

Jennings H.M., Dalgleish B.J. and Pratt P.L. (1988): Reactions between silicon and nitrogen, Part 2 Microstructure, J. Mat. Sci., No 23, pp 2573-83.

Kameda T., Asayama M., Komatsu M. and Komeya K. (1990): Effect of powder characteristics and sintering additives on high temperature strength of Si_3N_4, Ceramic Powder Science III, Ceramic Transactions, No 12, pp 827-34.

Kasai K., Nagata S., Arakawa T. and Tsukidale T. (1985): Synthesis of Si_3N_4 powder by thermal decomposition of $Si(NH)_2$ and sintering, Ceram. Eng. Sci. Proc., Vol 6, No 9-10, pp 1278-88.

Katayama Y. and Hattori Y. (1982): Effects of specimen size on strength of sintered silicon nitride, J. Am. Ceram. Soc., Vol 65, No 10, pp C-164-5.

Kingery W.D. (1959(a)): Densification during sintering in the presence of a liquid phase - I, Theory. J. App. Phys., Vol 30, No 3, pp 301-6.

Kleebe H.-J and Ziegler G. (1988): Influence of Si-powder characteristics on the pore structure of Si-powder compacts and of reaction-bonded Si_3N_4, Journal de Physique Colloque C1, Vol 47, No 2, pp C1-97-101.

Kobayashi S. and Wada S.(1988): Strengthening of Si_3N_4 ceramics by ZrO_2 additions, Advances in Ceramics No 24, Science and Technology of Zirconia III, Am. Ceram. Soc. Inc., pp 127-32.

Kohatsu I. and McCauley J.W. (1974): Re-examination of the crystal structure of α-Si_3N_4, Mat. Res. Bull., Vol 9, No 7, pp 917-920.

Komeya K., Komatsu M., Komeda T., Goto Y., Tsuge A. and Thomas G. (1990): High temperature strength microstrucutre in Si_3N_4-Y_2O_3 base ceramics, 7th CIMTEC, June 1990, Published by Elsevier Applied Science, pp 119-210.

Kulig M., Oroschin W. and Griel P. (1989): Sol-gel coating of silicon nitride with Mg-Al oxide sintering aids, J. Europ. Ceram. Soc., Vol 5, pp 209-17.

Lange F.F. (1978): Phase relations in the system Si_3N_4-SiO_2-MgO and their interrelations with strength and oxidation, J. Am. Ceram. Soc., Vol 61, No 1-2, pp 53-7.

Lange F.F., Falk L.K.L. and Davis B.I. (1987): Structural ceramics based on Si_3N_4-$ZrO_2(Y_2O_3)$ compositions, J. Mater. Res., Vol 2, No 1, pp 66-76.

Lange F.F. (1980): Silicon nitride polyphase systems: fabrication microstructure and properties, Int. Metals Review, Vol 1, pp 1-19.

Lange F.F. (1983): Fabrication and properties of dense polyphase silicon nitride, Ceramic Bulletin, Vol 62, No 12, pp 1369-74.

Lange F.F. (1983(b)): Importance of phase equilibria on process control of Si_3N_4 fabrication, Army Materials Tech. Conf., Vol. 6, pp 275-91.

Lee W.E., Drummond C.H., Hilmas G.E., Kiser J.D. and Sanders W.A. (1988): Microstructural evolution on crystallizing the glassy phase in a 6 weight % Y_2O_3-Si_3N_4 ceramic, Ceram. Eng. Sci. Proc., Vol 9, No 9-10, pp 1355-66.

Lee W.E. and Hilmas G.E. (1989): Microstructural changes in ß-silicon nitride grains upon crystallizing the grain boundary glass, J. Am. Ceram. Soc., Vol 72, No 10, pp 1931-37.

Lewis C.F. (1990): Testing ceramic fracture toughness, Materials Engineering, October 1990, pp 31-3.

Lourenz J., Weiss J. and Petzow G. (1982): Advanced powder technology, ASM Material Science Seminar, Ed G.Y. Chin, ASM Metals Park, Ohio, pp 289-308.

Lu H.Y. and Riley F.L. (1984): The analysis of silicon nitridation kinetic data, Science of Ceramics 12, pp 145-50.

Mangels J.A. and Tennenhouse G.J. (1980): Densification of reaction-bonded silicon nitride, Ceramic Bulletin, Vol 59, No 12, pp1216-22.

Mangles J.A. (1981(a)): Effect of rate-controlled nitriding and nitriding atmospheres on the formation of reaction-bonded Si_3N_4, Am. Ceram. Soc. Bull., Vol 60, No 8, pp 613-7.

Mangels J.A. (1981(b)): Sintered reaction-bonded silicon nitride, Cer. Eng. Sci. Proc., Vol 2, No 7-8, pp 589-603.

Mangels J.A. and Tennenhouse G.J. (1981): Sintering behavior and microstructural development of yttrium-doped reaction-bonded silicon nitride, Ceramic Bulletin, Vol 60, No 12, pp1306-10.

Matsuhiro K. and Takahashi T. (1989): Effect of grain size on the toughness of sintered Si_3N_4, Ceram. Eng. Sci. Proc., Vol 10, No 7-8, pp 807-16.

Martinengo P.C., Giachello A., Popper P., Buri A. and Branda F. (1978): Devitrification phenomena of a pressureless sintered silicon nitride, Proc. of Int. Symp. on Fators in Densification and Sintering of Oxide and Non-Oxide Ceramics, Japan, pp516-26.

McColm I.J. (1990): Ceramic Hardness, Published by Plenum Press, New York, pp 216-28.

Messier D.R. and Croft W.J. (1982): Preparation and properties of solid state materials, Vol 7, Chapter 2, pp131-213.

Messier D.R. and Wong P. (1973): Kinetics of formation and mechnical properties of reaction sintered Si_3N_4, in Ceramics for High Performance Applications, Ed J.J. Burke, A.E. Gorum and R.N. Katz, Brook Hill Chestnut Hill, Mass., pp 181-93.

Micski A. and Bergman B. (1990): High temperature strength of silicon nitride HIP with low amounts of yttria or yttria/alumina, J. Euro. Ceram. Soc., Vol 6, pp 291-301.

Moser W.R., Briere D.S. and Correia R. (1986): Kinetics of iron-promoted silicon nitride, J. Mat. Res. Vol 1, No 6, pp 797-802.

Moulson A.J. (1979): Review: reaction-bonded silicon nitride: Its formation and properties, J. Mat. Sci., No 14, pp 1017-51.

Moya J.S. and De Aza S. (1986): Equilibrium diagrams: A tool for designing new ceramics, Science of Ceramics 14, pp 27-40.

Mukerji J. (1984): Sintering of silicon nitride, in Sintered Metal-Ceramic Composites, ed. by G.S. Upadhyaya, Elsevier Science Publishers B.V. Amsterdam, pp 411-24.

Mukerji J. and Das P.K. (1986): Dense Si_3N_4 by liquid phase sintering, Indian Journal of Technology, Vol 24, April 1986, pp 209-14.

Mukhopadhyay A.K., Duta S.K. and Chakraborty D. (1990): On the microhardness of silicon nitride and sialon ceramics, J. Euro. Ceram. Soc., Vol 6, pp 301-11.

Mukhopadhyay A.K., Duta S.K. and Chakraborty D. (1991): Hardness of silicon nitride and sialon, Ceram. Int., Vol 17, pp 121-7.

Mustel W. and Broussaud P. (1984): Optimization of the silicon nitride process, Science of Ceramics 12, pp 131-7.

Negita, K. (1985): Effective sintering aids for Si_3N_4 ceramics, J. Mat. Sci. Letters, Vol 4, pp 755-8.

Neil J.T., Pasto A.E. and Bowen L.J. (1988): Improving the reliability of silicon nitride: a case study, Advanced Ceramic Materials, Vol 3, No, 3, pp 225-30.

Noakes P.B. And Pratt P.L. (1970): High-temperature mechanical properties of reaction sintered silicon nitride, in Special Ceramics 5, Ed. P. Popper, Published by The British Ceramic Research Association, pp 299-310.

Pasco W.D. and Greskovich C.D. (1982): Sintered Si_3N_4 for high performance thermomechanical applications, Final Report for US Department of Energy, No AMMRC TR 82-22.

Palm J.A. and Greskovich C.D. (1980): Thermomechanical properties of hot-pressed $Si_{2.9}Be_{0.1}N_{3.8}O_{0.2}$ ceramic, Ceram. Bull., Vol 59, No 4, pp447-52.

Park Ji Yeon, Kim Jae Ryong and Kim Chong Hee (1987): Effects of free Si on the α to β phase transformation in silicon nitride, J. Am. Ceram. Soc., Vol 70, No 10, pp C240-2.

Park Ji Yeon and Kim Chong Hee (1988): The α to β Si_3N_4 transformation in the presence of liquid silicon, J. Mat. Sci., No 23, pp 3049-54.

Paterson A.W. (1986): Fabrication of reaction bonded silicon nitride, Report CSIR-NIMR CMAT 293.

Paterson A.W. (1988): Effect of fabrication parameters on the hardness and microstructure of RBSN, Science of Ceramics 14, pp 677-82.

Petzow G., Telle R. and Danzer R. (1991): Microstructural defects and mechanical properties of high performance ceramics, Materials Characterization, Vol 26, pp 289-301.

Ponton C.B. and Rawlings R.D. (1989): Dependence of the Vickers indentation fracture toughness on the surface crack length, Br. Ceram. Trans. J., Vol 88, pp 83-90.

Popper P. (1978): Problems in sintering silicon nitride, Proc. of Int. Symp. of Factors in Densification and Sintering of Oxide and Non-Oxide Ceramics, Japan, pp 19-27.

Prokesová M. and Pánek Z. (1989): Particle rearrangement during liquid phase sintering of silicon nitride, Ceram. Int., Vol 15, pp 369-74.

Rae A.W.J.M., Thompson D.P. and Jack K.H. (1977): The role of additives in the densification of nitrogen ceramics, Proc. Army Mat. Tech. Conf. - Ceramic High Performance Applications, pp 1039-67.

Riley F.L. (1977): Nitridation and reaction bonding, in Nitrogen Ceramics (F.L. Riley, ed.) Noordhoff, Leyden, The Netherlands, pp 265-88.

Riley F.L. (1983): Silicon nitridation, in Progress in Nitrogen Ceramics, (F.L. Riley Ed.) NATO ASI Series, Series E, No 65, Martinus Nijhoff, The Hague, The Netherlands, pp 121-33.

Riley F.L. (1984): Silicon nitrides: An overview, Science of ceramics 12, pp 15-26.

Riley F.L. (1985): Production, properties and applications of silicon nitride ceramics, Sprechsaal, Vol 118, No 3, pp 225-33.

Riley F.L. (1989): Reaction-bonded silicon nitride, Materials Science Forum, Vol 47, pp 70-83.

Ritter J.E., Nair S.V., Gennari P.A., Dunlay W.A., Haggerty J.S. and Garvey G.J. (1988): High strength reaction-bonded silicon nitride, Advanced Ceramic Materials, Vol 3, No 4, pp 415-7.

Roy R. (1987): Ceramics by solution-sol-gel route, Science, Vol 238, pp 166

Russel G.J., Putch R. and Thorp J.S. (1985): A combined RHEED and SEM study of reaction bonded silicon nitride, Electron Microscopy and Analysis 1985, Int. Phys. Conf. Ser. No 78, Chapter 13, pp 535-8.

Schubert H. and Petzow G. (1988): What makes ceramics tougher?, J. Mater. Educ., Vol 10, pp 601-20.

Segal D. (1985): Developments in the synthesis of silicon nitride, Chemistry and Industry, 19 August, pp 544-5.

Shaw N.J. (1981): Nitridation of silicon, NASA Report NASA-TM-82722.

Shimada M., Koizumi M., Tanaka A. and Yamada T. (1982): Temperature dependence of K_{Ic} for high pressure hot-pressed Si_3N_4 without additives, Communications for Am. Ceram. Soc., April 1982, pp C48-50.

Smith J.T. and Quackenbush C.L. (1980(a)): Phase effects in Si_3N_4 containing Y_2O_3 and CeO_2: I, Strength, Am. Ceram. Soc. Bull., Vol 59, No 5, pp 529-32.

Soma T., Matsui M. and Oda I. (1985): Tensile strength of a sintered silicon nitride, in Technical Non-oxide Engineering Ceramics, Elsevier Applied Science, London, pp 361-74.

Sorrel C.C. (1982): Silicon nitride and related nitrogen ceramics - I: Phase equilibria and properties of reaction bonded and hot pressed M-Si-O-N systems, J. Aust. Ceram. Soc. Vol 18, No 2, pp 22-34.

Tajima Y., Urashima K., Watanabe M. and Matsuo Y. (1988): Fracture toughness and microstructure evolution of silicon nitride ceramics, Ceramic Transactions, Vol 1, Part B, Ceramic Powder Science, pp 1034-41.

Takatori K., Shimada M. and Koizumi M. (1981): Fabrication of highly dense Si_3N_4 ceramics without additives by high pressure sintering, NASA-TM-77425, Translation of "Nippon Kagaku Kaishi", 1981, pp 1506-7.

Tanaka H. and Baba H. (1984): Nitride based cutting tool and method for production of the same, European Patent 0113660 A2.

Tanaka I., Pezzotti G., Okamoto T., Miyamoto Y. and Koizumi M. (1989): Hot isostatic press sintering and properties of silicon nitride without additives, J. Am. Ceram. Soc., Vol 72, No 9, pp 1656-60.

Torizuka S., Yabuta K. and Nishio H. (1989(a)): Fabrication of Si_3N_4 by sinter/HIP, ISIJ International, Vol 29, No 9, pp 734-9.

Torizuka S., Yabuta K. and Nishio H. (1989(b)): Appropriate sinter/HIP conditions to fabricate high strength Si_3N_4 , ISIJ International, Vol 29, No 9, pp 740-5.

Tsuge A., Nishida K. and Komatsu M. (1975): Effect of crystallizing the grain-boundary glass phase on the high-temperature strength of hot pressed Si_3N_4 containing Y_2O_3, J. Am. Ceram. Soc., Vol 58, No 7-8, pp 323-9.

Vasilos T. (1977): Densification of nitrides by hot pressing, NATO Adv. Study, Inst. on Nitrogn Ceramics Series E, App. Sci. Vol 23, pp 367-82.

Weiss J. (1981): Silicon nitride ceramics: composition, fabrication parameters and properties, Ann. Rev. Mater. Sci, Vol 11, pp 381-99.

Weiss J. and Kaysser W.A. (1983): Liquid phase sintering, in Progress in Nitrogen Ceramics, Ed by F.L. Riley, Martinus Nijhoff Publishers, The Hague, The Netherlands, pp 169-86.

Wiederhorn S.M. (1984): Brittle fracture and toughening mechanisms in ceramics, Ann. Rev. Mater. Sci., Vol 14, pp 373-401.

Wötting G. and Ziegler G. (1984): Influence of powder properties and processing conditions on microstructure and mechanical properties of sintered silicon nitride, Ceram. Int., Vol 10, pp 18-27.

Wötting G. and Ziegler G. (1986(a)): Powder characteristics and sintering behaviour of Si_3N_4-powders, Part I: powder characteristics, Interceram. 2, pp 32-5.

Wötting G. and Ziegler G. (1986(b)): Powder characteristics and sintering behaviour of Si_3N_4-powders, Part II: sintering behaviour, Interceram. 3, pp 57-60.

Wötting G. and Ziegler G. (1986(c)): Powder characteristics and sintering behaviour of Si_3N_4-powders, Powder Metallurgy International, Vol 18, No1, pp 25-32.

Wötting G. and Ziegler G. (1988(a)): Gas pressure sintering of silicon nitride, Part 1, CFI/Ber. DKG, Vol 65, No 10, pp 364-8.

Wötting G. and Ziegler G. (1988(b)): Gas pressure sintering of silicon nitride, Part 2, CFI/Ber. DKG, Vol 65, No 11-12, pp 471-5.

Yamada T., Shimada M. and Koizumi M. (1981): Densification of Si_3N_4 by high pressure hot pressing, Ceram. Bul., Vol 60, No 12, pp 1281-3, 88.

Ziegler G. (1983): Microstructural effects on properties and new processing techniques of silicon nitride, Part II: New processing techniques of silicon nitride, Z. Werkstofftech., Vol 14, pp 189-96.

Ziegler G. and Wötting G. (1985): Post-treatment of pre-sintered silicon nitride by hot isostatic pressing, Int. J. High Technology Ceramics, Vol 1, pp 31-58.